Journal of Molecular Liquids 320 (2020) 114417

Contents lists available at ScienceDirect

Journal of Molecular Liquids

journal homepage: www.elsevier.com/locate/molliq

Enlightening binding behaviour of sulfonatocalix[4]arene receptor with 2-acetoxybenzoic acid through the lens of experiments and theory

Rupali G. Thorave [a], Dipali N. Lande [b], Uttam V. Shinde [a], Dipalee D. Malkhede [a,*], Shridhar P. Gejji [a,*]

[a] Department of Chemistry, Savitribai Phule Pune University, 411 007, India
[b] Chemistry Department, Sir Parshurambhau College, Pune 411 030, India

ARTICLE INFO

Article history:
Received 14 July 2020
Received in revised form 18 September 2020
Accepted 22 September 2020
Available online 28 September 2020

ABSTRACT

The inclusion behaviour of 2-acetoxy benzoic acid (ASA, aspirin) within the para-sulfonatocalix[4]arene (SCX4) host has been characterized employing UV–visible, ^{1}H NMR, vibrational spectroscopy, electrospray ionization mass spectrometry (ESI–MS) and chromatography experiments in conjunction with the density functional theory. It has been shown that the ASA ⊂ SCX4 complex possesses 1:1 stoichiometry and is more stable toward oxidative conditions than in acidic and basic media compared to the free ASA guest. The complexation of SCX4 with the ASA emerges with signature in the 'frequency up-shift' of its Ar-OH (~14 cm^{-1}) and SO_3^- (~36 cm^{-1}) stretching vibrations whereas the carbonyl stretching vibration from the ester group engenders shift in the opposite direction (red shift) in the measured infrared spectra. These inferences are corroborated through the density functional theory.

1. Introduction

Aspirin (ASA) has been recognized as an analgesic, antipyretic, anti-inflammatory, antiplatelet, and antithrombotic drug [1,2]. A regular dosage of aspirin is believed to prevent colorectal cancer [3]. Dovizio et al. have suggested the underlying mechanism of the anticancer action of aspirin and pointed out certain medical issues related to its applications [4]. The low to moderate doses of ASA inhibits cardiovascular diseases and minimize the risk of cardiac-cause mortality [5]. Low water solubility and gastrointestinal absorption, however limits bioavailability of the ASA [6–8]. It is thus crucial to develop new pharmaceutical formulations, for instance, granules and effervescent or micronized tablets [9]. The therapeutic drug carriers capable of binding to a substrate form the inclusion complex thereby providing an alternative strategy in this regard [10]. Such complexation enhances bio-distribution of a drug and enhances its water-solubility and its accumulation in sick tissues [11]. A family of macrocyclic hosts for example, cyclodextrins, calixarenes, cucurbiturils or pillararenes, have been explored as drug carriers for pharmaceutical applications [12–20]. Conducing of the inclusion complex shields a drug molecule from chemical reactions or photochemical degradation in biological environments which in turn, renders the prolonged therapeutic effect. An encapsulation of guest within the macrocyclic host(s) significantly alters its acidity/basicity [21,22], reactivity [23,24], conformation [25,26], or fluorescence behaviour [27].

It has earlier been shown that the solubility and permeability of aspirin (ASA) enhances dramatically on encapsulation within the β-cyclodextrin [28–34]. Porwanski et al. [35] synthesized the ASA complexes of bis-cellobiose and bis-glucose azacrown derivatives with the use of azacrownethers or azidosaccharides which were further characterized through the ^{1}H NMR experiments. Pursuance to this Adamiak [36] and coworker studied the complexation of bis-β-D-glucopyranosyldiazacrown derivative with ASA. Taking a clue from this in the present endeavour we explore the calixarene scaffold that has widely been employed as a major class of supramolecular hosts in pharmaceutical sciences.

Calixarene are cyclooligomers those were successfully synthesized by the reaction between the phenol derivatives and formaldehyde with an appropriate choice of solvent, base and temperature [37–41]. These macrocyclic hosts are endowed with a three- dimensional hydrophobic cavity that is capable of accommodating a variety of organic or cationic guests. The calix[*n*]arene hosts composed of n = 4, 6 or 8 phenol residues with varying cavity dimensions have thus been explored for diverse applications particularly in the domains of supramolecular chemistry [42]. Furthermore, the modification of such artificial receptors with nucleophilic and electrophilic aromatic substituents on upper or lower positions of its core annulus furnish newer cavitands those are largely flexible and rendered with the enhanced solubility [43]. It has also been demonstrated that functionalization of upper rim of calixarenes can be carried out with the electrophilic aromatic substitution that is, halogenation, nitration or sulphonation and other reactions [44–50]. To this direction the electrophilic substitution in concentrated sulfuric acid further has been carried out for tuning of

* Corresponding authors.
E-mail addresses: ddm@chem.unipune.ac.in (D.D. Malkhede), spgejji@chem.unipune.ac.in (S.P. Gejji).

https://doi.org/10.1016/j.molliq.2020.114417
0167-7322/

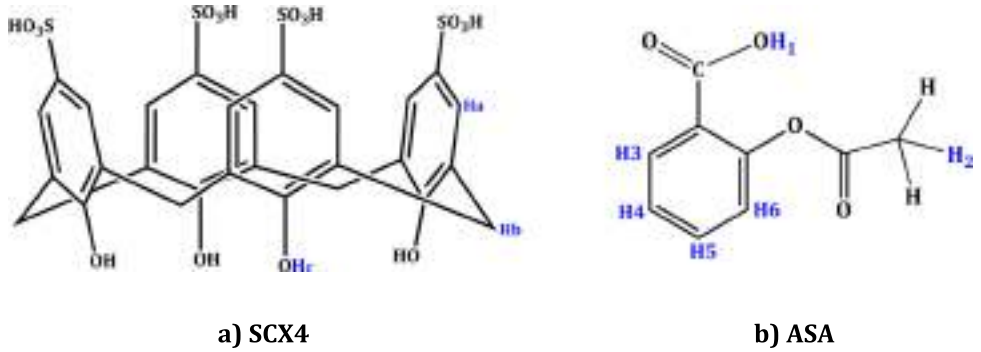

a) SCX4 **b) ASA**

Fig. 1. SCX4 host and guest Aspirin.

the desired chemical or physical properties on the calixarene hosts. Shinkai et al. [51] obtained para-sulfonato-calixarene derivatives as pure crystalline products which are highly soluble in water [52–57]. Their capability to encapsulate drugs, bioavailability, oral absorption and remarkable stability toward heat, light and acidic conditions, offered certain advantages in pharmaceuticals [58–67].

More interestingly para-sulfonatocalixarene derivatives serve as a remarkably efficient molecular receptor compared to other classes of hosts. These include: ease of chemical functionalization than for cucurbit[*n*]urils macrocycles, high binding affinity toward guest drugs likened with β-cyclodextrin and their bowl-shape cavity being distinct from those of barrel-shaped cucurbit[*n*]urils and cone shaped β-cyclodextrin or cylindrical pillar[n] arenes [68].

Despite of *afore* mentioned studies, almost no endeavour, within experimental as well as theory, appear to have been made toward the description of inclusion complex between para-sulfonatocalix[4]arene host (SCX4) and aspirin as a guest (cf. Fig. 1). In this spirit we employ a variety of spectroscopic techniques viz., ultra-violet (UV), ^{1}H nuclear magnetic resonance (NMR), Fourier transform infra-Red (FT-IR) and electrospray ionization mass spectrometry (ESI–MS). A comparison of stability of the isolated ASA and its inclusion complex has also been carried out through the forced degradation studies employing the chromatography experiments,

2. Experimental

2.1. Materials

The analytical grade *p*-sulfonatocalix[4]arene (SCX4) is obtained from TCI chemicals. The acetonitrile (HPLC grade), methanol (HPLC grade), hydrochloric acid, sodium hydroxide, hydrogen peroxide of AR grade and doubly distilled deionized water (milli-Q), were used.

2.2. Experimental

A stock solution of 100 μg/mL was prepared by dissolving 10 mg of aspirin in 100 ml milli-Q water. The SCX4 (10^{-3} M) solution was prepared by an appropriate amount of pure solid in water. The 1:1 equivalent ASA ⊂ SCX4 complex was prepared with the addition of 0.01 M ASA in methanol to a solution of 0.01 M SCX4 by using slow evaporation method. A white amorphous powder was obtained. These are used for UV, NMR, IR, ESI-MS analysis and chromatographic experiments.

To determine binding stoichiometry of the inclusion complex, ^{1}H NMR titration experiments (using D_2O as a solvent) were carried out on the 400 MHz Bruker spectrophotometer. ^{1}H NMR titration experiments were carried out and the Job's plot was obtained [69]. Further $\Delta\delta$ refers to a change in chemical shift upon addition of the host species to ASA compared to the isolated ASA (Table 1).

The infrared spectra were measured on the TENSOR-37 equipped with ATR. FTIR analyses in the 4000–400 cm^{-1} region. The mass evaluated on High resolution mass spectrometer (HRMS) Bruker model impact HD. Sample loaded through UHPLC (Thermoscientific, ultimate 3000) auto sampler. For instrument operation OTOF control and Hystar 3.2 software's were used. Data analysis was carried out by compass data analysis software. Compound isotope pattern software was used to predict theoretical mass and isotope pattern. Positive ion polarity with ESI source was used for the analysis. Nebulizer, dry heater and charging voltage was set at 1.7 bar, 200 °C temperature and 2000 V respectively. The solution (90:10) water:methanol was used with thoroughly the flow being 0.120 ml/min. The mass spectra scan in the range from 0 to 1200 *m/z* [70]. Data analyses were carried out by compass data analyser software. Absorbance was measured on the SHIMADZU UV-1800 spectrophotometer. The scans were registered in the range 200 nm to 400 nm.

HPLC was chosen since it is compatible with aqueous or organic solvents, sensitivity and ability to detect polar compounds. Early elution of highly polar compounds and retention of nonpolar compounds was carried out through isocratic elution. A chromatographic analysis of aspirin and its complex was performed on Agilent Eclipse plus C18, 250 × 4.6 mm × (5 μm) column with UV detector by using Acetonitrile: milliQ: methanol (25:45:30 v/v) mobile phase with an effluent flow rate of 0.5 ml/min. All determinations were performed for run time of 10 min.

Trial and error methods were used to select the appropriate mobile phases by varying the proportions as well as flow rate of combination of solvents viz., methanol, water, acetonitrile and acidic buffer. For the 25:45:30 v/v ratio of acetonitrile, water and methanol respectively, a

Table 1
Chemical shifts along with $\Delta\delta$ for SCX4 (0.01 mM), ASA (0.01 mM) and ASA ⊂ SCX4 in D_2O.

Δ ($\Delta\delta = \delta$-δ_0) (ppm)										
Protons	δ_0	3:1	2:1	1:1	1:2	1:3	3:1	2:1	1:1	1:2	1:3
H3	7.94	7.93	7.91	7.90	7.89	7.87	−0.01	−0.03	−0.04	−0.05	−0.07
H4	7.18	7.12	7.10	7.07	7.05	7.02	−0.06	−0.08	−0.11	−0.13	−0.16
H5	7.40	7.30	7.25	7.21	7.17	7.12	−0.1	−0.15	−0.19	−0.23	−0.28
H6	7.64	7.54	7.47	7.45	7.40	7.35	−0.1	−0.17	−0.19	−0.24	−0.29
H2	2.31	2.29	2.28	2.28	2.27	2.26	−0.02	−0.03	−0.03	−0.04	−0.05
Ha	7.53	7.53	7.56	7.56	7.57	7.57	0	0.03	0.03	0.04	0.04
Hb	3.99	3.99	3.99	3.98	3.96	3.99	0	0	0.01	0.03	0

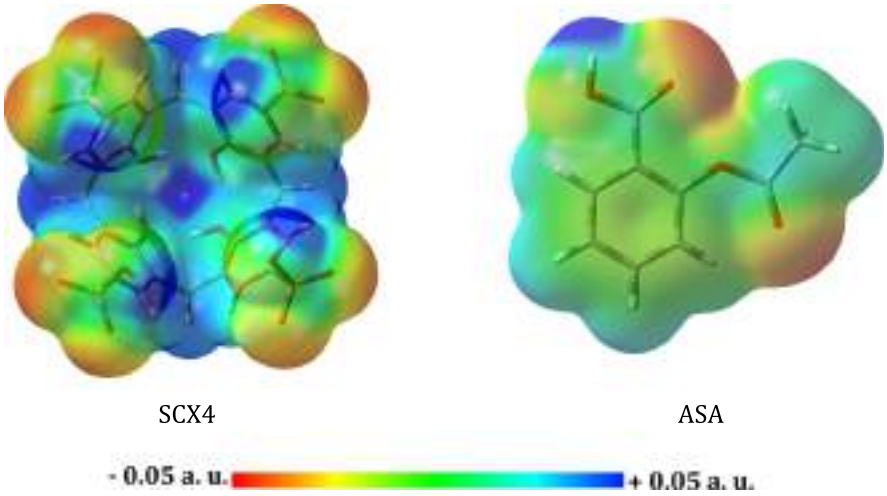

Fig. 2. Electron density isosurfaces (0.001 a.u.) overlaid with the MESP (−0.05 to +0.05 a.u.).

sharp symmetrical peak with minimum retention time (Rt) was then identified.

The standard stock solution of 100 μg/mL, complex was prepared by dissolving 10 mg of each in the milli-Q water (mobile phase) in 100 mL volumetric flask, ASA were prepared in milli-Q water and methanol (95:05). The solution was filtered by syringe filter 0.45 μM and further diluted with mobile phase so that a final concentration of 100 μg/mL was obtained.

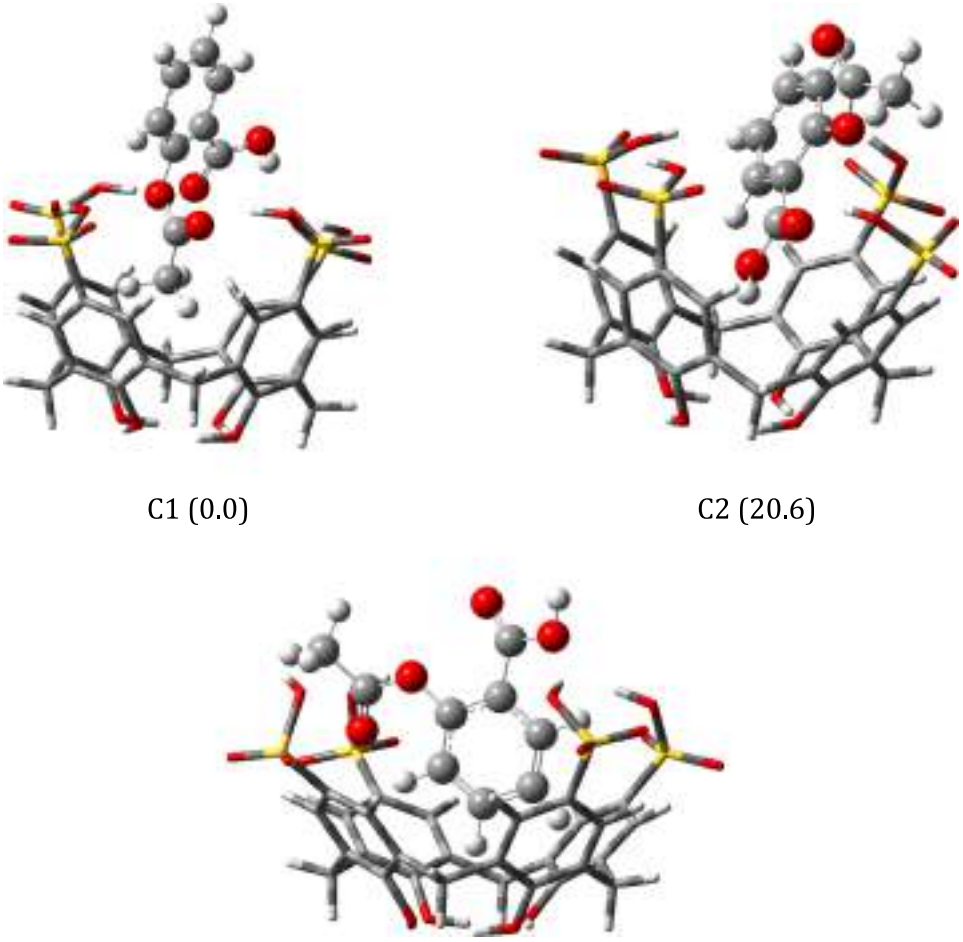

Fig. 3. Conformers of the ASA and SCX4 inclusion complexes along with relative stabilization energies (in kJ mol^{-1}).

Standard stock solution ranging from 1 mL to 5 mL were taken in10 mL volumetric flasks and diluted appropriately with mobile phase. The concentration of drug was varied from 10 to 50 μg/mL with 20 μL of each stock solution being injected under the standard chromatographic conditions. The peak area was recorded and the calibration curve obtained as a plot of peak area versus concentration of the ASA.

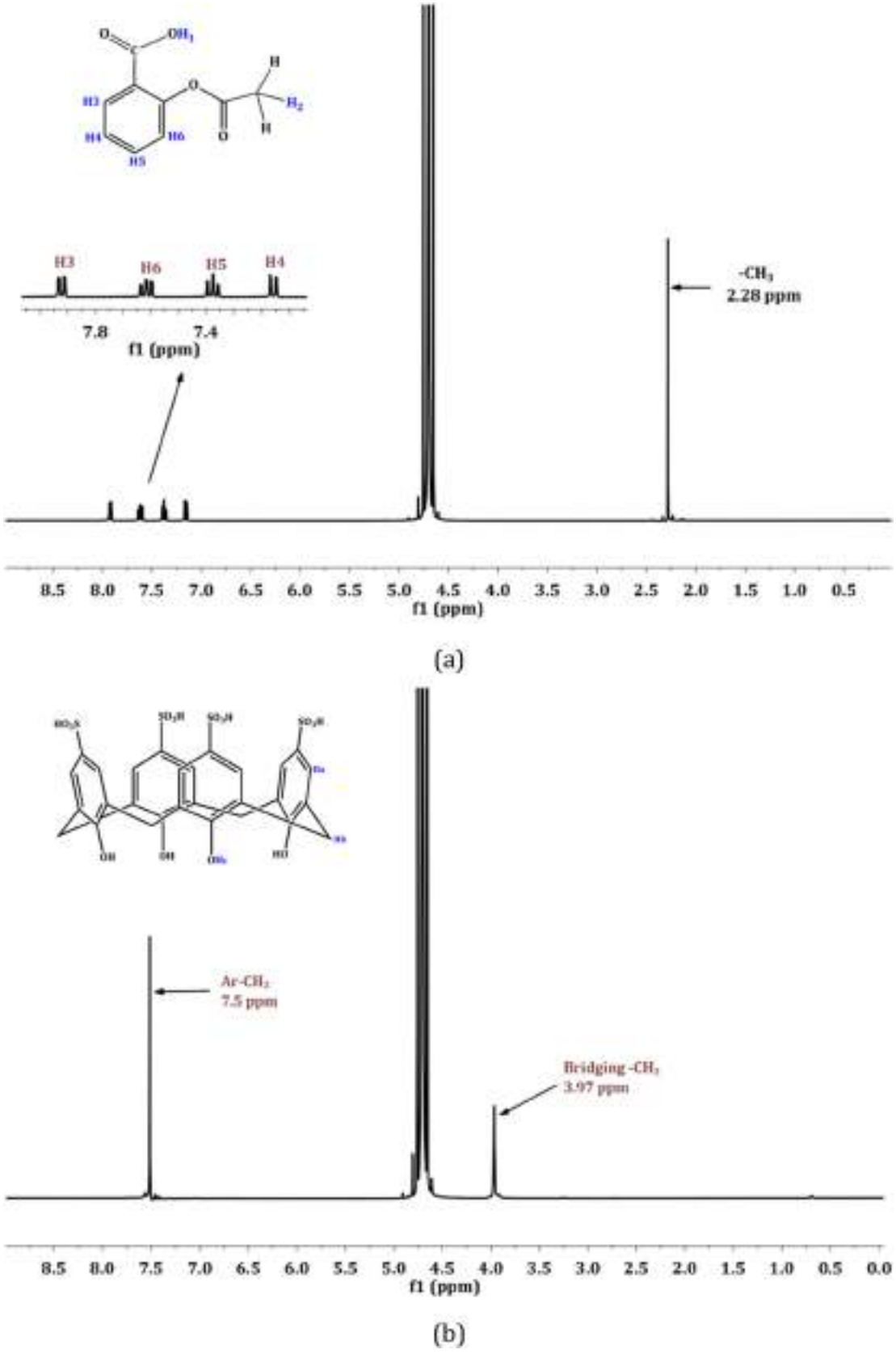

Fig. 4. ^{1}H NMR spectra of: a) ASA, b) SCX4 and c) ASA ⊂ SCX4 (400 MHz, D_2O, 298 K).

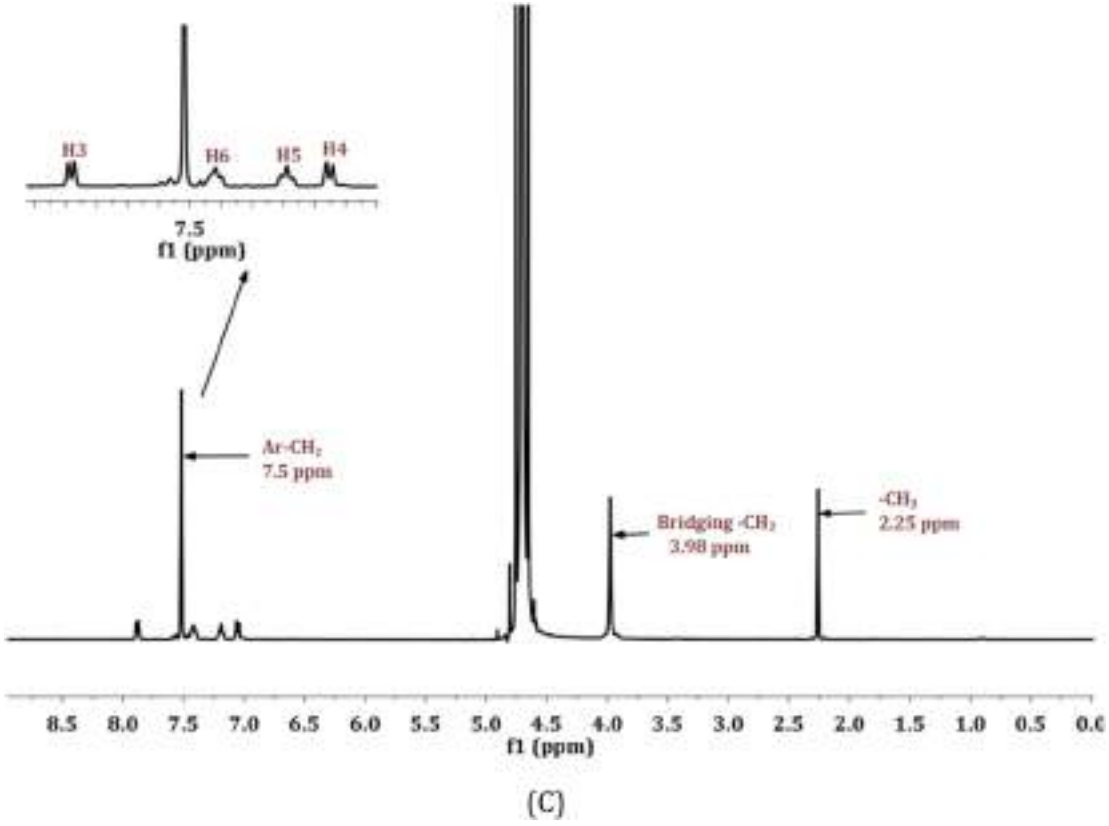

Fig. 4 (*continued*).

The guidelines prescribed by the International council on Harmonisation (ICH) were followed for the stress studies [71]. The acidic (0.1 N hydrochloric acid), basic (0.1 N sodium hydroxide), oxidative (0.3% H_2O_2), degradation was carried out at 0 h, 1 h, 2 h, 4 h, 8 h, 12 h, 16 h and 24 h.

3. Computational details

Optimizations of SCX4 host, ASA (guest) and its complex were carried out using the density functional theory with the help of Gaussian-09 suite of programme. The density functional theory (DFT) incorporating the dispersion corrected ωB97X-D hybrid exchange-correlation functional, designed to handle weak interactions was used in conjugation with the internally stored 6–311 + G(d,p) basis set, was employed [72,73]. Hydrogen bonding and dispersive interactions typifying non-covalent host-guest binding known to simulate well using this level of theory [74–77]. All the frequencies of normal vibrations in the stationary point structures of the SCX4, ASA and its complex turned out to be real which ascertained the local minima on the multivariate potential energy surfaces.

4. Results and discussion

Theoretical investigations shed light on binding patterns of ASA with the water soluble SCX4 macrocyclic host. The lowest energy truncated cone shaped SCX4 molecular scaffold was considered. Optimized structures of individual SCX4 macrocycle and ASA within the ωB97x-D/6-311+G(d,p) density functional framework.

In an effort to understand the binding modes of SCX4 macrocycle the MESP topography was used. It has earlier been shown that the three dimensional (3D) MESP maps give a direct perspective of the segments in the molecular system along with its reactivity and affinity toward different guests [78–82]. The electrostatic potential map overlaid on 0.001 au iso-density surface of an individual SCX4 host and the ASA guest has thus been displayed in Fig. 2. A difference MESP profile is depicted using a colour coding scheme: red indicating the most negative potential regions appropriate for the electrophilic attack while blue refers to most positive (large electron deficient) electrostatic potential regions. An emergence of green surface designates the potential halfway between the two extremes red and blue. The electrostatic potential intensifications follow the order: red < orange < yellow < green < blue. Here the hetero atoms (O and S) are rendered with relatively large negative electrostatic potential (dark red) and accordingly the lone pairs on oxygen and sulphur facilitate supramolecular interactions with the ASA. The sulfonato group at para position of the SCX4 macrocycle pulls π-electron density from aryl rings subsequently weakens the negative π potential inside the cavity. This is evidenced from the emergence of greenish yellow surfaces. The most acidic protons from the –OH and –SO_3H functionalities show a large brunt of positive charge (dark blue). MESP plot of ASA indicate the negative valued potential isosurfaces around oxygen atoms and appear as blue regions near the protons. A close contact of the complementary sites (red and blue) in the MESP topography would be required to allow allosteric binding of ASA with the SCX4 macrocycle. Taking a cue from these considerations different conformers of the host-guest complex that include (i) ester functional group of ASA inside the cavity, (ii) acid functional group of ASA within the cavity and (iii) benzene ring within the cavity the electrostatic docking of the electron deficient sites around the MESP critical points in the macrocycle were carried out which on subsequently optimizations yield different conformers those are depicted in Fig. 3. The relative stabilization energies (kJ mol^{-1}) of these relative to the lowest energy structure are given in parentheses. Among these conformers, the complex in which the guest penetrates via the ester functionality (C1 conformer) side within the SCX4 cavity turned out to be of the lowest energy which was subsequently characterized through an array of experiments outlined here.

Observed ^{1}H NMR spectra of the isolated ASA, SCX4 and their inclusion complex in D_2O are depicted in Fig. 4. Different types of protons in

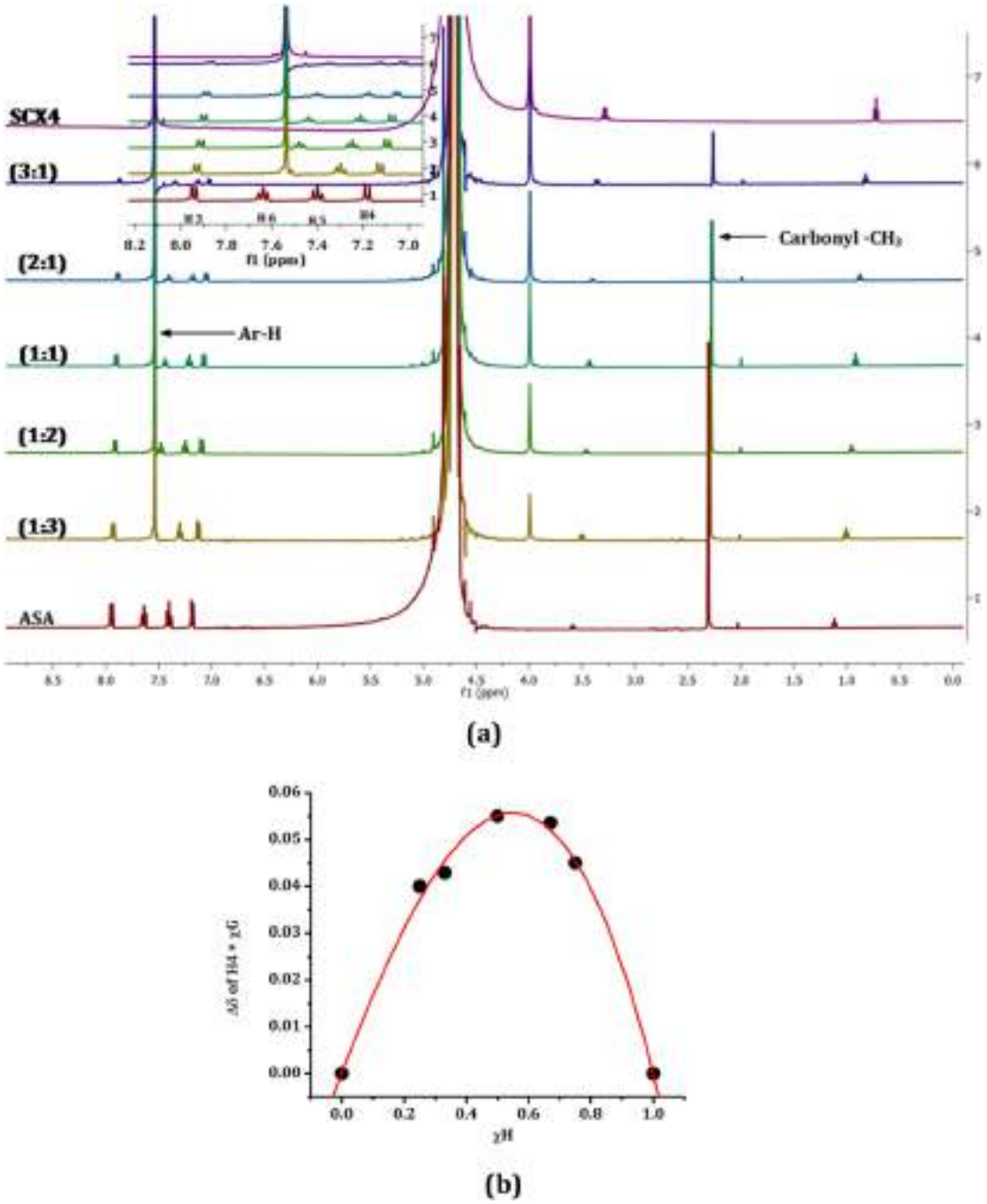

Fig. 5. (a) Partial ^{1}H NMR titration spectra (400 MHz, D_2O, 298 K) of aspirin at the concentration of (0.01 M) upon addition of SCX4 (0.01 M) (1) 3:1 equi., (2) 2:1 equi., (3) 1:1 equi., (4) 1:2 equi., (5) 1:3 equi. (b) Job's plot for the (ASA ⊂ SCX4) complex of 0.01 M where Δδ = change in chemical shifts in ppm, χ = mole ratio of host and guest.

ASA can broadly be classified as hydroxyl (H1), methyl (H2) and aromatic protons (H3-H6). The aromatic H3-H6 protons appear in 7–8 ppm region. The signals of methyl protons (H2) were observed as the further large upfield value at $\delta_H = 2.28$ ppm. An encapsulation of ASA within the bucket shaped cavity of SCX4 renders shielding of H2 to H6 protons that show up near ~0.3 ppm. The guest thus penetrates within the host cavity via the ester functionality; the inference which is consistent with the inference drawn earlier from the density functional theory. As far as the isolated SCX4 is concerned, the protons are of types: aromatic protons (Ha), methylene bridge protons denoted as Hb. The δ_H values in SCX4 host follows the order Ha (7.50 ppm) > Hb (3.97 ppm). Chemical shift values of host protons are insensitive to complexation. To determine stoichiometry in the complex ^{1}H NMR titration were carried out; the Job's plot (a continuous variation method) is displayed in Fig. 5. The 1:1 stoichiometry of the host and guest in the ASA ⊂ SCX4 complex was observed.

It has been realized that the host-guest binding leading to formation of the inclusion complex emerges with its signature in the 'frequency shifts' of characteristic vibrations in the infrared spectra those typify as the "fingerprint" of the noncovalent interactions underlying the supramolecular complexation. Encapsulation of the guest within a host cavity therefore, reflects in the 'frequency shift' of the characteristic stretching vibrations. The experimental infrared spectra of SCX4 macrocycle, ASA and the ASA ⊂ SCX4 complex are shown in Fig. 6. As

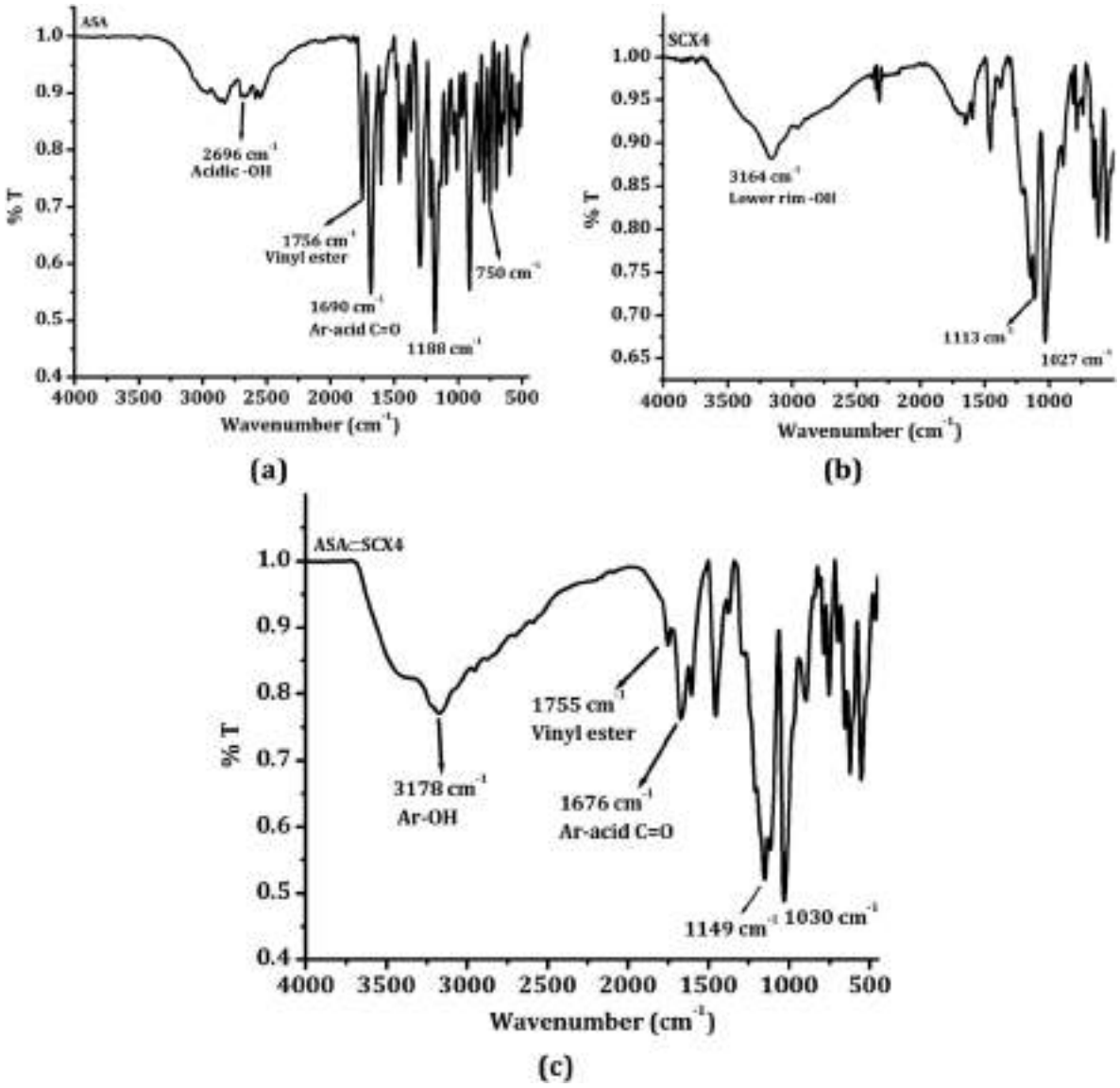

Fig. 6. Infrared spectra of a) ASA, b) SCX4 and c) ASA ⊂ SCX4 complex.

may readily be noticed, the isolated peak at 3164 cm^{-1} was assigned to O–H stretching of the free SCX4 host. Encapsulation of ASA in the SCX4 complexation shifts this vibration to higher wavenumber ~3178 cm^{-1}. The sulfonato vibrations in the SCX4 appear as two sharp peaks one near 1113 cm^{-1} and other at 1027 cm^{-1}; the former shows an up (blue) shift of ~36 cm^{-1} while only a marginal shift was noticed for the latter. As far as the ASA is concerned, the IR spectra reveal the characteristic broad band at 2969 cm^{-1} which was assigned to –OH stretching. Furthermore, two characteristic carbonyl stretching bands, corresponding to 1756 cm^{-1} and 1690 cm^{-1} respectively, were observed which arise from the acetoxy and acid vibrations. Of these the former peak shifts to the lower wavenumber 1746 cm^{-1} upon complexation with SCX4, which can be attributed to hydrogen bonding arising from the acetoxy group. The effective host-guest binding thus is ascertained. The inferences on the frequency up-shift of the OH vibrations (from 3137 cm^{-1} to 3157 cm^{-1}) is consistent with the experiment. A shift in the opposite direction that is, red shift (58 cm^{-1}) for the carbonyl stretching as noticed from the experiment also borne out from the present theoretical calculations.

The analytical characterization of host-guest complexes including their composition, stoichiometry and structural aspects was investigated through the electrospray ionization mass spectrometry (ESI–MS) in positive mode. The ESI-MS spectrum of ASA, SCX4 and relevant portions of ASA ⊂ SCX4 complex are shown in Fig. 7 and Figs. S1 through S3 of the ESI. As may readily be noticed the characteristic *m/z* peaks at 766.9839 and 383.0734 corresponds to isolated [SCX4 + Na^+] and [2ASA + Na^+], respectively. The peak at 943.9626 was assigned to [Na^+ ASA ⊂ SCX4] complex. The loss of methyl functionality from ASA of [Na^+ ASA ⊂ SCX4] upon fragmentation can be evidenced from the m/z 928.9744 peak. Further, the peak at 910.9101 results from the loss –CH_3 and –OH groups of ASA in [Na^+ ASA ⊂ SCX4] complex. The absence of peak corresponding to m/z value [SCX4 + 2ASA + Na^+] suggests the 1:1 stoichiometry is favored. These inferences are in consonance with the ^{1}H NMR experiments discussed earlier.

UV–Visible spectra of the ASA ⊂ SCX4 complex in Fig. 8 shows a band of ASA near 275 nm that exhibits a bathochromic shift, concomitant enhanced absorption intensity (nearly twice as large) was observed with addition of the SCX4. This signifies the effective improvement of water solubility of ASA as a result of the noncovalent host-guest binding. The calibration curve was obtained for a series of solutions by varying ASA concentrations and that of complex as 10, 20, 30, 40, 50, 60, 70

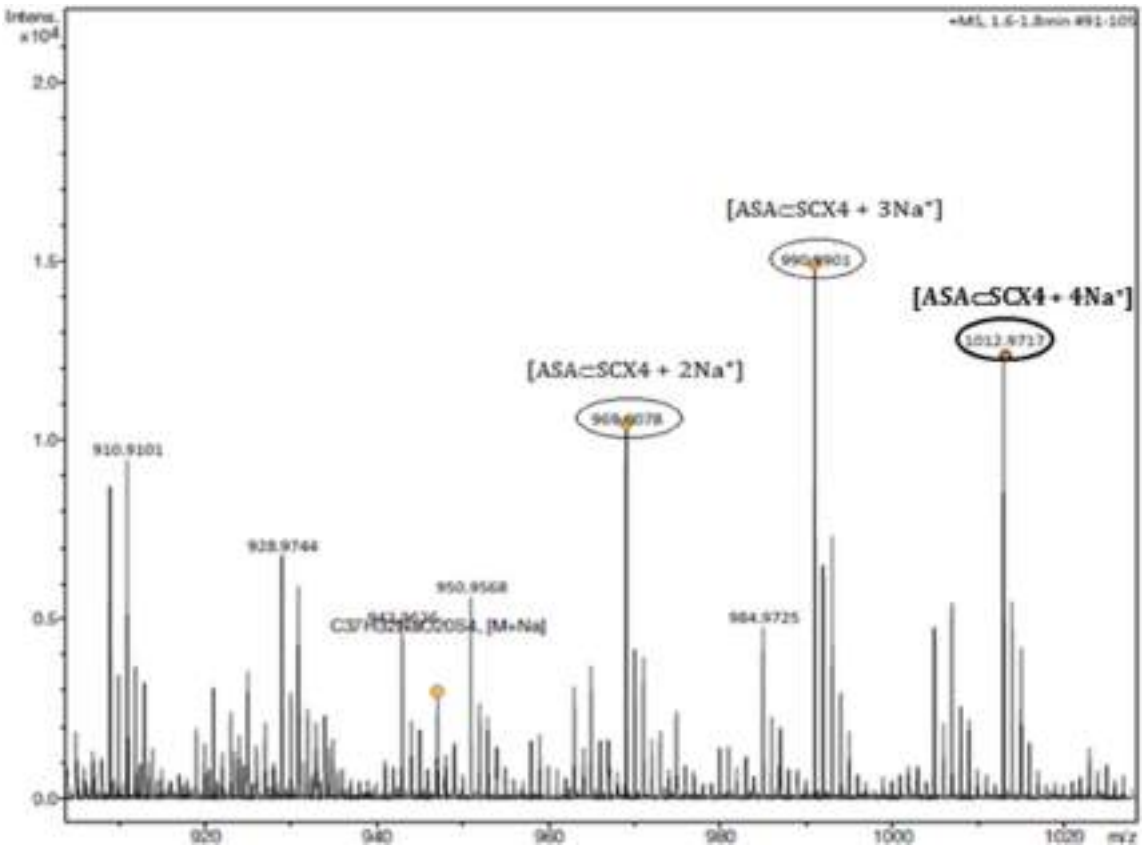

Fig. 7. Enlarged portion of HR-MS spectra of SCX4 complex with ASA (ASA ⊂ SCX4).

μg/mL. The absorbances were measured at the 275 nm; the corresponding graphs are displayed in Fig. 9a (aspirin in 95% water: 5% methanol) and Fig. 9b (ASA ⊂ SCX4 in water).

The chromatographic parameters were initially evaluated with Agilent Eclipse plus C18, 250 × 4.6 mm × (5 μm) column using Acetonitrile: milliQ: methanol as a mobile phase. The conditions for method development with the above column, with different proportions of mobile phase were subsequently optimized.

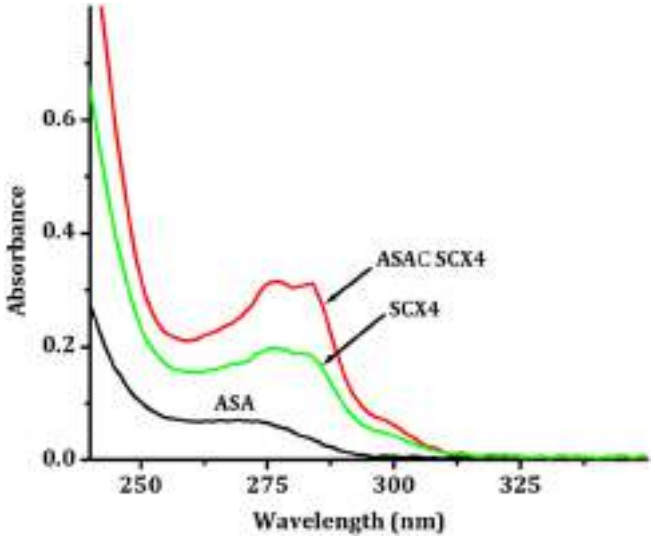

Fig. 8. Absorption spectrum of Aspirin and ASA ⊂ SCX4 complex at same conc. (10^{-5} M) in milli-Q.

The above method was applied to standard solutions of aspirin in the range of 10–50 μg/ml concentrations and chromatograms obtained are depicted in Fig. 10. An excellent correlation between the peak areas and concentrations of the ASA in mobile phase (R^2 = 0.9996) is further evident from Fig. 11. A reverse phase HPLC conditions were employed to determine the retention time of ASA and the ASA ⊂ SCX4 complex which were 2.48 min and 1.92 min; (cf. Fig. 12a and b). An early elution (low retention time) upon complexation further indicated increased polarity and in turn, the enhanced solubility of ASA.

Forced degradation studies were carried out to determine the stability indicating properties and specificity of the proposed method. Stress studies of ASA and the complex were performed by exposing analyte to acid, base and hydrogen peroxide mediated hydrolysis using reverse phase (RP) HPLC. The data on retention time, peak area, % height has been reported in Table 2. Chromatograms of the oxidative degradation at 275 nm of degraded sample appear in Fig. 12c and d. Moreover, the acidic and basic degradation are also reported in Figs. S4 and S5 of electronic supplementary information respectively. Furthermore, the percentage degradation of the isolated ASA was observed to be large in hydrogen peroxide mediated oxidative condition while the SCX4 host relatively stable in basic conditions. A comparison of ASA and its complex suggests that the inclusion complex is more stable than ASA under oxidative conditions. The method thus furnishes conditions for pre-formulation, stability and development of proper storage requirements for the ASA.

5. Conclusions

Molecular insights on host-guest binding of the SCX4 with aspirin were derived through various experiments in conjunction with the

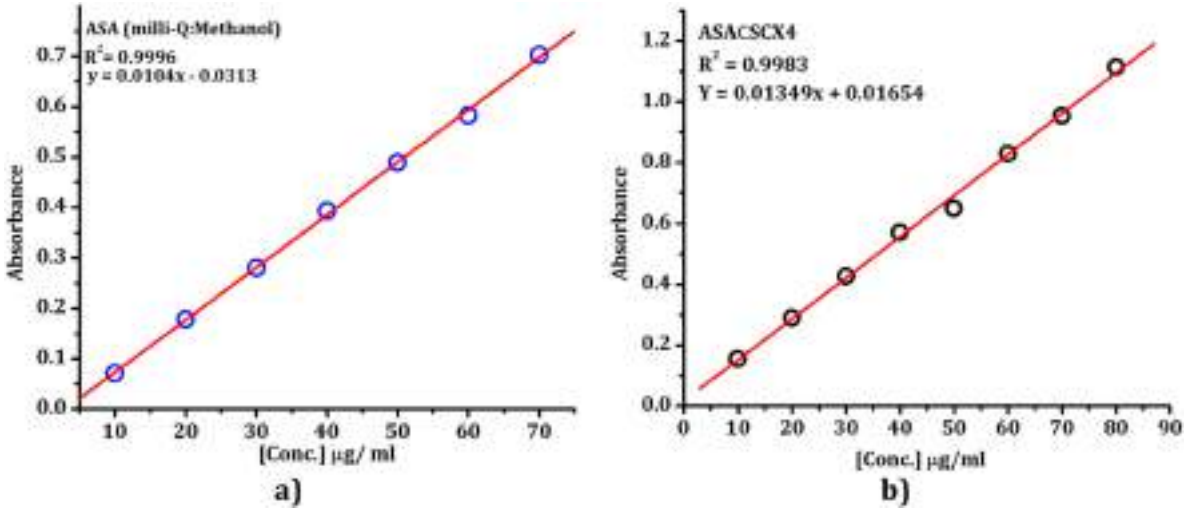

Fig. 9. Calibration graph for a) Aspirin in water: methanol (95:5) and b) ASA ⊂ SCX4 in water.

density functional theory. The characteristic bathochromic (red) shifts accompanied with the enhanced absorption intensity in the UV–visible spectra of the ASA ⊂ SCX4 complex. An encapsulation of ASA within the SCX4 engenders shielding of the methyl protons of the ester group in the measured ^{1}H NMR spectra. The ramifications of noncovalent binding accompanying the formation of the ASA ⊂ SCX4 complex to the 'frequency shifts' of the OH and C═O stretching in the infrared spectra have been discussed. The simple, precise HPLC based method to assess stability of the ASA ⊂ SCX4 complex has been developed. An early elution (low retention time) upon complexation indicated increased polarity and thus, enhanced solubility of the ASA.

The noncovalent interactions accompanying the complexation of the SCX4 host and ASA (guest) replicate in structural and spectral features that can be explored for a design and modelling of newer supramolecular assemblies with the increased bioavailability.

Linearity Assay of Aspirin:

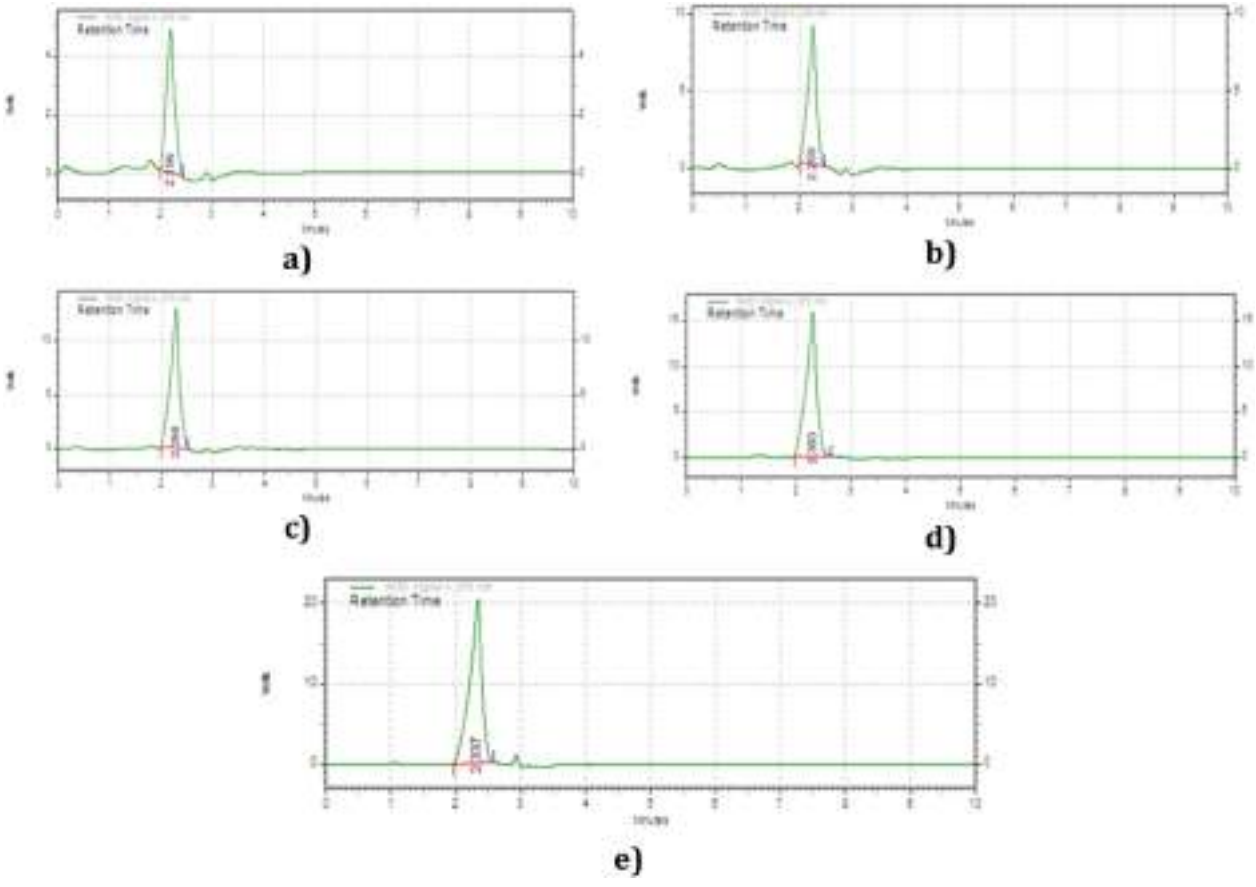

Fig. 10. Chromatographic plot of Aspirin at: a) 10 µg/mL, b) 20 µg/mL, c) 30 µg/mL, d) 40 µg/mL and e) 50 µg/mL.

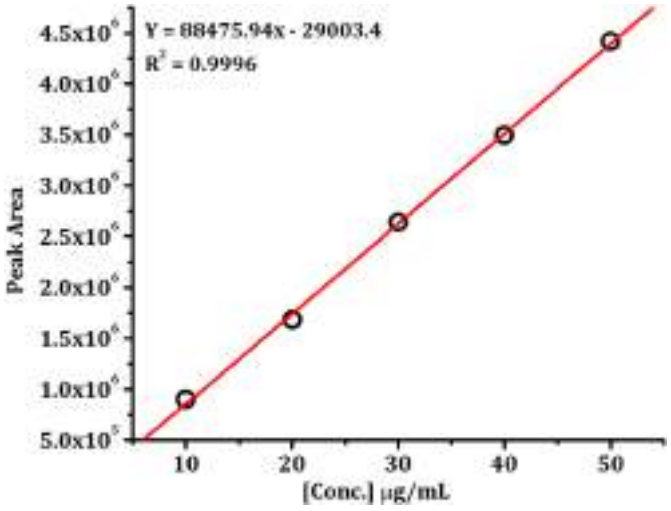

Fig. 11. Standard calibration curve of Aspirin ranging from 10 to 50 µg/mL in mobile phase.

Table 2
Forced degradation studies of ASA and their complex with SCX4.

Types of degradation	Retention time	Area	% Area	Height	% Height
ASA					
Acidic	2.48	2,755,185	100	403,751	100
Basic	2.21	2,709,479	89.41	315,822	83.69
Oxidative	2.24	2,000,046	48.01	227,740	47.22
ASA⊂SCX4					
Acidic	2.44	575,132	57.52	591,042	73.19
Basic	1.91	1,103,683	89.20	161,910	82.19
Oxidative	1.95	1,883,826	61.53	216,112	57.77

CRediT authorship contribution statement

Conception and design of study: Experimental data: Rupali G. Thorave, Uttam V. Shinde, Dipalee D. Malkhede. Computational and Theoretical data: Dipali N. Lande and Shridhar P. Gejji.

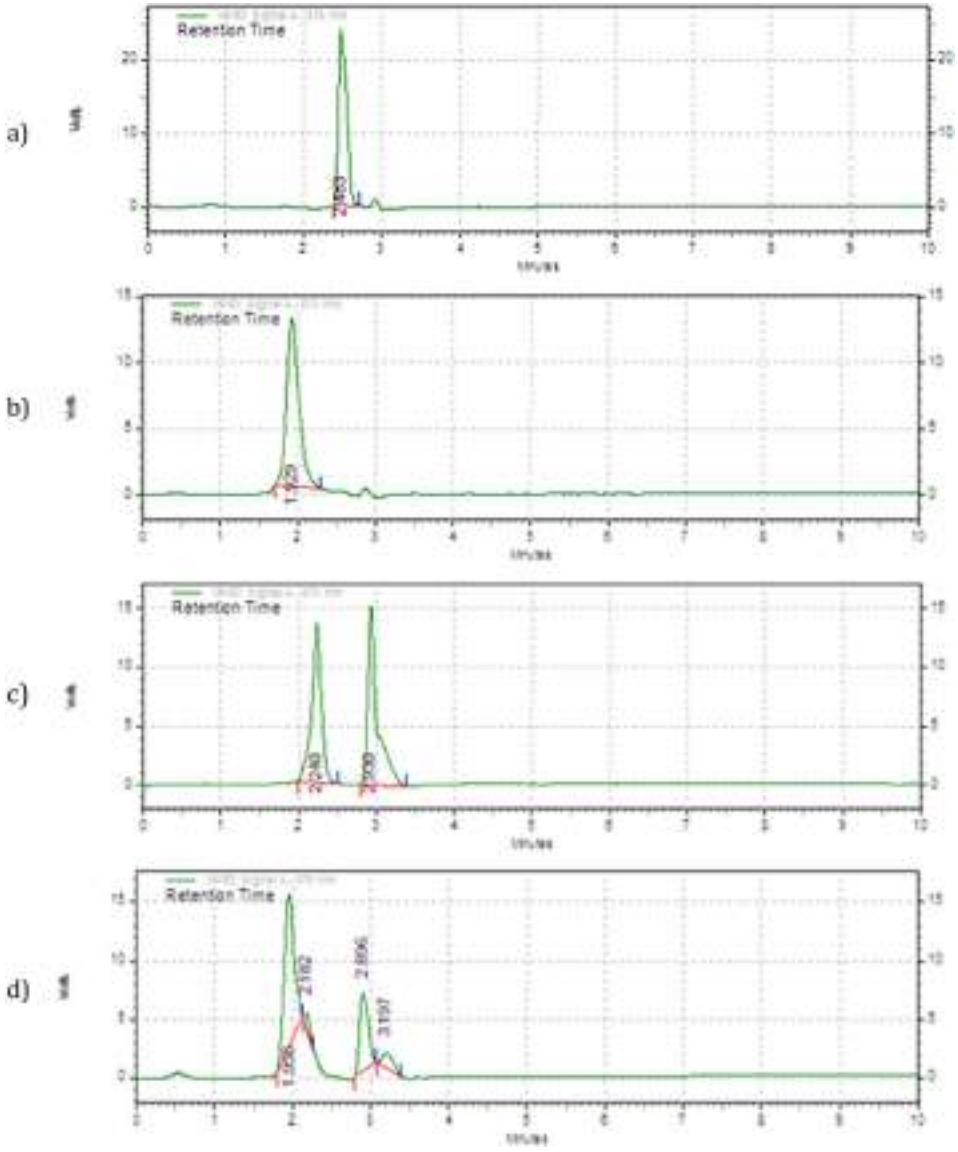

Fig. 12. a) Chromatographic analysis of ASA (100 µg/mL) at Retention time 2.48 min, b) Chromatographic analysis of ASA ⊂ SCX4 (100 µg/mL) complex at Retention time 1.92 min (c) oxidative degradation of ASA drug molecule with 0.3% H_2O_2 at retention time 2.24 min. d) oxidative degradation of ASA ⊂ SCX4 complex with 0.3% H_2O_2 at retention time 1.95 min.

Analysis and/or interpretation of data: Experimental part: Rupali G. Thorave, Uttam V. Shinde, Dipalee D. Malkhede and Shridhar P. Gejji. Computational and Theoretical: Dipali N. Lande and Shridhar P. Gejji.

Drafting the manuscript: Rupali G. Thorave, Dipali N. Lande and Shridhar P. Gejji. Revising the manuscript critically for important intellectual content: Shridhar P. Gejji.

Approval of the version of the manuscript to be published: Rupali G. Thorave, Dipali N Lande, Uttam V. Shinde, Dipalee D. Malkhede and Shridhar P. Gejji.

Declaration of competing interest

No any conflict Interest.

Acknowledgements

RGT is grateful Savitribai Phule Pune University for research fellowships disbursed through to UPE Phase (II) (University Potential Excellence) scheme and Sarthi (CMSRF) for the research fellowship. DDM acknowledge support from the research project from the University Grants Commission, New Delhi (F. No.42-289/2013). SPG thanks National Param Supercomputing Facility at the Centre for Development of Advanced Computing (CDAC), Pune, India where the molecular modelling studies were carried out.

Appendix A. Supplementary data

Supplementary data to this article can be found online at https://doi.org/10.1016/j.molliq.2020.114417.

References

[1] Y. Zhou, D.M. Boudreau, A.N. Freedman, Trends in the use of aspirin and nonsteroidal anti-inflammatory drugs in the general US population, Pharmacoepidem. Dr. S. 23 (2014) 43–50.
[2] L. Duley, S. Meher, K.E. Hunter, A.L. Seidler, L.M. Askie, Antiplatelet agents for preventing pre-eclampsia and its complications, Cochrane Db. Syst. Rev. 10 (2019) 1–18.
[3] S.V. Ittaman, J.J. Van Wormer, S.H. Rezkalla, The role of aspirin in the prevention of cardiovascular disease, J. Clin. Med. Res. 12 (3–4) (2014) 147–154.
[4] M. Dovizio, S. Tacconelli, C. Sostres, E. Ricciotti, P. Patrignani, Mechanistic and pharmacological issues of aspirin as an anticancer agent, Pharmaceuticals 5 (12) (2012) 1346–1371.
[5] P. Patrignani, C. Patrono, Aspirin and cancer, J. Am. Coll. Cardiol. 68 (9) (2016) 967–976.
[6] E. Bartsch, A.L. Park, J.G. Ray, Risk threshold for starting low dose aspirin in pregnancy to prevent preeclampsia: an opportunity at a low cost, PLoS One 10 (3) (2015) 1–10.
[7] S. Roberge, K. Nicolaides, S. Demers, J. Hyett, N. Chaillet, E. Bujold, The role of aspirin dose on the prevention of preeclampsia and fetal growth restriction: systematic review and meta-analysis, Am. J. Obstet. Gynecol. 216 (2) (2017) 110–120.
[8] G. Mao, D. Chen, H. Handa, W. Dong, D.G. Kurth, H. Möhwald, Deposition and aggregation of aspirin molecules on a phospholipid bilayer pattern, Langmuir 21 (2) (2005) 578–585.
[9] M. Voelker, M. Hammer, Dissolution and pharmacokinetics of a novel micronized aspirin formulation, Inflammopharmacology 20 (4) (2012) 225–231.
[10] D. Nevozhay, U. Kańska, R. Budzyńska, J. Boratyński, Current status of research on conjugates and related drug delivery systems in the treatment of cancer and other diseases, Med. Dosw. 61 (2007) 350–360.
[11] K. Wang, D.S. Guo, Y. Liu, Highly effective binding of viologens by p-sulfonatocalixarenes for the treatment of viologen poisoning, J. Med. Chem. 52 (2009) 6402–6412.
[12] M. Megyesi, L. Biczo'k, Considerable change of fluorescence properties upon multiple binding of coralyne to 4-sulfonatocalixarenes, J. Phys. Chem. B 114 (2010) 2814–2819.
[13] X. Ma, Y. Zhao, Biomedical applications of supramolecular systems based on host–guest interactions, Chem. Rev. 115 (2015) 7794–7839.
[14] F. Perret, A.N. Lazar, A.W. Coleman, Biochemistry of the para-sulfonato-calix[n]arenes, Chem. Commun. (2006) 2425–2438.
[15] B. Mokhtari, K. Pourabdollah, Applications of calixarene nano-baskets in pharmacology, J. Incl. Phenom. Macrocycl. Chem. 73 (2012) 1–15.
[16] Y.W. Yang, Towards biocompatible nanovalves based on mesoporous silica nanoparticles, Med. Chem. Commun. 2 (2011) 1033–1049.
[17] L. Gallego-Yerga, M. Lomazzi, F. Sansone, C.O. Mellet, A. Casnati, J.M.G. Fernández, Glycoligand-targeted core–shell nanospheres with tunable drug release profiles from calixarene–cyclodextrin heterodimers, Chem. Commun. 50 (56) (2014) 7440–7443.
[18] C. Wang, Z. Li, D. Cao, Y.L. Zhao, J.W. Gaines, O.A. Bozdemir, M.W. Ambrogio, M. Frasconi, Y.Y. Botros, J.I. Zink, J.F. Stoddart, Stimulated release of size-selected cargos in succession from mesoporous silica nanoparticles, Angew. Chem. Int. Ed. 51 (22) (2012) 5460–5465.
[19] Y.L. Sun, B.J. Yang, S.X.A. Zhang, Y.W. Yang, Cucurbit[7]uril pseudorotaxane-based photoresponsive supramolecular nanovalve, Chem. Eur. J. 18 (30) (2012) 9212–9216.
[20] Q. Duan, Y. Cao, Y. Li, X. Hu, T. Xiao, C. Lin, Y. Pan, L. Wang, pH-responsive supramolecular vesicles based on water-soluble pillar[6]arene and ferrocene derivative for drug delivery, J. Am. Chem. Soc. 135 (28) (2013) 10542–10549.
[21] H. Bakirci, A.L. Koner, T. Schwarzlose, W.M. Nau, Analysis of host-assisted guest protonation exemplified for p-sulfonatocalix[4]arene-towards enzyme-mimetic pKa shifts, Chem. Eur. J. 12 (2006) 4799–4807.
[22] M.D. Pluth, R.G. Bergman, K.N. Raymond, Acid catalysis in basic solution: a supramolecular host promotes ortho formate hydrolysis, Science 316 (2007) 85–88.
[23] L.S. Berbeci, W. Wang, A.E. Kaifer, Drastically decreased reactivity of thiols and disulfides complexed by cucurbit[6]uril, Org. Lett. 10 (2008) 3721–3724.
[24] N. Basilio, L. García-Río, J.A. Moreira, M.J. Pessêgo, Supramolecular catalysis by cucurbit [7] uril and cyclodextrins: similarity and differences, Org. Chem. 75 (2010) 848–855.
[25] A. Harada, J. Li, M. Kamachi, Double-stranded inclusion complexes of cyclodextrin threaded on poly (ethylene glycol), Nature 370 (1994) 126–128.
[26] L. Trembleau, J. Jr, Rebek, helical conformation of alkanes in a hydrophobic cavitand, Science 301 (2003) 1219–1220.
[27] R.N. Dsouza, U. Pischel, W.M. Nau, Fluorescent dyes and their supramolecular host/guest complexes with macrocycles in aqueous solution, Chem. Rev. 111 (2011) 7941–7980.
[28] D. Kumar, Y. Krishnan, M. Paranjothy, S. Pal, Analysis of molecular interaction of drugs within β-cyclodextrin cavity by solution-state NMR relaxation, J. Phys. Chem. B 121 (13) (2017) 2864–2872.
[29] T. Loftson, Cyclodextrins and the biopharmaceutics classification system of drugs, J. Incl. Phenom. Macrocycl. Chem. 44 (1–4) (2002) 63–67.
[30] T. Fukahori, M. Kondo, S. Nishikawa, Dynamic study of interaction between β-cyclodextrin and aspirin by the ultrasonic relaxation method, J. Phys. Chem. B 110 (9) (2006) 4487–4491.
[31] S.B. Carneiro, C. Duarte, F. Ílary, L. Heimfarth, S. Quintans, J. de Souza, L.J. Quintans-Júnior, V.F.D. VeigaJúnior, Á.A. Neves de Lima, Cyclodextrin–drug inclusion complexes: in vivo and in vitro approaches, Int. J. Mol. Sci. 20 (3) (2019) 642–664.
[32] G. Castronuovo, M. Niccoli, Thermodynamics of inclusion complexes of natural and modified cyclodextrins with acetylsalicylic acid and ibuprofen in aqueous solution at 298 K, Thermochimcai. Acta 557 (2013) 44–49.
[33] A. Rasheed, C.K.A. Kumar, Sravanthi, Cyclodextrins as drug carrier molecule: a review, V. V. N. S. S. Sci. Pharm. 76 (2008) 567–598.
[34] B. Cheirsilp, J. Rakmai, Inclusion complex formation of cyclodextrin with its guest and their applications, Biol. Eng. Med. 2 (1) (2016) 1–6.
[35] M. Pintal, B. Kryczka, A. Marsura, S. Porwański, Synthesis of bis-cellobiose and bis-glucose derivatives of azacrownmacrocycles as hosts in complexes with acetylsalicylic acid and 4-acetamidophenol, Carbohydr. Res. 386 (2014) 18–22.
[36] M. Adamiak, A. Ignaczak, Quantum chemical study of the complexation process of bis-β-d-glucopyranosyldiazacrown derivative with aspirin and paracetamol molecules, Comput. Theor. Chem. 1167 (2019) 112591–112599.
[37] S. Shinkai, Calixarenes-the third generation of supramolecules, Tetrahedron 49 (40) (1993) 8933–8968.
[38] C.D. Gutsche, The Royal Society of Chemistry, Cambridge (1989).
[39] J.S. Kim, D.T. Quang, Calixarene-derived fluorescent probes, Chem. Rev. 107 (2007) 3780–3799.
[40] S.B. Nimse, T. Kim, Biological applications of functionalized calixarenes, Chem. Soc. Rev. 42 (1) (2013) 366–386.
[41] M.J. Mclldowie, M. Mocerino, M.I. Ogden, A brief review of Cn-symmetric calixarenes and resorcinarenes, Supramol. Chem. 22 (2010) 13–39.
[42] S. Shinkai, Calixarenes as new functionalized host molecules, Pure Appl. Chem. 58 (11) (1986) 1523–1528.
[43] D. Coquiere, A. de la Lande, S. Martì, O. Parisel, T. Prangè, O. Reinaud, Multipoint molecular recognition within a calix[6]arene funnel complex, Proc. Natl. Acad. Sci. U. S. A. 106 (2009) 10449–10454.
[44] M. Conner, V. Janout, S.L. Regen, Synthesis and alkali metal binding properties of upper rim functionalized calix[4]arenes, J. Org. Chem. 57 (1992) 3744–3746.
[45] W. Verboom, A. Durie, R.J. Egberink, Z. Asfari, D.N. Reinhoudt, Ipso nitration of p-tert-butylcalix[4]arenes, J. Org. Chem. 57 (4) (1992) 1313–1316.
[46] A. Casnati, Y. Ting, D. Berti, M. Fabbi, A. Pochini, R. Ungaro, G.G. Lombardo, Synthesis of water soluble molecular receptors from calix[4]arenes fixed in the cone conformation, Tetrahedron 49 (43) (1993) 9815–9822.
[47] V.I. Kal'chenko, L.I. Atamas, V.V. Pirozhenko, L.N. Markovskii, Phosphorylation of the tetramethyl ether of 5, 11, 17, 23-tetrabromocalyx[4]arene, J. Gen. Chem. USSR. 62 (11) (1992) 2161–2162.
[48] S. Shinkai, T. Nagasaki, K. Iwamoto, A. Ikeda, G.X. He, T. Matsuda, M. Iwamoto, New syntheses and physical properties of p-alkylcalix[n]arenes, B. Chem. Soc. JPN. 64 (2) (1991) 381–386.
[49] A. Arduini, S. Fanni, G. Manfredi, A. Pochini, R. Ungaro, A.R. Sicuri, F. Ugozzoli, Direct regioselective formylation of tetraalkoxycalix[4]arenes, fixed in the cone conformation and synthesis of new cavitands, J. Org. Chem. 60 (5) (1995) 1448–1453.

[50] E. BahojbNoruzi, M. Kheirkhahi, B. Shaabani, S. Geremia, N. Hickey, F. Asaro, H.S. Kafil, Design of a thiosemicarbazide functionalized calix [4] arene ligand and related transition metal complexes: synthesis, characterization and biological studies, Front. Chem. 7 (2019) 663–703.
[51] D.S. Guo, V.D. Uzunova, K.I. Assaf, A.I. Lazar, Y. Liu, W.M. Nau, Inclusion of neutral guests by water-soluble macrocyclic hosts–a comparative thermodynamic investigation with cyclodextrins, calixarenes and cucurbiturils, Supramol. Chem. 28 (5–6) (2016) 384–395.
[52] D.S. Guo, Y. Liu, Supramolecular chemistry of p-sulfonatocalix[n]arenes and its biological applications, Acc. Chem. Res. 47 (7) (2014) 1925–1934.
[53] F. Perret, A.N. Lazar, A.W. Coleman, Biochemistry of the para-sulfonato-calix[n] arenes, Chem. Commun. (2006) 2425–2438.
[54] F. Perret, A.W. Coleman, Biochemistry of anionic calix[n]arenes, Chem. Commun. 47 (2011) 7303–7319.
[55] S. Shinkai, K. Araki, T. Tsubaki, T. Arimura, O. Manabe, New syntheses of calixarene-p-sulphonates and p-nitrocalixarenes, J. Chem. Soc. Perkin Trans. 1 (1987) 2297–2299.
[56] G.-S. Wang, H.-Y. Zhang, F. Ding, Y.J. Liu, Preparation and characterization of inclusion complexes of topotecan with sulfonatocalixarene, J. Incl. Phenom. Macro. 69 (2011) 85–89.
[57] A.W. Coleman, A.N. Lazar, K. Suwinska, O. Danylyuk, World Pat. PCT/FR2007/051129, 2007.
[58] W. Yang, D.P. Daniel, W. Liebenberg, M.M. de Villiers, Effect of para-sulfonato-calix[n]arenes on the solubility, chemical stability, and bioavailability of a water insoluble drug nifedipine, Curr. Drug Discov. Technol. 5 (2008) 129–139.
[59] E.S. Español, M.M. Villamil, Pharmacological properties of native plants from Argentina, Biomolecules 9 (2019) 90–104.
[60] K. Wang, D.S. Guo, X. Wang, Y. Liu, Multistimuli responsive supramolecular vesicles based on the recognition of p-sulfonatocalixarene and its controllable release of doxorubicin, ACS Nano 5 (4) (2011) 2880–2894.
[61] J.G. Panchal, R.V. Patel, S.K. Menon, Preparation and physicochemical characterization of carbamazepine (CBMZ): para-sulfonated calix[n]arene inclusion complexes, J. Incl. Phenom. Macrocycl. Chem. 67 (2010) 201–208.
[62] D. Hulmes, A. Coleman, E. Aubert-Foucher, Use of Calix(n)arenes for Treating Fibrotic Diseases. US Patent WO2000007585, 2000.
[63] A. Yousaf, S.A. Hamid, N.M. Bunnori, A.A. Ishola, Applications of calixarenes in cancer chemotherapy: facts and perspectives, Drug Des. Dev. Ther. 9 (2015) 2831–2849.
[64] R. Lamartine, M. Tsukada, D. Wilson, A. Shirata, Antimicrobial activity of calixarenes, Comptes. Rendus. Chimie. 5 (2002) 163–169.
[65] B. Mokhtari, K. Pourabdollah, Applications of calixarene nano-baskets in pharmacology, J. Incl. Phenom. Macrocycl. Chem. 73 (2012) 1–15.
[66] L. Mutihac, J.H. Lee, J.S. Kim, J. Vicens, Recognition of amino acids by functionalized calixarenes, Chem. Soc. Rev. 40 (2011) 2777–2796.
[67] Y. Zhou, H. Li, Y.-W. Yang, Controlled drug delivery systems based on calixarenes, Chin. Chem. Lett. 26 (2015) 825–828.
[68] E.B. Noruzi, M. Molaparast, M. Zarei, B. Shaabani, Z. Kariminezhad, B. Ebadi, V. Shafiei-Irannejad, M. Rahimi, J. Pietrasik, Para-sulfonatocalix[n]arene-based biomaterials: recent progress in pharmaceutical and biological applications, Eur. J. Med. Chem. (2020) 112121–112132.
[69] R.G. Thorave, D.N. Lande, S.V. Athare, S.P. Gejji, R.G. Gonnade, D.D. Malkhede, X-ray structure, spectral characteristics, thermal and redox behavior of quinoline encapsulated in sulfonatocalix [4] arene, J. Mol. Liq. 246 (2017) 187–196.
[70] V.S. Kalyani, D.D. Malkhede, *p*-Sulfonatocalix[8]arene and vitamin C complexation: assessment of photophysical, pKa and antioxidant property, J. Incl. Phenom. Macro. 87 (2017) 179–189.
[71] M. Blessy, R.D. Patel, P.N. Prajapati, Y.K. Agrawal, Development of forced degradation and stability indicating studies of drugs-a review, J. Pharm. Anal. 4 (3) (2014) 159–165.
[72] M. J. Frisch, G. W. Trucks, H. B. Schlegel, G. E. Scuseria, M. A. Robb, J. R. Cheeseman, G. Scalmani, V. Barone, B. Mennucci, G. A. Petersson, Gaussian 09 software, Inc., Wallingford, CT, (2009).
[73] A.D. McLean, G.S. Chandler, Contracted Gaussian basis sets for molecular calculations. I. Second row atoms, Z=11–18, J. Chem. Phys. 72 (1980) 5639–5648.
[74] K. Remya, C.H. Suresh, Which density functional is close to CCSD accuracy to describe geometry and interaction energy of small noncovalent dimers? A benchmark study using Gaussian 09, J. Comput. Chem. 34 (2013) 1341–1353.
[75] S.S. Rao, D.N. Lande, S.P. Gejji, Density functional theory investigations on binding and spectral features of complexes of ferrocenyl derivatives with cucurbit[7]uril, J. Mol. Liq. 216 (2016) 298–308.
[76] R. Das, P.K. Chattaraj, Host–guest interactions in $ExBox^{4+}$, ChemPhysChem 15 (2014) 4108–4116.
[77] D.N. Lande, S.P. Gejji, Cooperative hydrogen bonding, molecular electrostatic potentials, and spectral characteristics of partial thia-substituted calix[4]arene macrocycles, J. Phys. Chem. A 120 (2016) 7385–7397.
[78] J.S. Murray, P. Politzer, Molecular electrostatic potentials and noncovalent interactions, Comput. Mol. Sci. 7 (2017) 1–10.
[79] J.S. Murray, Z.P. Shields, P.G. Seybold, P. Politzer, Intuitive and counterintuitive noncovalent interactions of aromatic π regions with the hydrogen and the nitrogen of HCN, J. Comp. Sci. 10 (2015) 209–216.
[80] P. Politzer, J.S. Murray, T. Clark, Mathematical modeling and physical reality in noncovalent interactions, J. Mol. Model. 21 (2015) 52.
[81] J.S. Murry, J.M. Seminario, P. Politzer, A computational study of the structures and electrostatic potentials of some azines and nitroazines, J. Mol. Struct. (THEOCHEM) 87 (1989) 95–108.
[82] S.P. Gejji, C.H. Suresh, L.J. Bartolotti, S.R. Gadre, Electrostatic potential as a harbinger of cation coordination: $CF_3SO_3^-$ ion as a model example, J. Phys. Chem. A 101 (1997) 5678–5686.

e-ISSN: 2319-8753 | p-ISSN: 2320-6710

IJIRSET

International Journal of Innovative Research in
SCIENCE | ENGINEERING | TECHNOLOGY

INTERNATIONAL JOURNAL OF INNOVATIVE RESEARCH

IN SCIENCE | ENGINEERING | TECHNOLOGY

Volume 10, Issue 5, May 2021

INTERNATIONAL STANDARD SERIAL NUMBER INDIA

Impact Factor: 7.512

9940 572 462 | 6381 907 438 | ijirset@gmail.com | www.ijirset.com

International Journal of Innovative Research in Science, Engineering and Technology (IJIRSET)

| e-ISSN: 2319-8753, p-ISSN: 2320-6710| www.ijirset.com | Impact Factor: 7.512|

|| Volume 10, Issue 5, May 2021 ||

DOI:10.15680/IJIRSET.2021.1005259

Network Encoding Protocol for Power Management Scheme in WSN

Prof. Nanda S. Kulkarni

Professor, Department of Electronics & Telecommunication, Siddhant College of Engineering, Pune, India

ABSTRACT: Wireless Sensor Network (WSN) is that the key in addition to of wisdom and is extensively utilized at interims the structures bolstered Internet of Things (IoT). The sharp indicator center points are utilized in applications like system perceptive, therapeutic thriving consideration structures, and so forth. Anyway these centers are essentialness constraint devices. Efficient bundle and adequate group head (CH) assurance plans are required, in choose to advance essentialness stinting of finder center points. Amid this paper, vivacious CH assurance procedure (DCHSM) is utilized wherever CHs are picked in 2 phases. This computation advances imperativeness stinting on far reaching scale thus are frequently utilized for IoT applications. At first, QB Cluster chart is utilized to segment the insightful point plane figure molded groups. CH assurance is performed in 2 phases. To begin with course of CH is picked bolstered seen shot and in this manner the minute course is picked on the reason of survival time estimation. Entertainment examination appears that DCHSM defeats the standard strategies regarding get ready life expectancy Index.

KEYWORDS: Wireless Sensor Networks (WSN), Cluster Head (CH), Internet of Things, Voronoi Diagram, Dynamic Cluster Head Selection Method.

I.BACKGROUND

For applications from individual contraptions to mechanical devices, IoT is the rapidly creating development, where sensors are related remotely to web. IoT interfaces the world with recognizing, initiation, arranging and distributed computing [1– 3]. The possibility of adroit world is the consequence of mix of the world with web. IoT finds application in astute household, insightful city, sharp vehicles, related prosperity, related vehicle, keen structures, mechanical web and so forth. The Cluster of IoT is WSN. WSN goes about as the staggering structure for recognizing, arranging and directing [4– 6].

Minimal effort sensor and low power hubs are to be made for applications in prosperity care watching, mechanical watching, splendidly structures, military organizations, normal life checking, wild fire checking, and wisely transportation systems etc. In inside the checking range the sizable sensor center points arranged subjectively are webbed together using WSNs. Free of the serious condition, the sensor center point is careful to detect the watching range. The sweeping scale information collected by sizable number of sensor centers are used and finds application inside the field of IoT.

The sensor centers self-sort out and tracks the checking zone watchfully. For exact estimations, the centers should work botch free all through. Batteries are the in a manner of speaking source to supply essentialness to sensor centers. Sensor center points experienced the greater part of the essentialness while transmitting and tolerating sizable information. Because of the thick state of condition in which the center points are sent, it is difficult to displace the batteries of sensor center points. In order to push ahead the lifetime of WSN, it is most basic to lessen essentialness usage of individual sensor center points in this manner keeping up a vital separation from quick battery exhaust.

Specific boards of trustees directed a couple asks about on bunching strategies for imperativeness saving in WSN [7]. Arrange transmission eats up more control contrasted with bunching strategies, since every sensor center point discuss direct with the BS. In bunching strategies, in a manner of speaking the pioneer picked as the CH of the individual group,

| e-ISSN: 2319-8753, p-ISSN: 2320-6710| www.ijirset.com | Impact Factor: 7.512|

|| Volume 10, Issue 5, May 2021 ||

DOI:10.15680/IJIRSET.2021.1005259

discuss its information with the BS because of which pointless wastage of essentialness is discarded to a far reaching grow. To detect nature of speaking the non CH people are careful in a manner and

speak with the individual CHs. CHs of the individual group alone are able to gather the information and send it to BS when non CH people are idle when individual center point imperativeness is saved at whatever point. CHs of the individual group alone are able to gather the information and send it to BS at data transmission expel of other non CH people are diminished. Along these lines bunching methodologies push ahead imperativeness saving in WSN extending the mastermind lifetime. In organize to push ahead essentialness saving of sensor center points, efficient grouping and real CH decision systems are required. The two information traffic among all CH centers as such pushes ahead the lifetime of WSNs.

The computation join two phases to be explicit, set up stage and unflinching state arrange. In the midst of set up stage, CH is picked and bunches are formed. Predictable state organizes joins transmission of information.

A number is picked in stretch out of and 1 heedlessly for every center. If the discretionary number gotten for every center is not as much as its breaking point regard by then it can hold the situation of CH. Authentic CH decision plans are required, in orchestrate to push ahead essentialness saving of sensor center points. A deterministic part is incorporated to Filter figuring, to make deterministic Filter count, which focus fundamentally on CH decision criteria [10].

The deterministic part included to the edge regard pushes ahead essentialness saving of sensor center points by mulling over the rest of the imperativeness of individual hubs.

In IoT applications, dynamic gathering is an appropriate response for tremendous scale data assembling. Dynamic gathering got criticalness to alter the traffic load among various CHs [12]. Here periodic improvement of groups pulls in particular systems in improving the flexibility and essentialness saving in WSNs.

DCHSM examining a two phase bunching computation. At first, polygonal framed groups are made using Voronoi diagram [11]. By then CH is picked in two phases. The first course of CH is picked subject to seen likelihood and the moment course of CH is picked reliant on survival time estimation computation.

The work is sorted out as: Framework show is elucidated in Area II. Amusement examination is given in Area III taking after the end in Area

IV. PROPOSED SYSTEM

The proposed framework is separated into three stages: level task component, 2 associated Cluster organizes arrangement and at last steering. In to begin with stage, the base station relegates level to each sensor hub within the organize. In following stage, a 2-connected Cluster arrange is shaped utilizing CHs. In third stage, hubs forward their Both dispersed and centralized clustering plans play significant part in vitality sparing in WSN. Base station holds the prime position within the centralized strategy. Base station at first collects the vitality and area subtle elements of each hub will utilize the data to make clusters, choose CH, and shape the organize. Despite the way that brought together bunching pushes ahead efficiency of mastermind regarding imperativeness saving, it crashes and burns to push ahead efficiency for gigantic scale organize. In appropriated bunching methodology, the sensor centers self-sort out and are themselves skilled to make groups, pick CH and casing the compose and thusly pushes ahead efficiency of orchestrate as far as adaptability [8].

Investigators are pointing towards pushed ahead essentialness saving in Wireless sensor systems. Passed on grouping strategy is used to realize Moo imperativeness flexible bunching pecking request (Filter) estimation. In Filter estimation, CH center points are picked dependent on fated probability [9]. Non CH individuals screen the earth and bestow the data it assembled with the CH.CH transfer the information and communicate with the BS. Too the figuring businesses the idea of CH upheaval to change the packs to the lower level center points dependent on the weight fill in as low down in this manner.

International Journal of Innovative Research in Science, Engineering and Technology (IJIRSET)

| e-ISSN: 2319-8753, p-ISSN: 2320-6710| www.ijirset.com | Impact Factor: 7.512|

|| Volume 10, Issue 5, May 2021 ||

DOI:10.15680/IJIRSET.2021.1005259

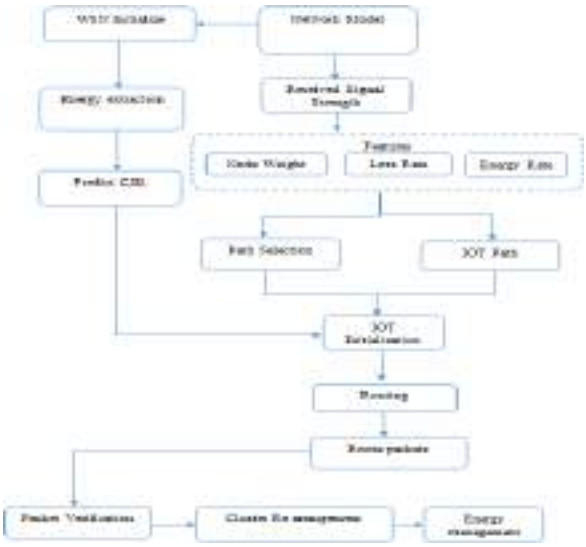

Fig 1. Proposed System Block Diagram

V.ASSIGNMENT LEVEL MECHANISM

In this stage, we dole out dimension (L) to each hub in the system relying upon its Distance from the base station. At first, dimension of the considerable number of hubs is zero including the base station. The total space between the last nodes from the base station called as the radius of the network. At that point we are applying the weight to the hubs by utilizing the separation from the base station. The nodes which are nearer to the base stations getting higher weight factor and nodes which are far from the base station getting lower weight factor. Then we are assigning the cluster head using the residual energy and based on the centroid approach, that is we are giving priority to the nodes which is nearer to the base station.

A. Connected Cluster Network Formation

In this stage, the Cluster organize is shaped with CHs in the system. Group run (BR) is utilized to give Cluster network. Group extend is the range between the associated CHs. Here, the group heads in level L1 are straightforwardly associated with the BS. Nonetheless, different CHs aside from hubs in L1 use their dimensions and BR for choosing next bounce CHs.

B. Routing in Weight Based

In this stage, directing is performed where group head in a dimension is just permitted to transmit the parcel to a next jump hub in next lower level dependent on a weight work. Here, the weight work considers lingering vitality level and connection separate.

C. Received Signal Strength Scheme

In the proposed methodology, there are three stages to accomplish the probabilistic forecast coefficient so as to gauge the connection security for solid information conveyance in the whole system.

The three steps incorporated in the distributed approach for determining the link stability are

a) Estimation of neighborhood solidness dependent on Energy

| e-ISSN: 2319-8753, p-ISSN: 2320-6710| www.ijirset.com | Impact Factor: 7.512|

|| Volume 10, Issue 5, May 2021 ||

DOI:10.15680/IJIRSET.2021.1005259

b) Estimation of neighbor steadiness dependent on connection misfortune
c) Manipulation of lifetime of mobile nodes

D. Cluster Reconfiguration Stage

System reconfiguration is vital to accomplish adjusted vitality utilization and furthermore to diminish the pointless systems administration overhead because of incessant re-bunching. N this system, the normal lingering vitality of CHs is contrasted and Maximum Threshold MAXTH just as Minimum Threshold MINTH esteem. It has three conceivable cases. These are:

1. On the off chance that the normal lingering vitality of CHs is higher than MAXTH, same forwarder set is utilized for information sending and Re grouping banner is set to 0.

2. In the event that the normal vitality of CHs is among MAXTH and MINTH, at that point another arrangement of forwarder hubs is browsed the current CHs and Clustering banner moves toward grouping.

3. In the event that the normal vitality is not exactly MINTH, re-grouping process is conjured so as to choose another arrangement of CHs and Re bunching banner is set to 1.

VI.NUMERICAL SIMULATIONS

In this segment, we present reenactment results on the system misfortune probabilities of our disseminated ideal development procedure under different setting of support sizes and the quantity of versatile operators just as various information entry examples to the system. Specifically, we here exhibit its impressive execution improvement over the standard arbitrary walk procedure in which an irregular stroll at the present hub moves to any of its goal hubs. In every one of these reproductions, we see that the system misfortune likelihood under our Network coding Algorithm is around multiple times littler than that of the Distributed ideal Movement Strategy. Note that the system misfortune probabilities for both the standard irregular walk methodology and system coding technique will in general increment with a bigger number of sensor hubs (n = 200), since the quantity of sensor hubs to be secured by a versatile authority itself increments. The measure of decrease in the system misfortune likelihood that we accomplish from Network coding procedure (in examination with the standard arbitrary walk strategy).is a lot more noteworthy than the current one. For every landing example (or every reproduction figure), the information focuses are gotten by taking the normal of the outcomes under 30 distinctive heterogeneous and spatially-connected information entry designs. We expect that our thinking behind the Network coding procedure can be pertinent for the plan of Markovian arbitrary walk- based applications test topologies of every sensor hubs. In every one of these reenactments, we see that the system misfortune likelihood under our Network coding Algorithm is around multiple times littler than that of the Distributed ideal Movement Strategy .display. In all cases, our coding procedure is reliably superior to the standard arbitrary walk system, and the proportion tends to decreased, inferring that our methodology is progressively more benifits as the cushion measure.

| e-ISSN: 2319-8753, p-ISSN: 2320-6710| www.ijirset.com | Impact Factor: 7.512|

|| Volume 10, Issue 5, May 2021 ||

DOI:10.15680/IJIRSET.2021.1005259

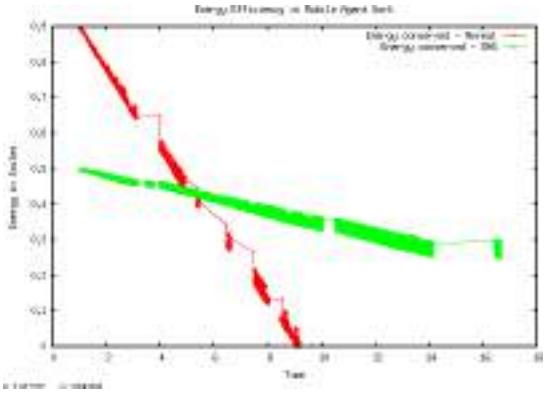

Fig 2. *Energy efficiency*

Represents to the vitality effectiveness concerning vitality and time. From this assessment the usage of vitality is diminished in system coding process as appeared in figure.

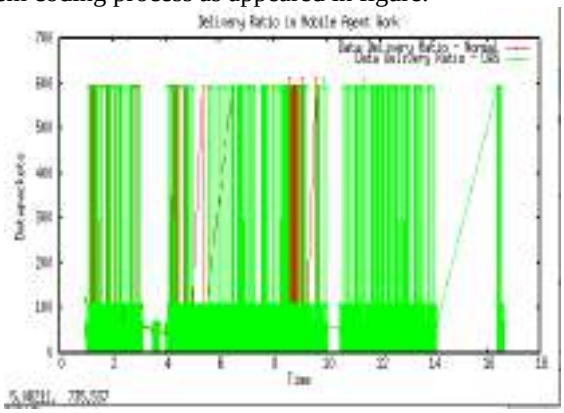

Fig 3. *Delivery ratio*

Represents to the conveyance proportion regarding time and number of information parcels. From this appraisal no of conveyance parcels is expanded contrasted with the appropriated ideal development methodology.

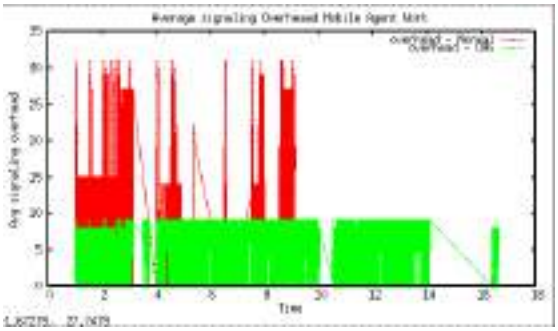

Fig 4. *Average signalling overhead*

Represents to the normal flagging overhead concerning time and number of sensor nodes. From this appraisal flagging secured over the whole system is similarly high than the current work.

| e-ISSN: 2319-8753, p-ISSN: 2320-6710| www.ijirset.com | Impact Factor: 7.512|

|| Volume 10, Issue 5, May 2021 ||

DOI:10.15680/IJIRSET.2021.1005259

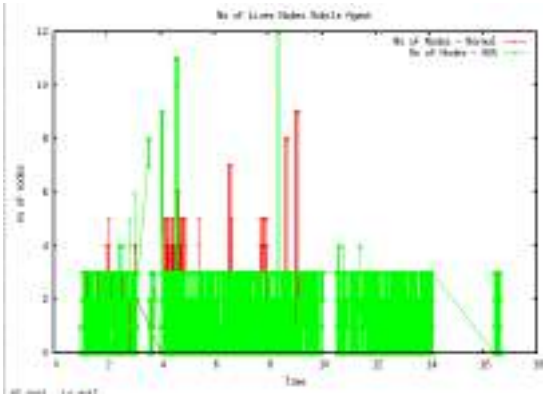

Fig 5. Number of live nodes

Speaks to the no of live hubs concerning time and no of nodes. From this recreation evaluation the general hub covers the system.

VII.CONCLUSION

In this exertion, we have tested the DCHSM execution in WSN. At first QB Cluster outline is utilized to acquire Rectangular molded groups. CHs are picked in two one of a kind stages. Results for 100 center points when striven for 2000 emphases shows that DCHSM improves the waiting imperativeness in WSN by 5.38% stood out from Deterministic LEACH and5.73% appeared differently in relation to LEACH. Thus DCHSM improves essentialness saving and constructs the framework lifetime. The test isn't striven for sizable centers. Thereafter, the comparable can be striven for sizable sensor centers. Also, clear imperativeness models are used in the computation, which identifies wrong for particular applications.

REFERENCES

1. Adrian Perrig, Robert Szewczyk, J. D. Tygar, Victor Wen, and David E. Culler. "SPINS: Security protocols for sensor networks." Wireless networks 8, no. 5 (2002): 521-534.
2. Ali Peiravi, and Maria Farahi. "Reliability of Wireless Body Area Networks used for Ambulatory Monitoring and Health Care." LifeScienceJoumal 7 (2005): 85.
3. Ameen, M. A., NiamatUUah, and KyungsupKwak. "Design and analysis of a MAC protocol for wireless body area network using wakeup radio." In Communications and Information Technologies (ISCIT), 2011 11th International Symposium on, pp. 148-153. IEEE, 2011.
4. AnirudhNatarajan, MehulMotani, Buddhika de Silva, Kok- Kiong Yap, and K. C. Chua. "Investigating network architectures for body sensor networks." In Proceedings of the 1st ACM SIGMOBILE international workshop on Systems and networking supportforhealthcare and assisted living environments, pp. 19-24. ACM, 2007.
5. Benoit Latre, Bart Braem, Ingrid Moerman, Chris Blondia, and Piet Demeester. "A survey on wireless body area networks." Wireless Networks 17, no. 1(2011): 1-18.
6. BoKeun Choi,, ByungSoo Kim, SangSeol Lee, KyuYeul Wang, YongJun
7. Kim, and DuckJin Chung. "Narrowband Physical Layer design for WBAN system."In Pervasive Computing Signal
8. Processing and Applications (PCSPA), 2010 First International Conference on, pp. 154-157.IEEE, 2010.
9. Changle Li, Huan-Bang Li, and Ryuji Kohno. "Performance evaluation of IEEE 802.15. 4 for wireless body area network (WBAN)." In Communications Workshops, 2009. ICC Workshops 2009. IEEE International Conference on, pp. 1-5. IEEE, 2009.
10. Charles E. Perskins, and Elizabeth M. Royer. "Ad-hoc on- demand distance vector routing." In Mobile Computing Systems and Applications, 1999. Proceedings. WMCSA'99. Second IEEE Workshop on, pp. 90-100. IEEE, 1999.
11. ChingYao Huang, MeiLing Liu, and ShihHeng Cheng. "WRAP: A weighted random value protocol for multiuser

| e-ISSN: 2319-8753, p-ISSN: 2320-6710| www.ijirset.com | Impact Factor: 7.512|

|| Volume 10, Issue 5, May 2021 ||

DOI:10.15680/IJIRSET.2021.1005259

wireless body area network." In Spread Spectrum Techniques and Applications (ISITA), 2010 IEEE 11th International Symposium on, pp. 116-119. IEEE, 2010.

12. Chris Karlof, and David Wagner. "Secure routing in wireless sensor networks:Attacks and countermeasures." Ad hoc networks 1, no. 2 (2003): 293-315.
13. [Dave Singelee, Benoit Latre, Bart Braem, Michael Peeters, Marijke De Soete, Peter De Cleyn, Bart Preneel, Ingrid Moerman, and Chris Blondia. "A secure cross-layer protocol for multi-hop wireless body area networks." Ad-hoc, Mobile and Wireless Networks (2008): 94-107.
14. C. Clavier, K. Gaj, C. De Canni'ere, O. Dunkehnan, and M. Knezevic, "KATAN and KTANTAN—a family of small and efficient hardware-oriented block ciphers," in Proceedings of the Cryptographic Hardware and Embedded Systems (CHES '09), pp. 272-288, Springer, Berhn, Germany, 2009.
15. Deva Seetharam and Sokwoo Rhee. "An efficient pseudo random number generator for low-power sensor networks [wireless networks]." In Local Computer Networks, 2004. 29th Annual IEEE International Conference on, pp. 560-562. IEEE, 2004.
16. Elaine Shi, and Adrian Perrig. "Designing secure sensor networks." Wireless Communications, IEEE 11, no. 6 (2004): 38-43.
17. Emil Jovanov, AleksandarMilenkovic, Chris Otto, and Piet
18. C. De Groen. "A wireless body area network of intelligent motion sensors for computer assisted physical rehabilitation." Journal of NeuroEngineering and rehabilitation 2, no. 1 (2005).
19. [10]Emil Jovanov, AleksandarMilenkovic, Chris Otto, Piet De Groen, Bruce Johnson, Steve Warren, and GueseppeTaibi. "A WBAN system for ambulatory monitoring of physical activity and health status: applications and challenges." In Engineering in Medicine and Biology Society, 2005. lEEE- EMBS 2005. 27th Annual International Conference of the, pp. 3810-3813. IEEE, 2006.

INNO SPACE
SJIF Scientific Journal Impact Factor

Impact Factor:
7.512

ISSN INTERNATIONAL STANDARD SERIAL NUMBER INDIA

निस्केयर
NISCAIR

INTERNATIONAL JOURNAL OF INNOVATIVE RESEARCH

IN SCIENCE | ENGINEERING | TECHNOLOGY

9940 572 462 6381 907 438 ijirset@gmail.com

www.ijirset.com

Scan to save the contact details

CERTIFICATION
OF PUBLICATION

IJIRSET

INTERNATIONAL JOURNAL OF INNOVATIVE RESEARCH IN SCIENCE, ENGINEERING AND TECHNOLOGY

Website: www.ijirset.com Email: ijirset@gmail.com

Impact Factor 7.512

This is hereby Awarding this Certificate to

PROF. NANDA S. KULKARNI

Professor, Department of Electronics & Telecommunication, Siddhant College of Engineering, Pune, India

Published a paper entitled

Network Encoding Protocol for Power Management Scheme in WSN

in IJIRSET, Volume 10, Issue 5, May 2021

e-ISSN: 2319-8753
p-ISSN: 2320-6710

ISSN INTERNATIONAL STANDARD SERIAL NUMBER

INNO SPACE SJIF Scientific Journal Impact Factor

P. Kumar
Editor-in-Chief

International Journal of Innovative Research in Science, Engineering and Technology (IJIRSET)

| e-ISSN: 2319-8753, p-ISSN: 2320-6710| www.ijirset.com | Impact Factor: 7.512|

||Volume 9, Issue 8, August 2020||

Internet of Things (IOT) Applications & Security: A Survey

Prof. Nanda Kulkarni

Assistant Professor, Department of Electronics & Telecommunication, Siddhant college of Engineering, Pune, India

ABSTRACT: Internet of things is going to lead the century with advent of 5G services.IoT system contain collection of sensors and devices. Because of an absence of security configuration just as the particular qualities of IoT gadgets, for example, the heterogeneity of processor engineering, IoT malware identification needs to manage exceptionally one of a kind difficulties, particularly on distinguishing cross-design IoT malware. In this manner, the IoT malware identification area is the focal point of exploration by the security network lately. There are numerous investigations exploiting notable dynamic or static examination for identifying IoT malware; be that as it may, static-based techniques are more compelling while tending to the multi-design issue. In this paper, we give an intensive study of static IoT malware location. We initially present the definition, advancement and security dangers of IoT malware. At that point, we sum up, look at and break down existing IoT malware discovery techniques proposed lately. At long last, we complete precisely the strategies for existing examinations dependent on the equivalent IoT malware dataset and a test design to assess impartially and expanding the unwavering quality of these investigations in recognizing IoT malware.

KEYWORDS*:* Internet of Things (IoT), Static-based, IoT botnet malware. Survey, IOT application

I. INTRODUCTION

Internet of Things (IoT) is the largest digital mega-trend that bridges physical and virtual worlds. The increment in the connectivity of people, objects, machines and the Internet is leading to the emergence of new business models as well as new interactions between mankind and the rest of the world. Due to the complexity of design and implementation in both hardware and software, as well as the lack of security functions and abilities, IoT devices are becoming an attractive target for cyber criminals who take advantage of weak authentication, outdated firmwares, and malwares to compromise IoT devices. By 2020, it is estimated that 25% of all cyber-attacks target IoT devices(https://www.gartner.com/). With the rapid adoption of IoT technologies in the industry, there will be an endless rise in these attacks. One of the most dangerous threats to IoT devices among them is malware. In Oct. 2016, Dyn (major US DNS service provider) was under one of the largest and most powerful DDoS attacks in recent history by Mirai malware family. The malware infected over 1.2 million IoT devices and targeted many popular online services such as Google, Amazon, etc.

Therefore, improving security aspects of IoT devices is becoming more and more urgent for researchers, especially when dealing with IoT malware. There are many research studies on security issues for IoT devices. Typical of such is Granjal et al. [1] who focused on analyzing extant protocols and mechanisms to secure communications for the IoT. Djamel Eddine Kouicem et al. [2] presented a comprehensive top down survey of the most existing proposed security and privacy solution in IoT. While, Djamel Eddine Kouicem et al. have categorized the various applications of IoT to identify security requirements and challenges for them, thereby analyzing traditional encryption solutions to deal with confidentiality, privacy, and availability. Besides, they also reviewed emerging technologies such as Blockchain and Software Defined Networking. In this perspective, a recent survey by Imran Makhdoom et al. [3] is quite comprehensive when presenting security issues and risks of threats to IoT devices. Besides, they emphasized that inherent safety provided by the communication protocols does not guard against harmful IoT malware and node compromise attacks. Hassan et al. [4] conducted a survey on security issues for IoT devices. However, the authors only focus on introducing solutions including lightweight authentication and encryption, not the IoT malware detection problem. Additionally, Felt et al. [5] reviewed the 46 pieces of mobile malware in the wild and collected dataset to evaluate the effectiveness of mobile malware identification and prevention methods. Costin et al. [6] only presented a comprehensive survey and analysis of all currently known IoT malware classes, without discussing IoT malware detection approaches.

IoT malware detection approaches could be classified into two main domains based on the type of strategy: dynamic and static analysis. Dynamic approach [7] consists of monitoring executables during run-time period and detecting abnormal behaviors. However, monitoring executing processes is resource-intensive, and in some cases,

malware could infect real environments. Besides, during execution time, it is not possible to fully monitor all their behaviors because many types of malware requiretrigger conditions to perform malicious behaviors. In addition to the common limitations of dynamic analysis, the execution of IoT executable files faces many issues such as diverse architectures (e.g., MISP. ARM, PowerPC, Sparc), and resource constraints of IoT devices. Therefore, it is difficult to configure an environment that meets the requirements for IoT executables to function correctly and fully. By contrast, static approach is performed by analyzing and detecting malicious files without executing them. One of the major advantages of static analysis is the ability to observe the structure of malware. In other words, we can explore all possible execution paths in malware sample without considering the diversity of processor architecture, thus making this approach effective to solve the heterogeneous issues of IoT devices. Thus, although there are many studies on security issues for IoT surveys, especially IoT malware detection, but no research has focused on methods of detecting IoT malware based on static analysis. Different from the existing survey studies when only evaluated based on the published results of the studies, this paper experimented exactly these methods with the same large dataset and the same system configuration.

In summary, the major contributions of this paper can be summarized as follows:

− First, we present a comprehensive overview of the interaction between the currently known IoT botnet families.

– Second, we provide a detailed taxonomy of static-features based IoT malware detection and discuss their shortcomings.

– Third, we accurately re-experimented the existing studies based on static analysis with the same large dataset and system configuration.

The rest of the paper is organized as follows: Section 2 provides an overview of IoT malware and its life-cycle, thereby better understanding the features that can be used by static analysis methods introduced in Section 3. Section 3 discusses the current IoT malware detection methods based on static features with their advantages and disadvantages. Section 4 presents and evaluates the methods by experiments. Furthermore, Section 5 shows the conclusion of this survey.

II. IOT MALWARE

In the past few decades, most malwares were designed to target personal computers running Microsoft Windows, the most popular operating system in the world with 83 percent of market share [8]. However, the diversity of computing devices has rapidly changed in recent years due to the Internet of Things technology. IoT devices are built upon a variety of CPU architectures, even on resource-constrained hardware such as Unix-based operating systems. Along with this change, IoT devices are becoming a favorite target by the attackers due to a lack of security design or implementation. In general, IoT malware has several characteristics such as IoT malware is used to perform DDoS attacks; IoT malware scans the open port of IoT services such as FTP, SSH or Telnet; IoT malware performs a brute-force attack to gain access to IoT devices.

Alex et al. [9] stated that most of the current malware generated by copying the source code according to online instructions or a variant of the same malicious code created by the malware writer. Through analysis, evaluation and synthesis of several studies such as [6], [10], [11] and manual analysis of some IoT malware samples this paper gives a brief chart of the recent development and evolution of IoT malware. Because IoT includes a vast and ever growing array of connected devices (e.g., smart meters, medical devices, public safety sensors, etc.), many IoT malware families such as Aidra, Bashlite and Mirai can utilize scanners that are designed to locate exposed ports and default credentials on these devices. In the last decade, IoT malware keeps developing and targeting new victims with various architecture. Mirai's evolution is gravitated toward changes in enterprise IT operations, extending its attack surface and bringing new zero-day exploits to consumer-level devices. In March 2019, IBM Xforce found a Mirai-like malware aimed at enterprises' IoT devices. These attacks drop crypto currency miners and backdoors onto affected devices.

There is a close correlation between IoT malware families reflected by the similarity of their functions as well as their source codes. Linux.Hydra as the first DdoS capable IoT malware that appeared since 2008. Since the release of Linux.Hydra's code, IoT malware developers have evolved into variants of Psybot, Chuck Norris and the last variation, Tsunami. However, part of the Tsunami's code was developed into the Remaiten and LightAidra, which are among the newest IoT malware. Also, the Tsunami is the ancestor of Bashlite and from Bashlite, the Mirai malware inherited and evolved more and more complex in 2016. From there, Mirai has continued to develop through variations that make it as a malware family rather than an individual stream of malware such as BrickerBot, VPNFilter. Accordingly, it cannot be denied that today's popularity of DDoS-capable IoT malware is steadily increasing because malware authors will continue to apply their creativity and programming skills to mutatetheir malwares for more critical infection on IoT devices. In summary, based on the analysis of the characteristics, evolution of IoT malware, we have found that there

are existing static characteristics of IoT malware that could be used as the features to detect malicious code, such as elf structure, strings, function call graph, grayscale image, etc. These features will be discussed in detail in Section 3

III. IOT MALWARE DETECTION BASED-ON STATIC FEATURE ANALYSIS

In this section, we discuss the static IoT malware detection methods that have been proposed since 2013. In static analysis, existing studies [7], [12], [13], [14], [15], [16], [17], [18], [19], [20], [21] commonly used the following static characteristics: control flow graph (CFG), operation codes (opcode), strings, file header, gray-scale image, etc. The way these features were extracted and processed greatly affects the accuracy and complexity of IoT malware detection methods. In the next subsection, we will demonstrate our method to divide these static-based features:

1) 3.1. Non graph-based IoT malware detection methods

Non graph-based detection methods aim at building a model that contains the properties of binary file structure to classify whether a binary file is malicious or benign. These methods rely on extracting the static features such as Operation Codes, Strings or File Structure to distinguish malicious samples. These characteristics can be divided into two groups: high-level features and low-level features. In particular, the low-level features can be obtained directly from binary file structure itself, while the high-level features must be extracted by disassembler (e.g., IDA Pro, radare2).

3.1.1. High-level features

Operation Code (Opcode) is one of the most popular features for malware detection. An Opcode is a single instruction that can be executed by the processor (CPU), which describes the behaviors of an executable file. In assembly language, an opcode is a command such as CALL, ADD or MOV. Based on this feature, Hamed HaddadPajouh et al. [12] proposed a method using Recurrent Neural Network (RNN) deep learning to detect IoT malware using the sequences of Opcodes. This method achieved the accuracy of 98.18 percent with the dataset of 281 ARM-based IoT malicious and 270 ARM-based IoT benign samples. Ensieh Modiri Dovom et al. [13] converted the executable files' Opcodes into a vector space and applied the fuzzy and fast fuzzy pattern tree methods to detect IoT malware. To prove this method in malware detection, they conducted an experiment on an ARM-based IoT dataset, comprising 1078 benign and 128 malware samples, and the experimental results achieved an accuracy of 99.83%. In similarity, Hamid Darabian et al. [14] presented a sequential opcode-based technique for IoT malware detection. By counting the number of opcode repetitions in executable files, the authors found that some opcodes in malware samples have higher frequency of repetition than benign files. Their experimental result achieved 99% accuracy and F-measure in the detection of IoT malware from benign samples. Nghi Phu et al. [22] proposed a feature selection method to detect cross-architecture malware, called CFDVex. The experiment achieved good results for cross-architecture malware detection. The experimental results show that the method is positive when it can detect the IoT malware for the MIPS architecture samples with a 95,72% accuracy rate by only train Intel 80386 architecture samples.

Strings — A string in an executable file is a sequence of characters such as "gayfgt" that is usually stored in ASCII (1 byte per character) or Unicode (2 bytes per character) format. Each printable string within an executable file could extract valuable information such as IP address, URL to connect, etc., to determine whether an executable is malicious or not [23]. Mohannad Alhanahnah et al. [15] generated good signatures for multi-architecture IoT malware classification based on printable strings. For evaluations, they used two IoTPOT malware datasets with 5150 malware samples, and with this signature-based detection mechanism, their experimental results achieved 95.5% IoT malware detection rate

3.1.2. Low-level features

ELF file header — An ELF (Executable and Linkable format) file format contains lots of interesting information that can be used in the malware detection. Based on this context, Farrukh Shahzad and Muddassar Farooq [16] presented a Linux malware detection tool, called ELF-Miner. To demonstrate their method, the dataset comprising 709 ELF samples was used and achieved more than 99.9% detection accuracy with less than 0.1% false alarm rate. In another work, Jinrong Bai et al. [17] introduced a method that extracts system call information from the symbol table of ELF files, they applied four machine learning algorithms for Linux malware detection. Using a dataset consisting of 756 benign and 763 malware samples, the experimental results achieved more than 98% accuracy on detecting an ELF file is malicious or benign.

Grayscale images — A grayscale image is type of image that each pixel has a value in the range from 0 to 255. In the malware detection problem, the executable files are analyzed and converted into binary strings 0 and 1, then combining those binary values into 8-bit vector segments that represent hex value from 00 to FF. These vectors are eventually converted into image data with a pixel value range between 0 and 255, where 0 as black and 255 as white. In this perspective, Su et al. [18] proposed a lightweight solution to distinguish between IoT malware and benign samples by feeding these gray-scale images to convolutional neural network model for detection. Besides, files of any size will

| e-ISSN: 2319-8753, p-ISSN: 2320-6710| www.ijirset.com | Impact Factor: 7.512|

||Volume 9, Issue 8, August 2020||

be normalized to fit with a 64 × 64 grayscale image and its remaining content will be deleted if redundant or covered with zero values if missing. The experiments achieved 93.33% accuracy for detecting IoT malware.

2) 3.2. Graph-based IoT malware detection methods

The most popular feature for malware detection is the Control Flow Graph. A control flow graph is a directed graph that represents all the possible execution paths that can be taken during the program, where each vertex (node) is represented by a basic block and each directed edge represents a possible control flow between the basic blocks. Control flow information in two key forms (1) inter-procedural control flow and (2) intra-procedural control flow. The interprocedural control flow graph demonstrates the association between functions and procedures in an executable file as a single CFG. Meanwhile, the intra-procedural control flow graph is demonstrated as a set of control flow graphs with one graph for a procedure or a function. Hisham Alasmary et al. [19] used the control flow graph (CFG) as an abstract structure to highlight the similarities and differences between IoT and Android malware binaries. Experimental results on the dataset consisting of 2.874 IoT malware samples and 201 android malware samples showed that IoT malware is more likely to contain a lesser amount of nodes and edges than Android malware, and graph-theoretic features between the IoT and android malware CFGs have a major variation. Therefore, they demonstrate the usefulness of CFGs in detecting IoT malware and android malware. Continuing to improve and expand this research direction in detecting IoT malware, Hisham Alasmary et al. [20] showed an IoT malware detection method that utilized Control Flow Graphs (CFGs) by using 23 static features to represent the characteristic of the CFG of IoT malware. By using this simple approach, this work achieved the accuracy of 99.66 percent with the dataset of 6000 malware and benign samples.

Follow the same approach, Azmoodeh et al. [21] proposed a deep learning-based method to detect Internet Of Battlefield Things (IoBT) malware that is based on the Opcodesequence graph. They evaluated the proposed method with a dataset including 128 malwares and 1078 benign files then achieved accuracy and precision rate of 98.37 percent and 98.59 percent respectively. HT Nguyen et al. [7] proposed an IoT botnet detection method based-on tracking footprints leaving at the steps of the botnet life cycle. These footprints were displayed as Printable String Information (PSI) which are used in the programming phase of any program such as IP address, username/ password patterns. In this work, they defined a graph-based data structure called PSI-Graph to represent the life cycle behavior of IoT botnet. On the dataset of more than 10000 samples, this study achieved the accuracy of more than 98 percent. In comparison with other methods, this work shows a better result in both detection rate and classifying time. Based on the above literature review, we compare the static IoT malware detection methods in Table 1 regarding their features used for detection, classification algorithms as well as the weaknesses that could affect the performance of these methods.

Method	Features	Mechanism	Passive technique	Weakness
[12]	Opcode	Identify malicious code through the sequences of Opcode	Neural networks	Only for ARM-based samples
[13]	Opcode	Apply fuzzy pattern tree to detect malicious sample	Fuzzing	Only for ARM-based samples. The dataset is not had enough samples.
[14]	Opcode	Detect malware by analyzing Opcode frequency	Machine learning	Only for ARM-based samples.
[22]	Opcode	Detect malware by using Vex intermediate representation	Machine learning	Only experiment with MIPS-based samples
[15]	Strings	Generate signature to classify IoT malware	Clustering	Time consuming Only for 4 malware families
[16]	ELF header	Extract features from sections of a binary file to detect malware	Machine learning	The structure of binary file is easy to modify.
[18]	Grayscale Image	Represent binary sample as grayscale image to detect malicious code	Neural network	Lose the accuracy when obfuscation or encrypt technique was applied

| e-ISSN: 2319-8753, p-ISSN: 2320-6710| www.ijirset.com | Impact Factor: 7.512|

||Volume 9, Issue 8, August 2020||

Method	Features	Mechanism	Passive technique	Weakness
[20]	CFG (Function Call Graph)	Calculate 23 properties of CFG to separate malicious and benign samples	Machine learning, Neural network	Time consuming The defined properties is not correct.
[21]	Opcode graph	Construct Opcode graph as a type of CFG to detect malware	Graph theory	Only for ARM-based samples
[7]	PSI graph	Use the PSI-Graph extracted from function call graph to detect malware	Neural network	Transforming graphs into vector data is time consuming

IV. CONCLUSION

IoT security is turning into an inexorably earnest issue in guaranteeing the wellbeing of the Internet framework and private information. This paper gave a deep reaching survey of developed IoT security and static-based recognition strategies. We talked about the principle methods just as qualities and shortcomings in existing static IoT malware discovery. In short, IoT malware location strategies can be separated into two gatherings: non diagram based and chart based techniques. The non diagram based strategies can accomplish a decent outcome when identifying "basic" and "direct" malware without customization or muddling, yet conceivably loses precision when distinguishing inconspicuous malware. In actuality, the chart based strategies show points of interest while dissecting the control stream of IoT malware, in this way can possibly precisely identify inconspicuous or muddled malignant code in spite of the unpredictability of these techniques. To think about the exhibition of these investigations. In light of the component, location examination and preparing time, we summed up the focal points and confinements of these investigations that can be utilized to improve the proficiency in future explores. As further augmentation of this work, we intend to structure and build up a chart based lightweight recognition technique that will assist with managing recognize malevolent executable record in IoT gadgets.

REFERENCES

[1] Granjal J., Monteiro E., Silva J.S. Security for the internet of things: a survey of existing protocols and open research issues
IEEE Commun. Surv. Tutor., 17 (3) (2015), pp. 1294-1312
[2] Kouicem Djamel Eddine, Bouabdallah Abdelmadjid, Lakhlef HichamInternet of things security: a top-down surveyComput. Netw., 141 (2018), pp. 199-221
[3] Makhdoom Imran, et al.Anatomy of threats to the internet of thingsIEEE Commun. Surv. Tutor., 21 (2) (2018), pp. 1636-1675
[4] Hassan W.H., et al.Current research on internet of things (IoT) security: A surveyComput. Netw., 148 (2019), pp. 283-294
[5] Felt A.P., Finifter M., Chin E., Hanna S., Wagner D.A survey of mobile malware in the wildPresented at the Security and Privacy in Smartphones and Mobile Devices (SPSM) (2011), pp. 3-14
[6] Costin Andrei, Zaddach JonasIot malware: Comprehensive survey, analysis framework and case studiesBlackHat USA (2018)
[7] Nguyen H.T., Ngo Q.D., Le V.H.A novel graph-based approach for IoT botnet detectionInt. J. Inf. Secur. (2019), pp. 1-11
[8] Cozzi Emanuele, et al.Understanding linux malwareIEEE Symposium on Security and Privacy (2018), pp. 161-175
[9] Allix K., Jerome Q., Bissyande T.F., Klein J., State R., Traon Y.L.A forensic analysis of android malware – How is malware written and how it could be detected?Presented at the IEEE 38th Annual Computer Software and Applications Conference (2014), pp. 384-393
[10] Angrishi KishoreTurning internet of things (IoT) into internet of vulnerabilities (IoV): IoT botnets(2017)arXiv preprint arXiv:1702.03681
[11] De Donno Michele, Dragon Nicola, Giaretta AlbertoDDoS-Capable IoT malwares: Comparative analysis and mirai investigationSecurity and Communication Networks, Wiley (2018)

[12] HaddadPajouh Hamed, Dehghantanha Ali, Khayami Raouf, Choo Kim-Kwang RaymondA deep recurrent neural network based approach for internet of things malware threat huntingFuture Gener. Comput. Syst., 85 (2018), pp. 88-96
[13] Dovom Ensieh Modiri, et al.Fuzzy pattern tree for edge malware detection and categorization in IoT J. Syst. Archit. (2019)
[14] Darabian Hamid, et al.An opcode-based technique for polymorphic Internet of Things malware detection Concurr. Comput.: Pract. Exper. (2019)
[15] Alhanahnah Mohannad, Lin Qicheng, Yan QibenEfficient signature generation for classifying crossarchitecture IoT malware Commun. Netw. Secur. (2018), pp. 1-9
[16] Shahzad F., Farooq M.Elf-miner: Using structural knowledge and data mining methods to detect new (linux malicious executablesKnowl. Inf. Syst., 30 (3) (2012), pp. 589-612
[17] Bai Jinrong, Yang Y., Mu S., Ma Y. Malware detection through mining symbol table of Linux executables Inf. Technol. J., 12 (2) (2013), pp. 380-383
[18] Su Jiawei, Vargas Danilo Vasconcellos, Prasad Sanjiva, Sgandurra Daniele, Feng Yaokai, Sakurai Kouichi Lightweight classification of IoT malware based on image recognition 2018 IEEE 42nd Annual Computer Software and Applications Conference (COMPSAC), Vol. 2 (2018), pp. 664-669
[19] Alashmary Hisham, et al. Graph-based comparison of IoT and android malware International Conference on Computational Social Networks (2018), pp. 259-272
[20] Alasmary Hisham, et al. Analyzing and detecting emerging internet of things malware: A graph-based approach IEEE Internet Things J., 6 (5) (2019), pp. 8977-8988
[21] Azmoodeh Amin, et al. Robust malware detection for internet of (battlefield) things devices using deep eigenspace learning IEEE Trans. Sustain. Comput. (2018), pp. 88-95
[22] T.N. Phu, L.H. Hoang, N.N. Toan, N.D. Tho, N.N. Binh, CFDVex: A novel feature extraction method for detecting cross-architecture IoT malware, in: Proceedings of the Tenth International Symposium on Information and Communication Technology, 2019, pp. 248–254.
[23] Islam Rafiqul, et al. Classification of malware based on integrated static and dynamic features J. Netw. Comput. Appl. (2013), pp. 646-656
[24] Pa Y.M.P., Suzuki S., Yoshioka K., Matsumoto T., Kasama T., Rossow C. CIoTPOT: A novel honenypot for revealing current IoT threatsJ. Inf. Process., 24 (2016), pp. 522-533

CERTIFICATION
OF PUBLICATION

IJIRSET

INTERNATIONAL JOURNAL OF INNOVATIVE RESEARCH IN SCIENCE, ENGINEERING AND TECHNOLOGY

Website: www.ijirset.com Email: ijirset@gmail.com

This is hereby Awarding this Certificate to

PROF. NANDA KULKARNI

Assistant Professor, Department of Electronics & Telecommunication, Siddhant College of Engineering, Pune, India

Published a paper entitled

Internet of Things (IOT) Applications & Security: A Survey

in IJIRSET, Volume 9, Issue 8, August 2020

Impact Factor 7.512

e-ISSN: 2319-8753
p-ISSN: 2320-6710

ISSN INTERNATIONAL STANDARD SERIAL NUMBER

INNO SPACE SJIF Scientific Journal Impact Factor

Editor-in-Chief

ISSN (Online) 2581-9429

IJARST

International Journal of Advanced Research in Science & Technology (IJARST)

Volume 8, Issue 3, August 2020

Optimization of Heat Treatment Process Parameter for High Speed Steel Taper Shank Drill

Mr. Rushikesh S. More[1] and Prof. Bhagwat B. Kedar[2]

PG Student, Mechanical Engineering, Siddhant College of Engineering, Pune, India[1]

Asst. Professor, Mechanical Engineering, Siddhant College of Engineering, Pune, India[2]

Abstract: *Drilling is a cutting process that uses a drill bit to make or widen a hole of circular cross section in solid material. The Bit is pressed against the work piece and rotates at high speed, Due to the increasing competitiveness in the market; the performance of drill bit must be increased. There are various methods to improve the performance of Tool Steel like Surface coating, cryogenic treatment, and optimization of heat treatment process parameter to obtain best possible metallurgical properties. By comparing with other competitor it is revealed that there is gap in performance of Taper Shank Drill. This project based on Optimization of Heat Treatment Process Parameter to improve performance with reduction in cost per component. High Speed Steel M2 material is used as drill material for experimentation. There are four parameter in heat treatment process i.e. soaking temperature, soaking time, tempering temperature and tempering time. Different experiments are performed, for that Taguchi orthogonal array (L9) is used with three levels of heat treatment process parameter. From the response of design of experiments the desired heat treatment cycle is selected. The performance of Taper shank drills in terms of number of holes drilled between two re-sharpening has to be measured. And it is expected from project that the performance of drill in terms of number of drill to be improved with a best possible temp-time relation.*

Keywords: HSS M2, drill bit, Taguchi Orthogonal Array, Hardness, Heat treatment, hardness.

I. INTRODUCTION

Metal cutting process forms the foundation of the engineering industry and is involved either directly or indirectly in the manufacture of nearly every manufactured goods of our modern civilization. The cutting tool is one of the important elements in realizing the full budding out of any metal cutting operation. Over the years the burdens of economic competition have motivated a lot of research in the arena of metal cutting leading to the development of new tool materials of remarkable performance and vast potential for a remarkable increase in productivity. Changes in work piece materials, manufacturing processes and even government guidelines catalyse parallel advances in metal cutting tooling technology.

As manufacturers continually seek and apply new engineering materials that are lighter and tougher and therefore more fuel efficient it follows that cutting tools must be so established that can machine new materials at the highest possible productivity. The most important basics in the design of cutting tools is the material construction and there judicious selection The properties that a tool material must possess are as follows:

1. Capacity to hold firm stability at elevated temperatures during high cutting speeds.
2. Cost and easiness of fabrication.
3. Resistance to thermal and mechanical shock.
4. Highly resistance to brittle fracture.

Developmental activities in the area of cutting tool materials are guided by the knowledge of the extreme circumstances of stress and temperature produced at the tool-work piece interface. Tool wear happens by one or more complex mechanisms which comprises abrasive wear, chipping at the cutting edge, thermal cracking etc. Since most of these processes are significantly accelerated by increased temperatures, the more obvious requirements for tool materials are enhancements in physical, mechanical and chemical properties at elevated temperature. Traditional tool materials such as HSS continue to experience considerable improvement in their properties through suitable alterations in their composition by optimizing the processing method as well as incorporating various surface treatments. As a result of these technological developments HSS are still in use having surviving rivalry from carbides and ceramics.

IJARST
ISSN (Online) 2581-9429
International Journal of Advanced Research in Science & Technology (IJARST)
Volume 8, Issue 3, August 2020

Carbide because of the ability to hold its strength and hardness at very high temperatures, to withstand cutting speeds 6 or more than 6 times advanced than tools of HSS and the cost-effective price has become a logical choice of many cutting industries. However with the combination of suitable surface treatments, its service life as well as its properties can be enhanced even more.

II. OBJECTIVE

1. To improve the Performance of drill in terms of number of holes to be drilled.
2. To obtain better hardness of the tool material.
3. To optimize heat treatment process parameter that will give desired temperature time relation.

III. LITERATURE REVIEW

V.K. Murugan, P. Koshy [1] Mathewshas discussed in his paper an optimal setting of carburizing process parameters (carburizing temperature, soaking time, gas diffusion effect ,furnace air circulation) causing in optimal values of the correct depth of the case in the surface of the components. Taguchi method is a influential design of the experiment (DOE) tool for engineering optimization of a process and they concluded that The Taguchi method efficiently, obtains optimal heat treatment parameters for the plain low carbon steel, reduces the number of experiments, and analyzers the effect of each heat treatment parameter on the experiment results and the contribution of individual parameters.

S.Z. Qamar [2] has analysed results of mechanical testing performed on variously heat treated H11 steel samples, to arrive at an optimum heat treatment strategy for hot work applications. The tensile and impact test specimens were fabricated using precision milling and EDM. These samples were exposed to various heat treatment arrangements, consisting of annealing, hardening, air and oil quenching, and tempering at different temperatures. Heat treated samples then mechanically tested for hardness (Rockwell), impact toughness (Charpy), and tensile properties (yield strength, ultimate strength, ductility). The paper concludes that mechanical testing of H11 samples revealed that with increasing temper temperatures hardness first increases to a maximum and then gradually decreases; impact toughness first decreases to a minimum and then increases.

Harvinder Singh, Aneesh Goyal [3] found out that the Cryogenic treatment process uses sub-zero temperatures down to -184°C to modify the micro-structure and properties of material. This process is an extension of heat treatment which further improves the properties of material. This paper focuses on the effect of cryogenic treatment on High Speed Steel (T-15) tool material. Cryogenic treatment at -184°C is conducted in this research and its properties compared with untreated material. It has been found that as the temperature is decreased, microstructure of material is refined and more number of carbide precipitates appeared on the surface after the treatment. Interestingly to note that the retained austenite is completely converted into marten site after subjecting the T42 HSS specimen to cryogenic treatment. The micro structural changes results in improvement of properties of HSS, (T-15) tool material.

O.O. Joseph, R.O. Leramo [4] has studied The effect of heat treatment at 850oCon the microstructure and mechanical properties of SAE 1025 carbon steel has been studied. Annealing, normalizing and age-hardening heat-treatments at 850oC were used for the experimental work. Hardness tests, tensile tests and metallography were done on the heat-treated and controlled samples. The results were additionally analysed using the one-way ANOVA test. Results obtained showed significant differences in the microstructure and mechanical properties of the different heat-treated samples. And observed that higher tensile strength was observed for the annealed samples than for the control, normalized and age-hardened samples. A microstructure of improved quality was obtained with normalizing heat treatment whereas a lesser quality was obtained by age-hardening.

Dennis W. Hetzner, William Van Geertruyden [5] studied crystallography and metallography of carbides in high alloy steels. The carbides in high carbon, high chromium bearing steels, high chromium carburizing steels, newly settled easily carburizable low carbon, low chromium high speed steels and M62 high speed steel fabricated by powder metal processing were studied. The particular steels assessed include 440C, BG42.M50-Nil, CHS1, M2, CHS50, and M62. The morphology and structure of the carbides were evaluated by means of metallography, X-ray diffraction and

IJARST
ISSN (Online) 2581-9429
International Journal of Advanced Research in Science & Technology (IJARST)
Volume 8, Issue 3, August 2020

electron beam backscattered diffraction. The combination of these three techniques has provided new insight into how different carbide morphologies form throughout processing and the carbide structures that can be expected to be present in components fabricated from these steels by various types of heat treating.

The literature survey concludes optimization of heat treatment plays a vital role in the consistent performance of cutting tools. Hardening and Tempering cycle need to be optimally managed for getting required toughness in order to absorb shocks during application. The present paper discusses the optimization of Hardening & Tempering process of Taper Shank Drills manufactured to improve the performance, hole quality thereby reducing CPC (cost per component)

IV. MATERIAL

HSS M2 Material- commonly used tool material. M recognizes molybdenum content. Its bending strength can reach 4700 MPa.

Table 1: Composition of alloying element

Alloying element	(By % wt.)
C	0.95
Cr	4
Mo	5
W	2

V. METHODOLOGY

The objective of this project is to improve quality & consistency in the performance of Taper Shank Drills. For this project, DMAIC methodology is followed:

A. Define Phase

Define phase is the first & most important activity in quality improvement activity. Define phase involves problem details, identifying of the process to be improved, objectives of the project etc.

Sr. No.	Parameter	Details
1	Problem Statement	Less Performance
2	Part number selected for study	14mm, 16mm, 26mm dia.
3	Suspected manufacturing process	Heat Treatment
4	Process stages where the problem is inspected	Endurance Testing
5	Objective of the project	To improve the performance of Taper Shank Drills

Table 2: Define Phase

B. Measure (Benchmarking)

Product Benchmarking was carried out with the leading competitors: Following are the performance test parameters:

1. Column Drilling M/C
2. Cutting Speed- 500 RPM
3. Cutting Feed- 100 mm/min
4. Depth of Hole- 48 mm
5. Test Specimen- EN9 (C: 0.45%-0.65%
6. Testing Block Hardness- 229 BHN
7. No. of Holes after Two Regrinding

Performance Test Results

Size (mm)	Performance (No. of Holes)		
	Existing Performance	Competitor I	Competitor II
14	37	59	63

ISSN (Online) 2581-9429

IJARST

International Journal of Advanced Research in Science & Technology (IJARST)

Volume 8, Issue 3, August 2020

16	35	50	53
26	19	30	32

Table 3: Performance Test Results

C. Analysis of Hardness

After Analysis of Hardness, it is observed that the hardness of Taper Shank Drills manufactured, is lesser than those which are manufactured by Competitor I and Competitor II. The performance of Taper Shanks Drills primarily depends on the hardness. Hardness is most important stipulated property that any cutting tool must have.

Size (mm)	Hardness (VHN)		
	Existing hardness	Competitor I	Competitor II
14 mm	798	849	856
16 mm	792	856	869
26 mm	804	856	869

Table 4

VI. IMPROVEMENT AREAS

When a system is subjected to free vibration and the system is considered as continuous system in which the beam mass is considered as distributed along with the stiffness of the shaft. In such case the equation of motion of a cantilever beam is given as (Meirovitch, 1967)

A. Problems Identified in Existing Heat Treatment Practice

1. Inconsistent soaking time
2. Variation in hardness
3. Poor control over grain sizes
4. Over heating: It results in excessive distortion, irregular grain growth, loss of ductility and low strength
5. under heating: It results in low hardness and low wear resistance

B. Improvement in Existing Heat Treatment Process

Hardening and tempering process is to be optimized for the different diameters of Taper Shank Drills: 14mm, 16mm, and 26mm.

For this purpose, Taguchi design (DOE) (L9) will be used by three deferent levels of Soaking Temperature, Soaking Time, tempering temperature & tempering time to arrive at the optimum Hardness with the approach of "Larger the better" The effect of these parameters (between low, medium and high) on hardness is to be measured.

Symbol	Factor	Unit	Range
A	Soaking Temperature	°C	1190 – 1220
B	Soaking Time	Seconds	220–280
C	Tempering temperature	°C	540–590
D	Tempering time	min	75–120

Table 5: Fermentation factor

c) Experimental Details

Design of experiment is powerful tools for analyzing the influence of the process variables covers some specific variable, which is a unknown function of these process variable. The major step in the taguchi method is the selection of the factors affecting the performance measures. The table shows the parameters and the corresponding levels chosen for the investigations. The multiple response characteristics including four heat treatment parameters are chosen on the output parameter to validate the effectiveness. The standard experiment layout 3 level OA L9 (34) for factors are listed

ISSN (Online) 2581-9429

IJARST

International Journal of Advanced Research in Science & Technology (IJARST)

Volume 8, Issue 3, August 2020

for this cases and shown in the following table. The experiments are performed for the various heat treatment cycles as per the layout. And the response or hardness will be measured for various experiments. At the optimum Hardness with the approach of "Larger the better". The cycle will select which will be the optimal solution for existing problem.

Sr. No	Soaking temp	Soaking time	Tempering temp	Tempering Time	hardness
1	1190	205	545	90	690
2	1190	225	560	105	710
3	1190	245	575	120	720
4	1205	205	575	105	810
5	1205	225	545	120	829
6	1205	245	560	90	842
7	1210	180	560	120	790
8	1210	210	575	90	823
9	1210	245	545	105	836

Table 6: Experimental Details For 16 mm Subgroup, Taper Shank Drills

VII. Result and Discussion

Hardness: The experiments were performed by varying the heat treatment parameters and the average response of the factors is measured. with three deferent levels of Soaking Temperature, Soaking Time, tempering temperature & tempering time to arrive at the optimum Hardness with the approach of "larger the better." This will give desired temperature time relation. Similarly for other drill the experiments were performed. Table shows the optimized hardness with best temp time relation.

Sr. No.	Drill Size	Hardness(VHN)
1	14	849
2	16	845
3	26	835

Table 7: Result table with optimized temperature time Relation

Size (mm)	Performance (No. of Holes)		
	Existing Performance	Competitor I	Competitor II
14	52	59	63
16	49	50	53
26	32	30	32

Table 8: Performance test with optimized temperature time Relation

VIII. Conclusion

Experiments have to be performed for optimization of Heat Treatment of Taper Shank Drills. The hardness & performance has to evaluate. Significant improvement expected in the performance of Taper Shank Drills. Including following points.

1. Maximum Hardness should be achieved which get up to 849 VHN.
2. Performance of Taper Shank Drills is improved to in comparison with other competitors.
3. Optimization of heat treatment significantly improves the performance of tool.

ISSN (Online) 2581-9429

IJARST

International Journal of Advanced Research in Science & Technology (IJARST)

Volume 8, Issue 3, August 2020

ACKNOWLEDGMENT

First and foremost, I would like to express my deep sense of gratitude and indebtedness to my Guide Prof. B. B. Kedar and Prof. N. S. Bagal PG coordinator, Department of Mechanical Engineering for his invaluable encouragement, suggestions and support from an early stage of this Project.

REFERENCES

[1]. V. K. Murugan, P. Koshy Mathews "Optimization of Heat Treatment Processes Using Taguchi "Parameter Design Approach" International Journal of Research in Mechanical Engineering Volume1, Issue1, July-September, 2013, pp. 16-21.

[2]. S.Z. Qamar, "Effect of heat treatment on mechanical properties of H11 tool steel" Journal of Achievements in Materials and Manufacturing Engineering, VOLUME 35 ISSUES 2 August 2009.

[3]. Harvinder Singh, Aneesh Goyal, "Effect Of Cryogenic Treatment On Microstructure Of T-15 Tool steel" International Journal Of Engineering Sciences& Research Technology, ISSN: 2277-9655, December, 2015

[4]. O.O. Joseph, R.O. Leramo, "Effect of Heat Treatment on Microstructure and Mechanical Properties of SAE 1025 Steel: Analysis by one-way ANOVA" J. Mater. Environ. Sci. 6 (1) (2015) 101-106

[5]. Dennis W. Hetzner,William Van Geertruyden, "Crystallography and Metallography of Carbides In High Alloy Steels", Journal of MaterialsEngineering and Performance Volume, July 2008, Pages 825–841

[6]. S. Sendooran, P Raja, "Metallurgical Investigation on Cryogenic Treated HSS Tool", International Journal of Engineering Science and Technology (IJEST), Volume 3 No. 5 May 2011.

[7]. Amit Kumar Tanwer "Effect of Various Heat Treatment Processes on Mechanical Properties of Mild Steel and Stainless Steel" American International Journal of Research in Science, Technology & Engineering" ISSN (Print): 2328-3491, 2014,

[8]. T. Senthilkumar and T. K. Ajiboye, "Effect of Heat Treatment Processes on the Mechanical Properties of Medium Carbon Steel", Journal of Minerals & Materials Characterization & Engineering, Vol. 11, No.2 pp.143-152, 2012.

International Journal of Advanced Research in Science, Communication and Technology

IJARSCT

Certificate of Publication

INTERNATIONAL STANDARD SERIAL NUMBER
ISSN NO: 2581-9429

This is to certify that

Mr. Rushikesh S. More

Siddhant College of Engineering, Pune, India

has published a research paper entitled

Optimization of Heat Treatment Process Parameter for High Speed Steel Taper Shank Drill

in IJARSCT, Volume 8, Issue 3, August 2020

Certificate No: 082020-A667
www.ijarsct.co.in

Scientific Journal Impact Factor 4.819 Journal Impact Factor

www.sjifactor.com

Editor-in-Chief

Journal of Civil Engineering and Environmental Technology
p-ISSN: 2349-8404; e-ISSN: 2349-879X; Volume 7, Issue 2; April-June 2020, pp. 174-178

http://www.krishisanskriti.org/Publication.html

SEISMIC STUDY OF DIAGRID STRUCTURE WITH BRACE FRAME AND DAMPER FRAME SYSTEM OF DIFFERENT ARRANGEMENT

Vikash Yadav[1] and Anurag Bajpai[2]

[1]PG Student(Structural Engineering), Civil Engineering Department, Institute of Engineering and Technology, Lucknow
[2]Assistant Professor(Structural Engineering) Civil Engineering Department, Institute of Engineering and Technology, Lucknow
Email: [1]vk.141993@gmail.com, [2]bajpai.ced.cf@ietlucknow.ac.in

Abstract—*In the current situation, population and industrialization are growing rapidly over time. Architects and engineers want to focus on the growth and vertical development of tall buildings and skyscrapers. However, increasing the height of the building is not easy. Several parameters play an important role in construction, including lateral loads. (i.e. wind or seismic force). The next task of the designer is to design a type of building that will be more sustainable. In this study structural analysis of G+44 story steel frame, diagrid structure with grid angle 67.32. In other two frame using x-bracing at all faces, at corner, at centre and damper at corner, at centre. The plan considered for all models was 30m X 30m and the method use for analysis was Response spectrum analysis method. All the member was designed as per IS456:2000, IS800:2007 and load combination for seismic force were considered as per IS1893(Part-1):2016. The procedure of modelling also analysis was done on ETABSv17.0.1 software. The performance was evaluated from various. The result was expressed in forms of graphs, tables and figures while comparison was done with the limitation as per IS1893(Part-1):2016.*

It was found that maximum story displacement and story drift lies within the permissible value as per IS1893(Part-1):2016. Comparing the specified parameters, it was found that the diagrid frame structure performing better than the x-bracing and damper frame structure thus can be consider to be more effective for high rise construction. From all the six-models diagrid gives less value of story displacement and story stiffness compare to other models. Hence, the diagrid can be considered as the sustainable solution in terms of high-rise construction.

Keyword*: Diagrid; X-bracing, Damper; Lateral load; Response spectrum analysis; ETABs software.*

1 INTRODUCTION

In the current situation, population and industrialization are growing rapidly over time. Architects and engineers want to focus on the growth and vertical development of tall buildings and skyscrapers. However, increasing the height of the building is not easy. Several parameters play an important role in construction, including lateral loads. (i.e. wind or seismic force). The next task of the designer is to design a type of building that will be more sustainable. Diagrid is a construction made of steel, concrete and wooden blocks and arranged diagonally at the time of constructions of buildings, roofs. As the height of the building increases, the lateral drag mechanism from the gravitational system becomes more and more important. The physical stability of the diagonal structure has a triangular shape, which resists gravity and lateral loads due to the axial pressure of its elements. Some of these systems include pipe designs, gaskets, transverse joints, cantilever joints, transition walls, and diode structures. The diagrid system is used as a roof to create a large transparent area without columns. Use 20%-25% less building material in comparison to others.

Bracing are a method used to build seismic structures. Elements in a lattice frame are designed to work with skeletal or push structures. Braking maintains the lateral load of the seismic force by terminating the inclined elements. The brake frame is on the screen; They move along spiral axes and columns. Since the diagonal buffer operates under axial load, the amplifier is the most efficient, therefore, the minimum size of the element gives it greater rigidity and strength in the horizontal section. Concentric bracing and eccentric bracing are being used here. Bracing system are very efficient in resisting lateral load as they provide strength in lateral direction.

The damper uses lateral force to hold the structure in place. A damper is a power distribution device that limits evacuation from a home during an earthquake. This helps the structure to reduce the bending of columns and supports and increase the rigidity of the structure.

2: OBJECTIVES OF WORK

1.Study of seismic behaviour of buildings for regular plan under seismic loads and combinations according to IS 1893: 2016.

2. To assess the report of diagrid and braced frame lateral resisting force system structure.

3. To stimulate seismic parameter that are base shear, modes of vibration, time period, story deracination, story drop off and story constrain.

3: DESCRIPTION OF BUILDING

S. No.	Structural Part	Dimension
1.	Type of building	Commercial(G+44)
2.	Type of structure	Steel structure
3.	Length in X-Dir	30m
4.	Length in Y-Dir	30m
5.	No of bays in X-Dir.	7No@5m
6.	No of bays in Y-Dir.	7No@5m
7.	Floor to floor height	3.m
8.	Total height of buildings	132 m
9.	Slab thickness	150mm
10.	Column	ISHB 600-2
11.	Beam	ISMB 600
12.	Diagrid (Tube section)	385.6mm X 385.6mm X 11mm
13.	Grid Angle	67.32
14.	Secondary Beam	ISLB 400
15.	Bracing	ISMB 300
16.	Fluid Viscous Damper	500kN, 98Kg.
17.	Thickness of core	400mm

Table 3(a) Geometrical Properties

S. No.	Material	Grade
1.	Concrete (slab)	M25
2.	Concrete (Core)	M40
3.	Steel section (I-shape)	Fe345
4.	Re-bar	HYSD550
5.	Density of Steel	7850 kg/m^3
6.	Young Modulus E	2.1 X 10^5 N/mm^2
7.	Shear Modulus	80000 N/mm^2
8.	Poisson's Ratio	0.3

Table 3(b) Material Properties (IS 456:2000 & IS 800:2007)

1.	Earthquake Zone	III
2.	Zone factor (Z)	0.16 (Table 3, clause 6.4.2)
3.	Damping Ratio	5% (clause 7.2.4)
4.	Important Factor(I)	1.2 (Table 8, clause 7.2.3)
5.	Type of soil	Medium soil (clause 6.4.2.1)
6.	Response Reduction Factor (R)	5(SMRF) (Table-9, clause 7.2.6)

Table 3(c) Seismic Data (IS 1893:2016 (part 1)

4: STRUCTURAL MODELLING

Model-1 Diagrid Structure

Model-2 X-Bracing Structure (All faces)

Model-3 X-Bracing Structure (Corner)

Model-4 X-Bracing Structure (Centre)

Model-5 Damper Structure (Corner)

Model-6 Damper Structure (Centre)

Modelling done by the help of ETAB'S 2017 software.

5: ANALYSIS AND RESULTS

Time period

When the structure is considered for analysis, it is considered as lumped mass. General building act as inverted pendulum. With increase in the storey one lumped mass get increased. When earthquake occur building start vibrating under forced vibration. General earthquake lasts for few minutes. After completion of earthquake building vibrated as free vibration and it vibrate at natural frequency. Natural time period is the time required to complete one cycle of oscillation when it was disturbed and left free i.e. no external force is applied. Natural time period is inverse of natural frequency. It depends mass and stiffness of the building.

$$Tn = 2\pi\sqrt{m/k}$$

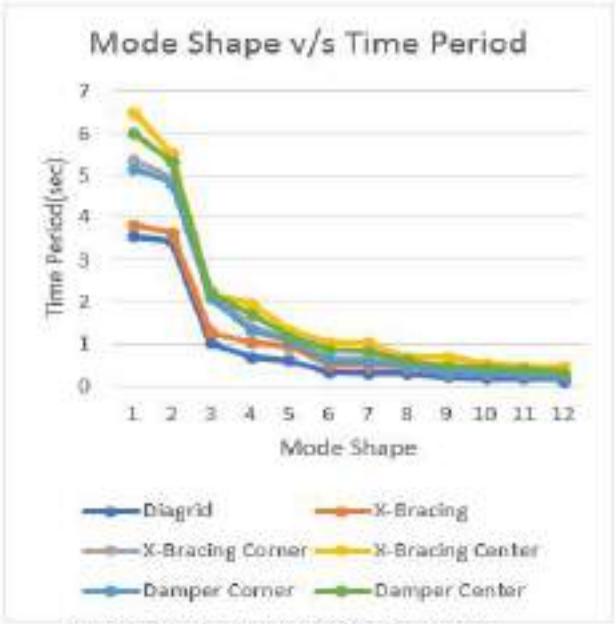

Graph 5. Mode v/s Time Period of All Models

From the above table and graph, we can see that Diagrid structure having less time period value then X-Bracing at all faces and maximum value of time period in all model having X-Bracing at centre. We can say that Diagrid structure is more efficient in all six models.

6: STORY DRIFT

As mentioned before building act as spring mass system. Every storey's slab part act as mass and column part provide stiffness. When building subjected to seismic load each mass vibrated differently according to its location and value. The relative displacement between adjacent storey has been termed as storey drift. Codes have prescribed its value H/250. Where H represent storey height.

In Eurocode 8:2004 Part 1 specifies allowable maximum story drift is 1% of story height therefore as per Eurocode permissible limit of drift will be 0.01 X 3000 = 30 mm.

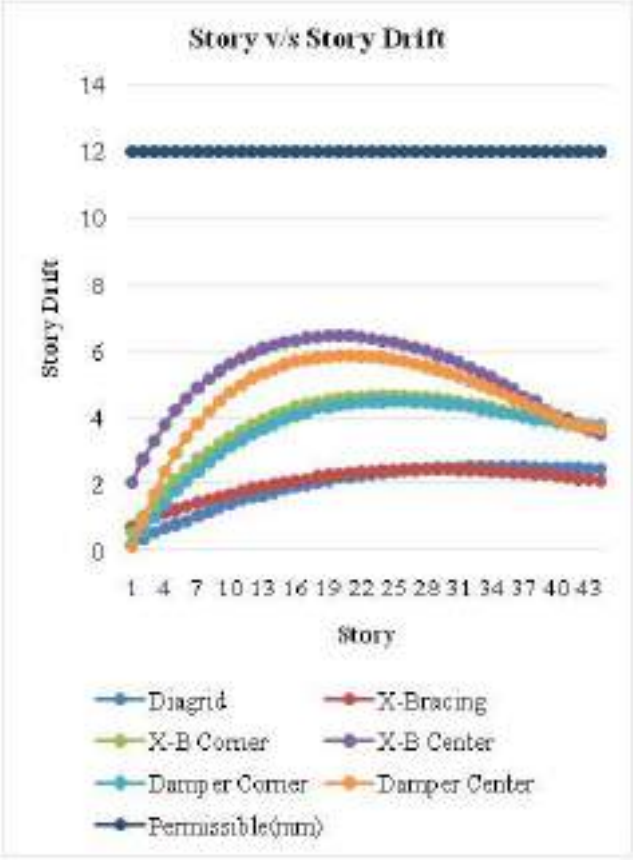

Graph 6 Story v/s Story Drift of All Models

From the above table and graph, we can see that in begging Diagrid structure having less story drift value but after 28 story X-Bracing at all faces having less value from the Diagrid structure. And maximum value of story drift is X-Bracing at centre.

7: BASE SHEAR

Base shear is the sum of all storey shear acting in lateral direction. Base shear plays important role in deciding the type of foundation used. High base shear required strong foundation as compared to lower value of base shear. Base shear can be calculated used given formula.

$V_b = A_h x W$

Where, Ah= Design horizontal seismic coefficient for structure.

W= Seismic weight of the building

Model	Base Shear (kN)
Model-1	2103.8416
Model-2	2682.3112
Model-3	2593.8597
Model-4	2529.938
Model-5	2523.47
Model-6	2520.6485

Table 8 base shear of all models

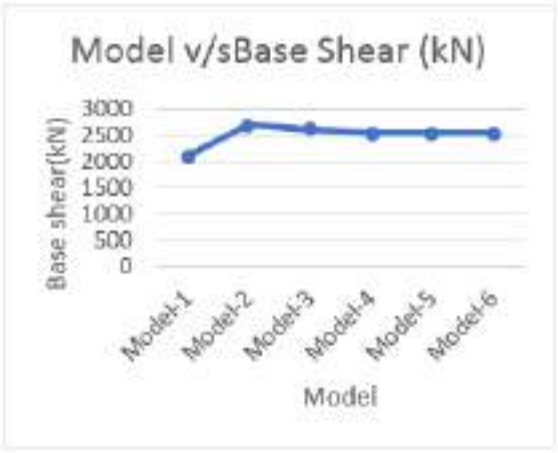

Graph 8 Model v/s Base Shear

From the above table and graph, we can see that Diagrid structure having less base shear value and maximum value of base shear in all model having X-Bracing at all faces. We can say that Diagrid structure is more efficient in all six models.

8: STORY DISPLACEMENT

When the building is excited with lateral force, it tends to move from its original position. This displacement with reference to fixed point that is base is termed as storey displacement. As per Indian standard code, the storey displacement is restricted to H/250 where H is storey height form base. Eurocodes have higher allowable value of storey displacement i.e. H/100.

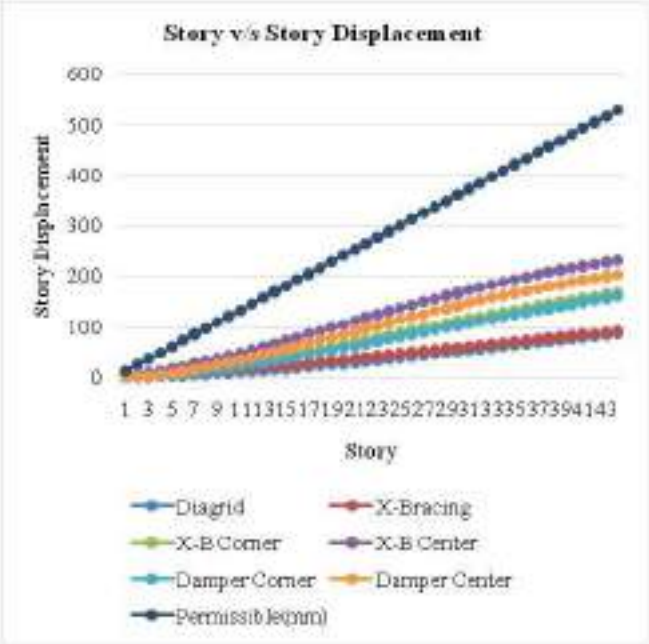

Graph 5.4 Story Displacement of All Models

From the above table and graph, we can see that Diagrid structure having less Story Drift value then X-Bracing at all faces and maximum value of Story Drift in all model having X-Bracing at centre. We can say that Diagrid structure is more efficient in all six models.

9: STORY STIFFNESS

The term story stiffness is defined as capability of resisting force/load acting on any story. It is depending on material property, if the story is stiffer it means less flexible.

Graph 9 Story v/s Story stiffness

From the above table and graph, we can see that Diagrid structure having maximum Story stiffness value then X-Bracing at all faces in all models. We can say that Diagrid structure is more efficient in Y-dir. from all six models.

10: CONCLUSION93

1. Time taken in first mode is minimum in diagrid structure and in other all with respect to diagrid structure, 10.66% more in X-bracing in all faces, 55.46% more in X-bracing at corner, 89.27% more in X-bracing in centre.
2. Drift is minimum in X-bracing in all faces after 27 story before 27 story Diagrid structure having minimum vale but overall comparisons shows with respect to diagrid structure, maximum value of drift is 5.16% less in X-bracing in all faces, 81.5% more in X-bracing at corner, 150.5% more in X-bracing in centre.
3. Displacement is minimum in diagrid structure and in other all with respect to diagrid structure, 4.49% more in X-bracing in all faces, 95.69% more in X-bracing at corner, 169.75% more in X-bracing in centre.
4. Base shear is minimum in diagrid structure cause of less weight of structure and in other all with respect to diagrid structure, 27.49% more in X-bracing in all faces, 23.29% more in X-bracing at corner, 20.25% more in X-bracing in centre.
5. Story stiffness is maximum for Diagrid structure from all four models.
6. In all four models, model 1 perform best.

From above all I can say, Diagrid structure is much better than other all considered models. And also, in diagrid structure using 20-25% less building material by which weight of building is reduces. For seismic effect one of the major factors is weight of building.

REFRENCES

[1] Ali, M.M. and Moon, K.S., 2007. Structural developments in tall buildings: current trends and future prospects. *Architectural science review*, *50*(3), pp.205-223.

[2] Moon, K.S., 2008. Practical Design Guidelines for Steel Diagrid Structures. In *AEI 2008: Building Integration Solutions* (pp. 1-11).

[3] Kim, J. and Lee, Y.H., 2010. Seismic performance evaluation of diagrid system buildings. *The Structural design of tall and special buildings*, *21*(10), pp.736-749.

[4] Eghtesadi, S., Nourzadeh, D. and Bargi, K., 2011. Comparative Study on Different Types of Bracing Systems in Steel Structures. *World Academy of Science, Engineering and Technology*, *73*, p.2011.

[5] Sangle, K.K., Bajoria, K.M. and Mhalungkar, V., 2012. Seismic analysis of high-rise steel frame building with and without bracing. *15wcee, Lisboa*.

[6] Jani, K. and Patel, P.V., 2013. Analysis and design of diagrid structural system for high rise steel buildings. *Procedia Engineering*, *51*, pp.92-100.

[7] MOON, K., 2013, September. Optimal structural configurations for tall buildings. In *Proceedings of the Thirteenth East Asia-Pacific Conference on Structural Engineering and Construction (EASEC-13)* (pp. G-4). The Thirteenth East Asia-Pacific Conference on Structural Engineering and Construction (EASEC-13).

[8] Yadav, S. and Garg, V., 2015. Advantage of steel diagrid building over conventional building. *International Journal of Civil and Structural Engineering Research (ISSN)*, *3*(01), pp.394-406.

[9] Pawar, D.S., Phadnis, S.A.U. and Shinde, R.S.,2015. Analysis of multistoried braced frame subjected to seismic and gravity loading.

[10] Bhale, P. and Salunke, P.J., 2016. Analytical Study and Design of Diagrid Building and Comparison with Conventional Frame Building. *International Journal of Advanced Technology in Engineering and Science*, (4).

[11] Shah, M.I., Mevada, S.V. and Patel, V.B., 2016. Comparative study of diagrid structures with conventional frame structures. *Int. J. Eng. Res. Appl. (IJERA)*, *6*(5), pp.22-29.

[12] Khaleel, M.T. and Dileep Kumar, U., 2016. Seismic Analysis of Steel Frames with Different Bracings using ETABS Software. *International Research Journal of Engineering and Technology*, *3*(08).

[13] Sreeshma. K.K. Nicy Jose (2016). Seismic Performance Assessment of Different Types of Eccentric Braced System. IJIRST, ISSN 2349-6010, Volume 3, Issue 4, Sept 2016, pp123-127.

[14] Joshi R. S. and Dhyani D. J. (2017), A Review on Novel Structure Development in Tall Building: Diagrid Structure, IJAERD.

[15] Shankar, B., Dheekshith, K. and Hijaz, S.N., 2017. Study On Behaviour of Diagrids Under Seismic Loads Compared to Conventional Moment Resisting Frames.

[16] Jain, S.K., Bhadoria, S.S. and Kushwah, S.S.,2017. Comparative Study and Seismic Analysis of a Multistorey Steel Building.

[17] Mangalore, S.S.E. and Bangalore, T.O.C.E., 2017. Comparative Study of Different Types of Bracing Systems by Placing at Different Locations.

[18] Suyog Sudhakar Shinde, Abhijeet A. Galatage, Dr. Sumant K. Kulkarni (2017). Evaluation Seismic Efficiency of Combination of Bracing for Steel Building. IJARIIT, ISSN: 2454-132X (Volume3, Issue5), pp 46-55.

[19] Asadi, E., Li, Y. and Heo, Y., 2018. Seismic performance assessment and loss estimation of steel diagrid structures. *Journal of Structural Engineering*, *144*(10), p.04018179.

[20] Saurabh Kanungo & Komal Bedi (2018). Analysis of a Tall Structure with X-Type Bracing Considering Seismic Loan Using Analysis Tool Stadd. Pro. IJESRT, ISSN: 2277-9655, PP 366-373.

[21] Safvana p, Anila s (2018). Seismic Analysis of Braced System in RCC, Steel and Composite Structure. IJIRSET, Volume 7 Issue 3, pp 3019-3032.

[22] Abhishek R I, Rajeeva S V2 (2019). Seismic Behaviour of Steel Bare Frame Building with Outrigger and Bracing with Outrigger Structure. IRJET, Volume: 06, Issue: 01. Jan 2019, pp161-165.

[23] Vishwakarma A., Rai A. (2019). Seismic Analysis of Steel Frame with Bracings Using Response Spectrum Method. IRJET, 2019.

[24] Meghna, Singh V. K. (2019) Structural Performance of Four Storey Diagrid Tall Building. JETIR, 2019 May, Volume 6, Issue 5 (ISSN-2349-5162)

[25] Radmard Rahmani, H. and Könke, C., 2019. Seismic control of tall buildings using distributed multiple tuned mass dampers. *Advances in Civil Engineering*, *2019*.

[26] Dadkhah, H. and Mohebbi, M., 2019. Performance assessment of an earthquake-based optimally designed fluid viscous damper under blast loading. *Advances in Structural Engineering*, *22*(14), pp.3011-3025.

[27] S. Lakshmi Shireen Banu, Kothakonda Ramesh (2019). Seismic Response Study and Evaluation of Vibration Control of Elevated RCC Structure using Friction Damper. IJITEE, 2019.

[28] S.lakshmishireenbanu, pathaushasri,(2019). Study of Seismic Energy Dissipation and Effect in Multistory RCC Building with and Without Fluid Viscous Dampers. IJITEE, 2019.

[29] De Domenico, D. and Ricciardi, G., 2019. Earthquake protection of structures with nonlinear viscous dampers optimized through an energy-based stochastic approach. *Engineering Structures*, *179*, pp.523-539.

[30] Dadkhah, H. and Mohebbi, M., 2019. Performance assessment of an earthquake-based optimally designed fluid viscous damper under blast loading. *Advances in Structural Engineering*, *22*(14), pp.3011-3025.

[31] De Domenico, D., Ricciardi, G. and Takewaki, I., 2019. Design strategies of viscous dampers for seismic protection of building structures: a review. *Soil Dynamics and Earthquake Engineering*, *118*, pp.144-165.

[32] Del Gobbo, G.M., 2019, June. Placement of fluid viscous dampers to improve total-building seismic performance. In *Proceedings of the CSCE Annual Conference, Laval, Montreal, QC, Canada* (pp. 12-15).

[33] Patle, Y.Z., Gajghate, V. and Manchalwar, A., Seismic Response Control of Adjacent Building Using Fluid Viscous Damper.

[34] Sahu, G. and Sahu, P., 2019. COMPARATIVE ANALYSIS OF EFFECTS OF BASE ISOLATOR & FLUID VISCOUS DAMPER ON RESPONSE OF A RCC STRUCTURE.

[35] Koshti, A., Shinde, S., Yamagar, K. and Shegunshi, S., Seismic Response of Structure with Fluid Viscous Damper (FVD).

[36] IS: 800:2007 General Construction of Steel- Code of Practice.

[37] IS: 456:2000 Plain and Reinforced Concrete- Code of Practice.

[38] IS: 1893(Part-1):2016 Criteria for Earthquake Resistant Design of Structures.

[39] IS: 875 (Part 2) - 1987, Code of Practice Design Loads (Other Than for Earthquake) For Buildings and Structures.

[40] IS: 13920:2016 Ductile Design and Detailing of Reinforced Concrete Structures Subjected to Seismic Forces- Code of Practice.

[41] Eurocode 8:2004 Design of structures for earthquake resistance.

Journal of Civil Engineering and Environmental Technology
p-ISSN: 2349-8404; e-ISSN: 2349-879X; Volume 7, Issue 2; April-June 2020, pp. 158-163

http://www.krishisanskriti.org/Publication.html

SEISMIC STUDY OF DIAGRID STRUCTURE WITH BRACE FRAME STRUCTURE OF DIFFERENT ARRANGEMENT

Vikash Yadav[1] and Anurag Bajpai[2]

[1]PG Student(Structural Engineering), Civil Engineering Department, Institute of Engineering and Technology, Lucknow
[2]Assistant Professor(Structural Engineering) Civil Engineering Department, Institute of Engineering and Technology, Lucknow
E-mail: [1]vk.141993@gmail.com, [2]bajpaianurag5@gmail.com

Abstract—*In the current situation, population and industrialization are growing rapidly over time. Architects and engineers want to focus on the growth and vertical development of tall buildings and skyscrapers. However, increasing the height of the building is not easy. Several parameters play an important role in construction, including lateral loads i.e. seismic or wind force. The next task of the designer is to design a type of building that will be more sustainable. In this study structural analysis of G+44 story steel frame, diagrid structure with grid angle 67.32. And X-bracing at all faces, at corner, at centre. The plan considered for all models was 30m X 30m and the method use for analysis was Response spectrum analysis method. All the member was designed as per IS456:2000, IS800:2007 and load combination for seismic force were considered as per IS1893(Part-1):2016. ETABSv17 software has been used for modelling and analysis. Latest 2017 version has been used for analysis. The performance was evaluated from various. The result was expressed in forms of graphs, tables and figures while comparison was done with the limitation as per IS1893(Part-1):2016.*

It was found that maximum story displacement and story drift lies within the permissible value as per IS1893(Part-1):2016. Comparing the specified parameters, it was found that the diagrid frame structure performing better than the x-bracing and damper frame structure thus can be consider to be more effective for high rise construction. From all the six-models diagrid gives less value of story displacement and story stiffness compare to other models. Hence, the diagrid can be considered as the sustainable solution in terms of high-rise construction.

Keyword: *Diagrid, X-Bracing, Lateral load, ETAB'S.*

INTRODUCTION

In the current situation, population and industrialization are growing rapidly over time. Architects and engineers want to focus on the growth and vertical development of tall buildings and skyscrapers. However, increasing the height of the building is not easy. Several parameters play an important role in construction, including lateral loads. The next task of the designer is to design a type of building that will be more sustainable. Recently diagrid structure are more popular due to aesthetics. They have very attractive look. Diagrid is a construction made of steel, concrete and wooden blocks and is used diagonally in the construction of buildings and roofs. As the height of the building increases, the lateral drag mechanism from the gravitational system becomes more and more important. The physical stability of the diagonal structure has a triangular shape, which resists gravity and lateral loads due to the axial pressure of its elements. Some of these systems include pipe designs, gaskets, transverse joints, cantilever joints, transition walls, and diode structures. The diagrid system is used as a roof to create a large transparent area without columns. Use 20%-25% less building material in comparison to others.

Bracing are a method used to build seismic structures. Elements in a lattice frame are designed to work with skeletal or push structures. Braking maintains the lateral load of the seismic force by terminating the inclined elements. The brake frame is on the screen; They move along spiral axes and columns. Since the diagonal buffer operates under axial load, the amplifier is the most efficient, therefore, the minimum size of the element gives it greater rigidity and strength in the horizontal section. Concentric bracing and eccentric bracing are being used here. Bracing system are very efficient in resisting lateral load as they provide strength in lateral direction.

There is recent revision of earthquake code 1893:2016. This code has been revised after 14 year. In this code some strict norm has been added in design of earthquake resistance structure. The definition of soft storey and weak storey have been revised and importance factor have also been increased for some structures. This code has altered the value of Sa/g. In this paper the study has been done using latest code.

OBJECTIVE OF WORK

1. Study of seismic behaviour of buildings for regular plan under seismic loads and combinations according to IS 1893: 2016.

2. To assess the report of diagrid and braced frame lateral resisting force system structure.

3. To stimulate seismic parameter that are base shear, modes of vibration, time period,story deracination, story drop off and story constrain.

DESCRIPTION OF BUILDING

Building type- Commercial
Plan area- 30m X 30m
Number of story- 44
Height of each story- 3m
Total height of building- 132m
Core thickness- 400mm
Size of steel square tube section used for Diagrid 385.6mm X 385.6mm X 11mm.
Steel section used for Beam- ISMB 600
Steel section used for Column- ISWB 600-2
Steel section used for brace- ISMB 300
Concrete grade used for core- M40
Concrete grade used for Deck slab- M25
Grade of steel- Fe345
Dead load counterweight of structure
Live load – 4kN/m^2

EARTHQUAKE DATA

Zone-III
Zone factor = 0.16
Importance factor =1.2
Response reduction factor =5
Soil type-II

MODELLING

MODEL 1- DIAGRID STRUCTURE
MODEL 2- X-BRACEING (ALL FACES)
MODEL 3- X-BRACEING (At CORNER)
MODEL 4- X-BRACEING (At CENTER)
Modelling done by the help of ETAB'S 2017 software.

Plan, Elevation and 3D

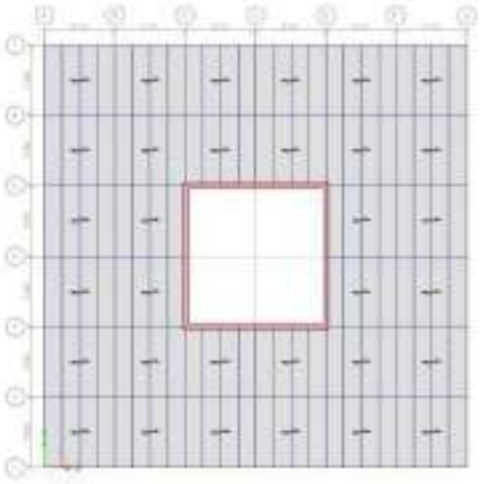

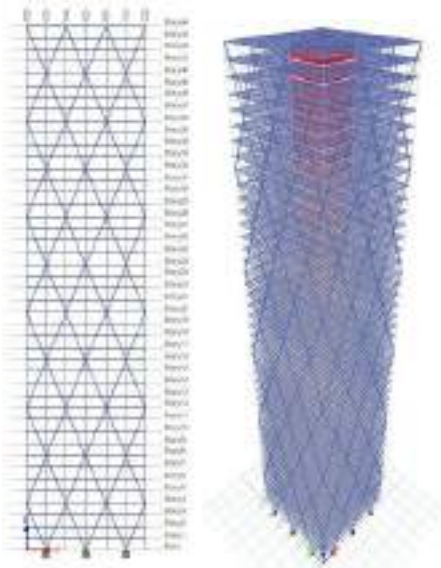

Fig. Plan, Elevation and 3D (Model 1)

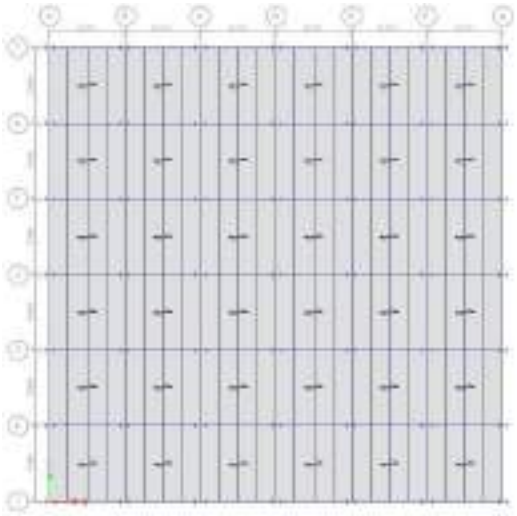

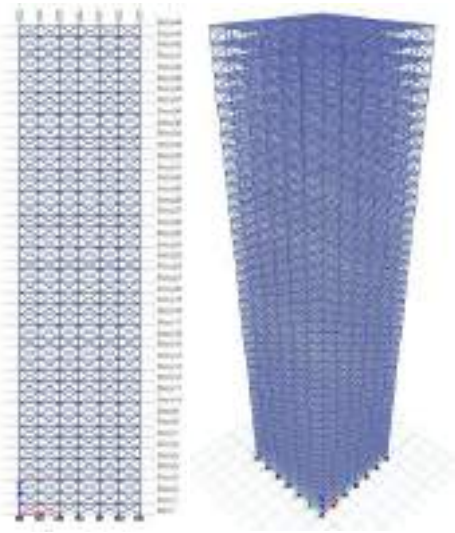

Fig. Plan, Elevation and 3D (Model 2)

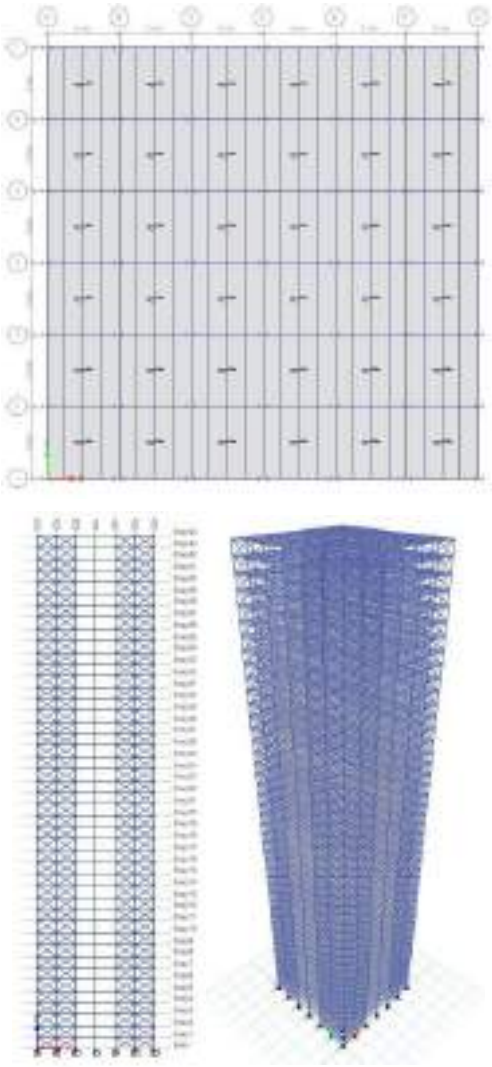

Fig. Plan, Elevation and 3D (Model3)

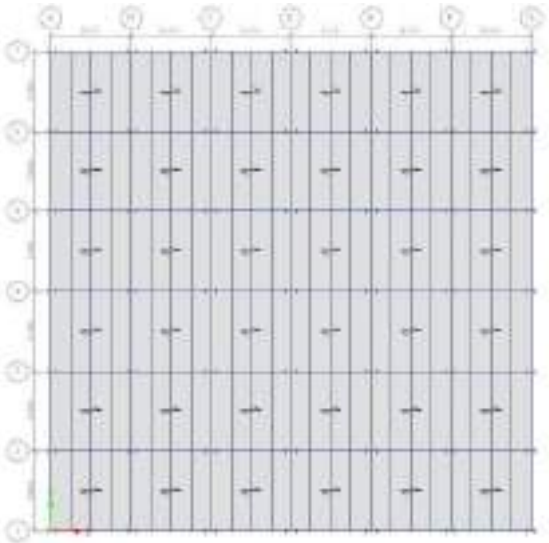

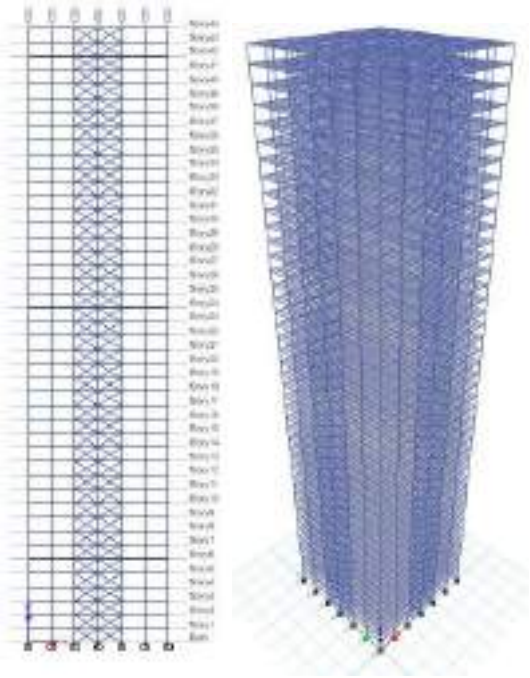

Fig. Plan, Elevation and 3D (Model 4)

ANALYSIS AND RESULTS

Time period

When the structure is considered for analysis, it is considered as lumped mass. General building act as inverted pendulum. With increase in the storey one lumped mass get increased. When earthquake occur building start vibrating under forced vibration. General earthquake lasts for few minutes. After completion of earthquake building vibrated as free vibration and it vibrate at natural frequency. Natural time period is the time required to complete one cycle of oscillation when it was disturbed and left free i.e. no external force is applied. Natural time period is inverse of natural frequency. It depends mass and stiffness of the building.

$$Tn = 2\pi\sqrt{m/k}$$

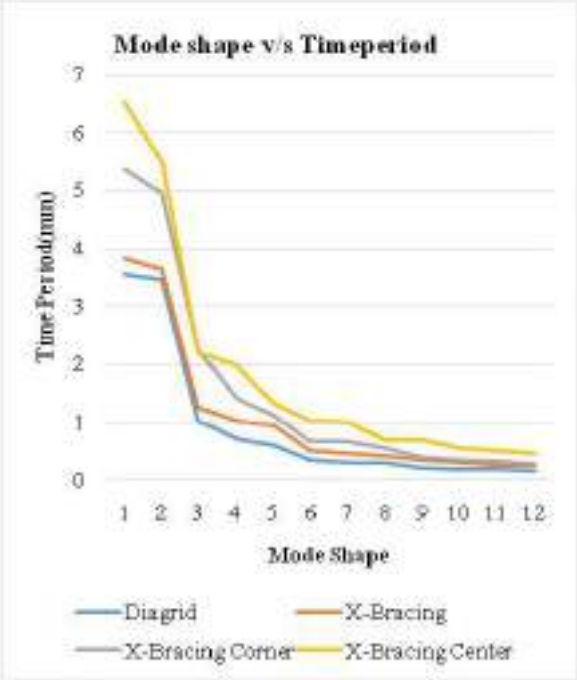

Graph: Fundamental natural time period

STORY DRIFT

As mentioned before building act as spring mass system. Every storey's slab part act as mass and column part provide stiffness. When building subjected to seismic load each mass vibrated differently according to its location and value. The relative displacement between adjacent storey has been termed as storey drift. Codes have prescribed its value H/250. Where H represent storey height.

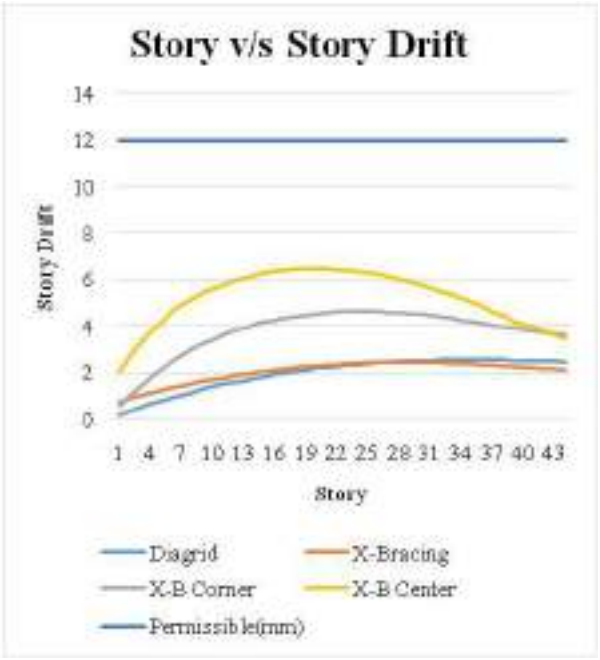

Graph: Story v/s Story drift

STORY DISPLACEMENT

When the building is excited with lateral force, it tends to move from its original position. This displacement with reference to fixed point that is base is termed as storey displacement. As per Indian standard code, the storey displacement is restricted to H/250 where H is storey height form base. Eurocodes have higher allowable value of storey displacement i.e. H/100.

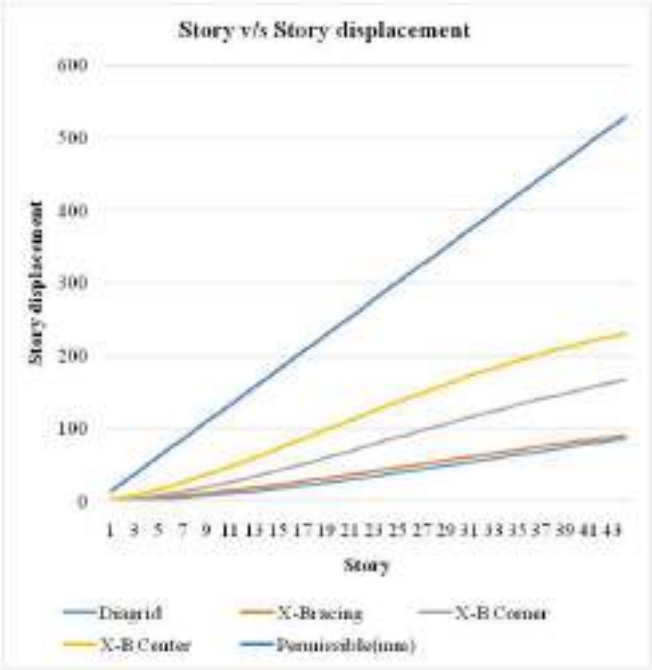

Graph: Story v/s Story displacement

BASE SHEAR

Base shear is the sum of all storey shear acting in lateral direction. Base shear plays important role in deciding the type of foundation used. High base shear required strong foundation as compared to lower value of base shear. Base shear can be calculated used given formula.

$$V_b = A_h X W$$

Where, Ah= Design horizontal seismic coefficient for structure.

W= Seismic weight of the building

Model	Base Shear (kN)
Diagrid	2103.8416
X-Brace	2682.3112
X-Brace corner	2593.8597
X-Brace centre	2529.938

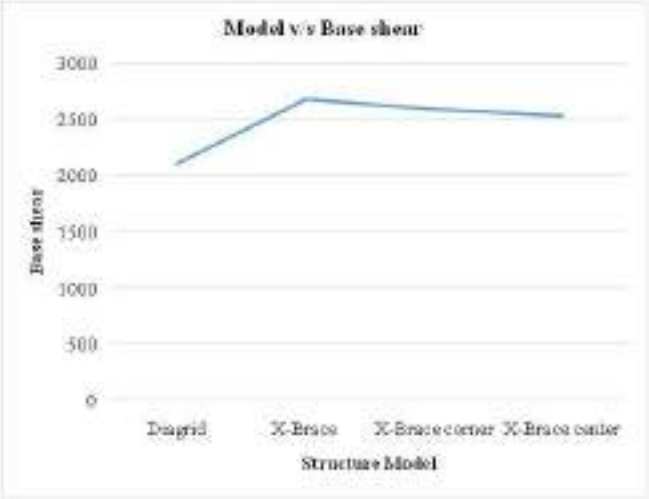

Graph: Model v/s Base shear

STORY STIFFNESS

The term story stiffness is defined as capability of resisting force/load acting on any story. It is depending on material property, if the story is stiffer it means less flexible.

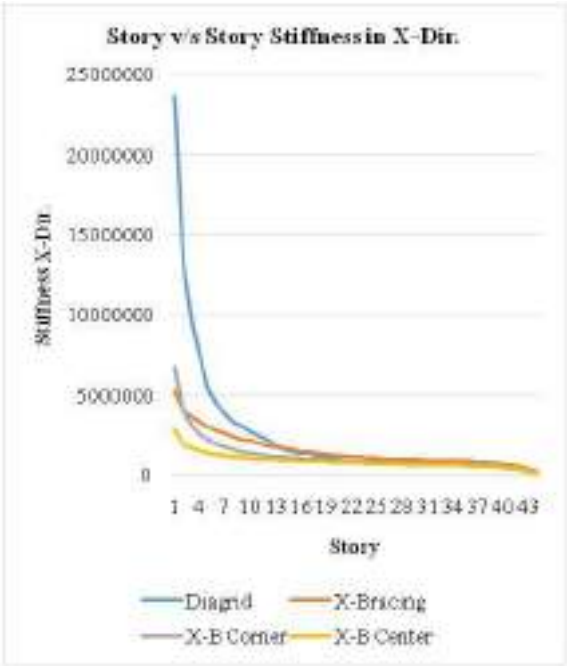

Graph: Story v/s Stiffness

CONCLUSION

1. Time taken in first mode is minimum in diagrid structure and in other all with respect to diagrid structure, 10.66% more in X-bracing in all faces, 55.46% more in X-bracing at corner, 89.27% more in X-bracing in centre.

2. Drift is minimum in X-bracing in all faces after 27 story before 27 story Diagrid structure having minimum vale but overall comparisons shows with respect to diagrid structure, maximum value of drift is 5.16% less in X-bracing in all faces, 81.5% more in X-bracing at corner, 150.5% more in X-bracing in centre.

3. Displacement is minimum in diagrid structure and in other all with respect to diagrid structure, 4.49% more in X-bracing in all faces, 95.69% more in X-bracing at corner, 169.75% more in X-bracing in centre.

4. Base shear is minimum in diagrid structure cause of less weight of structure and in other all with respect to diagrid structure, 27.49% more in X-bracing in all faces, 23.29% more in X-bracing at corner, 20.25% more in X-bracing in centre.

5. Story stiffness is maximum for Diagrid structure from all four models.

6. In all four models, model 1 perform best.

REFRENCES

[1] Ali, M.M. and Moon, K.S., 2007. Structural developments in tall buildings: current trends and future prospects. *Architectural science review*, *50*(3), pp.205-223.

[2] Moon, K.S., 2008. Practical Design Guidelines for Steel Diagrid Structures. In *AEI 2008: Building Integration Solutions* (pp. 1-11).

[3] Kim, J. and Lee, Y.H., 2010. Seismic performance evaluation of diagrid system buildings. *The Structural design of tall and special buildings*, *21*(10), pp.736-749.

[4]Eghtesadi, S., Nourzadeh, D. and Bargi, K., 2011. Comparative Study on Different Types of Bracing Systems in Steel Structures. *World Academy of Science, Engineering and Technology*, *73*, p.2011.

[5]Sangle, K.K., Bajoria, K.M. and Mhalungkar, V., 2012. Seismic analysis of high-rise steel frame building with and without bracing. *15wcee, Lisboa*.

[6] Jani, K. and Patel, P.V., 2013. Analysis and design of diagrid structural system for high rise steel buildings. *Procedia Engineering*, *51*, pp.92-100.

[7] MOON, K., 2013, September. Optimal structural configurations for tall buildings. In *Proceedings of the Thirteenth East Asia-Pacific Conference on Structural Engineering and Construction (EASEC-13)* (pp. G-4). The Thirteenth East Asia-Pacific Conference on Structural Engineering and Construction (EASEC-13).

[8] Yadav, S. and Garg, V., 2015. Advantage of steel diagrid building over conventional building. *International Journal of Civil and Structural Engineering Research (ISSN)*, *3*(01), pp.394-406.

[9]Bhale, P. and Salunke, P.J., 2016. Analytical Study and Design of Diagrid Building and Comparison with Conventional Frame Building. *International Journal of Advanced Technology in Engineering and Science*, (4).

[10] Shah, M.I., Mevada, S.V. and Patel, V.B., 2016. Comparative study of diagrid structures with conventional frame structures. *Int. J. Eng. Res. Appl. (IJERA)*, *6*(5), pp.22-29.

[11] Khaleel, M.T. and Dileep Kumar, U., 2016. Seismic Analysis of Steel Frames with Different Bracings using ETABS Software. *International Research Journal of Engineering and Technology*, *3*(08).

[12] Sreeshma. K.K. Nicy Jose (2016). Seismic Performance Assessment of Different Types of Eccentric Braced System.

IJIRST, ISSN 2349-6010, Volume 3, Issue 4, Sept 2016, pp123-127.

[13] Suyog Sudhakar Shinde, Abhijeet A. Galatage, Dr.Sumant K. Kulkarni (2017). Evaluation Seismic Efficiency of Combination of Bracing for Steel Building. IJARIIT, ISSN: 2454-132X (Volume3, Issue5), pp 46-55.

[14]Asadi, E., Li, Y. and Heo, Y., 2018. Seismic performance assessment and loss estimation of steel diagrid structures. *Journal of Structural Engineering*, *144*(10), p.04018179.

[25] Saurabh Kanungo &KomalBedi (2018). Analysis of a Tall Structure with X-Type Bracing Considering Seismic Loan Using Analysis Tool Stadd. Pro. IJESRT, ISSN: 2277-9655, PP 366-373.

[16] Safvana p, Anila s (2018). Seismic Analysis of Braced System in RCC, Steel and Composite Structure. IJIRSET, Volume 7 Issue 3, pp 3019-3032.

[17] Abhishek R I, Rajeeva S V2 (2019). Seismic Behaviour of Steel Bare Frame Building with Outrigger and Bracing with Outrigger Structure. IRJET, Volume: 06, Issue: 01. Jan 2019, pp161-165.

[18] Meghna, Singh V. K. (2019) Structural Performance of Four Storey Diagrid Tall Building. JETIR, 2019 May, Volume 6, Issue 5 (ISSN-2349-5162)

[19] IS: 800:2007 General Construction of Steel- Code of Practice.

[20] IS: 456:2000 Plain and Reinforced Concrete- Code of Practice.

[21] IS: 1893(Part-1):2016 Criteria for Earthquake Resistant Design of Structures.

[22] IS: 875 (Part 2) - 1987, Code of Practice Design Loads (Other Than for Earthquake) For Buildings and Structures.

[23] IS: 13920:2016 Ductile Design and Detailing of Reinforced Concrete Structures Subjected to Seismic Forces- Code of Practice.

[24] Eurocode 8: Design of structures for earthquake resistance, 2004.

International Conference

on

Innovative Research in "Architecture, Civil, Built Environment Environmental Engineering for Sustainable Development" (ACBES- 2020)

Organized by: The Gyan Bindu Educational Society
Supported by: "Dr. G. C. Mishra Educational Foundation"

on

2nd May, 2020

Venue: Jawaharlal Nehru University, New Delhi

Research Paper Oral Presentation / Contribution Certificate

Certified that Prof./Dr./ Mr./Mrs./Ms **Vikas Yadav**.....of **PG Student(Structural Engineering), Civil Engineering Department, Institute of Engineering and Technology, Lucknow**.....Presented/Contributed a Research Paper titled **SEISMIC STUDY OF DIAGRID STRUCTURE WITH BRACE FRAME AND DAMPER FRAME SYSTEM OF DIFFERENT ARRANGEMENT**.....

Authored by **Vikash Yadav and Anurag Bajpai**.....

in one day International Conference held in Jawaharlal Nehru University (J.N.U.), New Delhi.

Dr. G.C. Mishra
Organizing Secretary

Dr. Vikas Rai
Convener

SEISMIC STUDY OF DIAGRID STRUCTURE WITH DAMPER OF DIFFERENT ARRANGEMENT

[1] Vikash Yadav, [2] Anurag Bajpai

[1] Student (M. Tech Structural Engineering), [2] Assistant Professor

[1] Civil Engineering Department,

[1] Institute of Engineering and Technology, Lucknow, India.

Abstract: In the current situation, population and industrialization are growing rapidly over time. Architects and engineers want to focus on the growth and vertical development of tall buildings and skyscrapers. However, increasing the height of the building is not easy. Several parameters play an important role in construction, including lateral loads. (Examples of wind and seismic loads). The next task of the designer is to design a type of building that will be more sustainable. In this paper study about 30m X 30m plan of diagrid structure and damper structure of different arrangement. Seismic zone III, soil type II, analysis done by the response spectrum method on ETAB'S 2017. Result in terms of time period, story drift, story displacement, story stiffness and base shear. After analysis diagrid structure is perform better then damper.

Keyword: Diagrid, Damper, Lateral load, ETAB'S.

INTRODUCTION: In the current situation, population and industrialization are growing rapidly over time. Architects and engineers want to focus on the growth and vertical development of tall buildings and skyscrapers. However, increasing the height of the building is not easy. Several parameters play an important role in construction, including lateral loads. (Examples of wind and seismic loads). The next task of the designer is to design a type of building that will be more sustainable. Diagrid is a construction made of steel, concrete and wooden blocks and is used diagonally in the construction of buildings and roofs. As the height of the building increases, the lateral drag mechanism from the gravitational system becomes more and more important. The physical stability of the diagonal structure has a triangular shape, which resists gravity and lateral loads due to the axial pressure of its elements. Some of these systems include pipe designs, gaskets, transverse joints, cantilever joints, transition walls, and diode structures. The diagrid system is used as a roof to create a large transparent area without columns. Use 20%-25% less building material in comparison to others.

The damper uses lateral force to hold the structure in place. A damper is a power distribution device that limits evacuation from a home during an earthquake. This helps the structure to reduce the bending of columns and supports and increase the rigidity of the structure.

Different types of damper are Viscous Dampers, Viscoelastic Dampers, Friction Dampers, Tuned Mass Damper (TMD), Yielding Dampers and Magnetic Damper.

OBJECTIVE OF WORK

1. To study seismic behaviour of building for regular plan under seismic loads and load combinations as per IS 1893:2016.

2. To evaluate the response of diagrid and damper system different arrangement.

3. To determine seismic parameter that are time period, modes of vibration, base shear, story displacement, story drift and story stiffness.

DESCRIPTION OF BUILDING

Building type- Commercial

Plan area- 30m X 30m

Number of story- 44

Height of each story- 3m

Total height of building- 132m

Core thickness- 400mm

Size of steel square tube section used for Diagrid 385.6mm X 385.6mm X 11mm.

Steel section used for Beam- ISMB 600

Steel section used for Column- ISWB 600-2

Fluid viscous damper- 98Kg, 500 kN

Concrete grade used for core- M40

Concrete grade used for Deck slab- M25

Grade of steel- Fe345

Dead load self-weight of structure

Live load – 4kN/m^2 as per IS-875(Part 2)

SEISMIC DATA

Seismic zone-III

Zone factor (Z)=0.16(table3, clause 6.4.2)

Importance factor (I)=1.2(table8, clause 7.2.3)

Response reduction factor I=5 (SMRF) (table9, clause 7.2.6)

Soil type-II (Medium soil)

MODELLING

MODEL 1- DIAGRID STRUCTURE

MODEL 2- DAMPER (At CORNER)

MODEL 3- DAMPER (At CENTER)

Modelling done by the help of ETAB'S 2017 software.

Fig. Plan, Elevation and 3D of Model 1

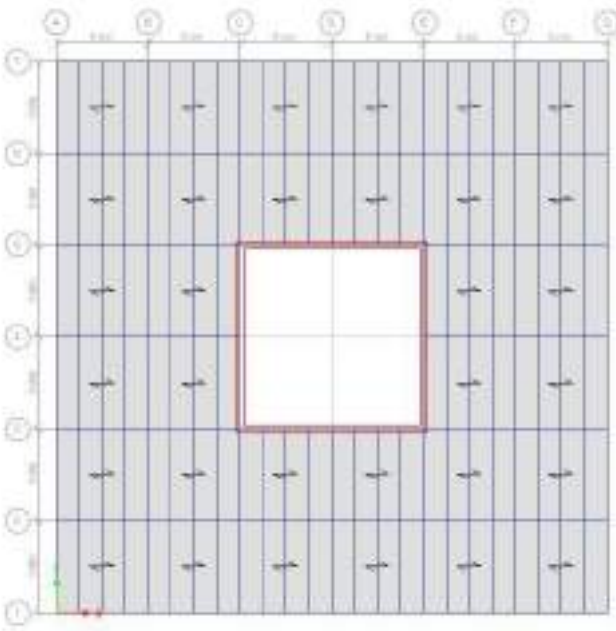

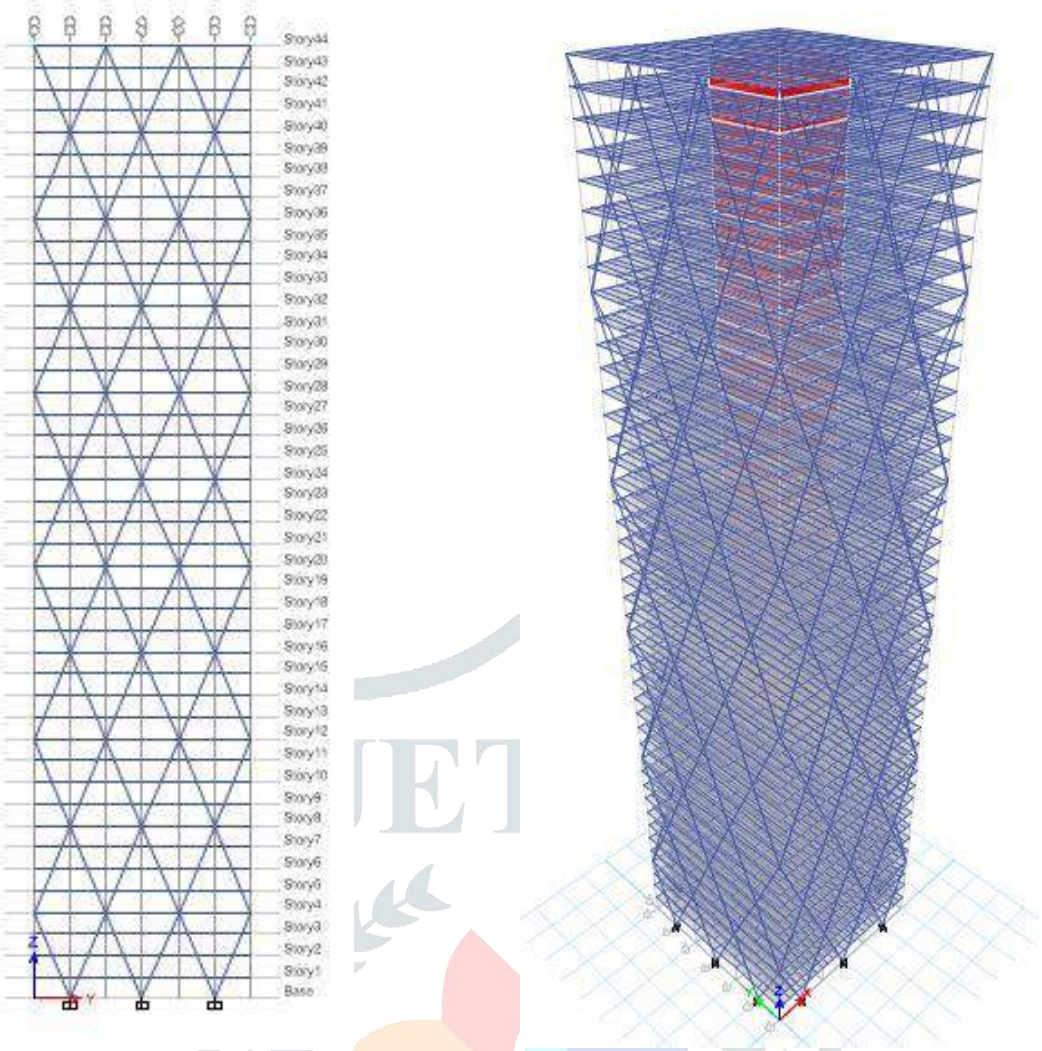

Fig. Plan, Elevation and 3D of Model 2

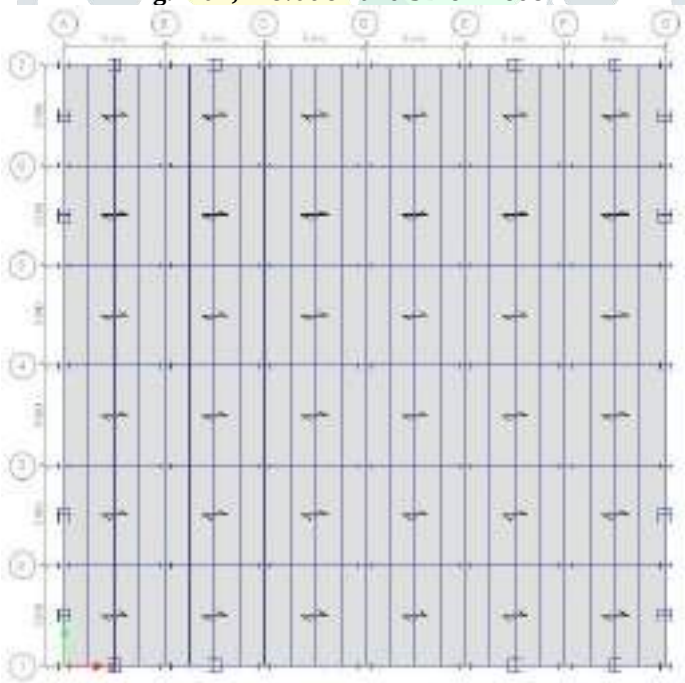

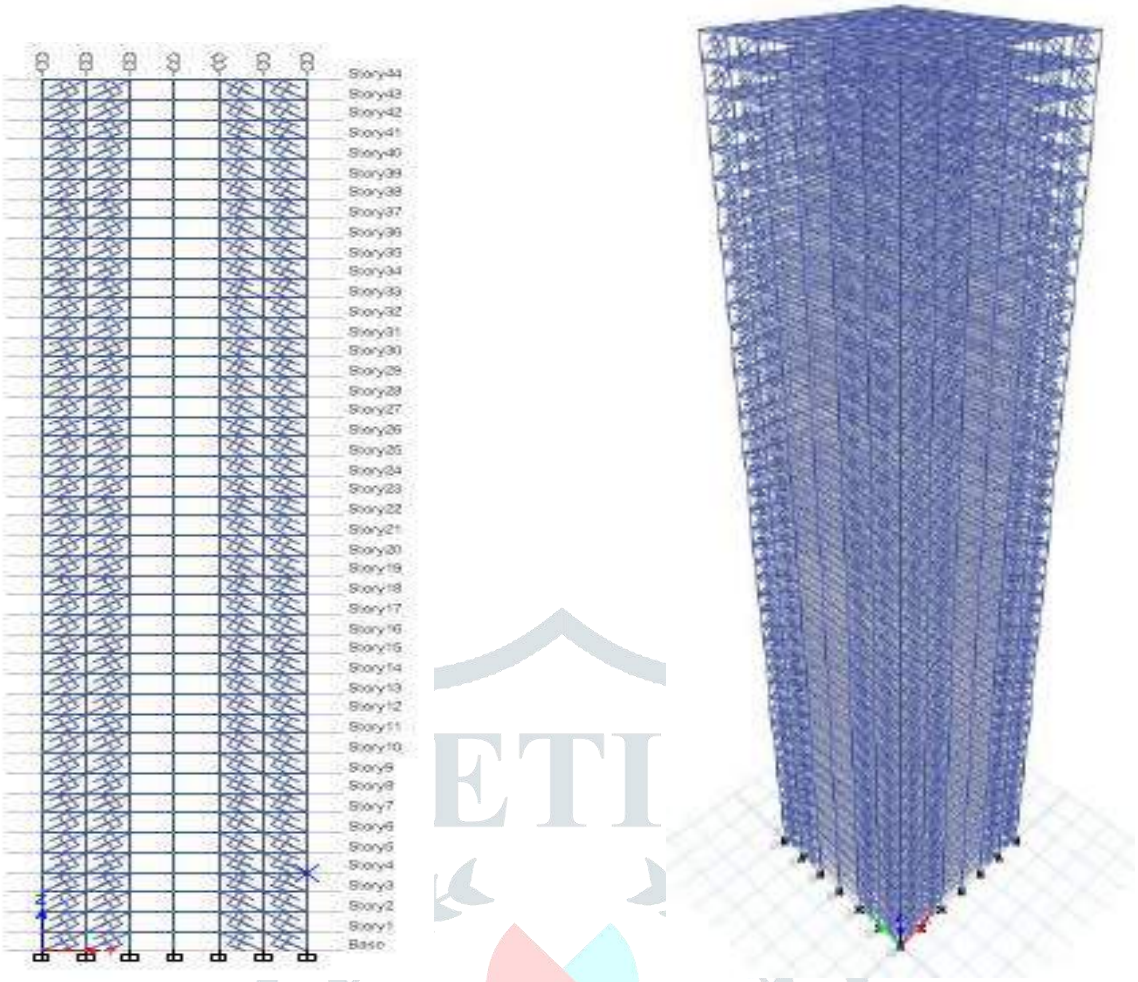

Fig. Plan, Elevation and 3D of Model 3

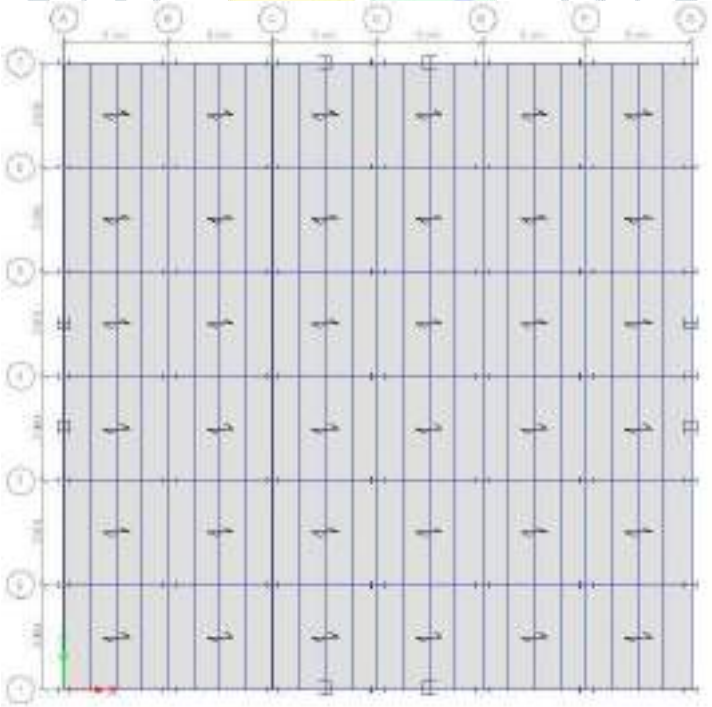

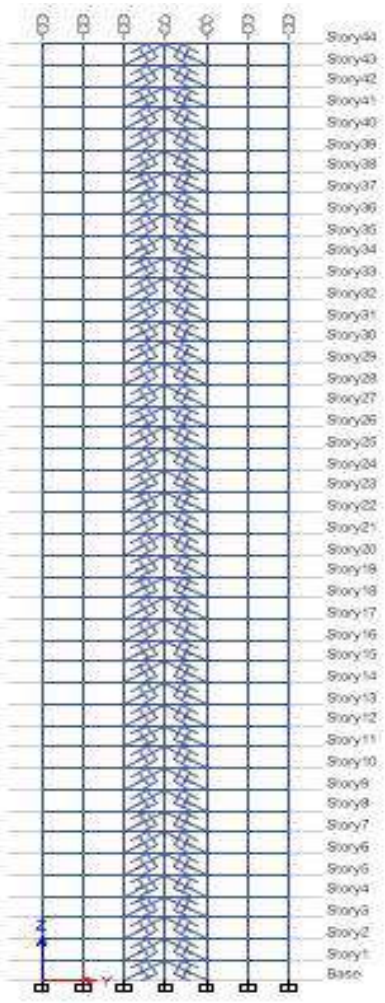

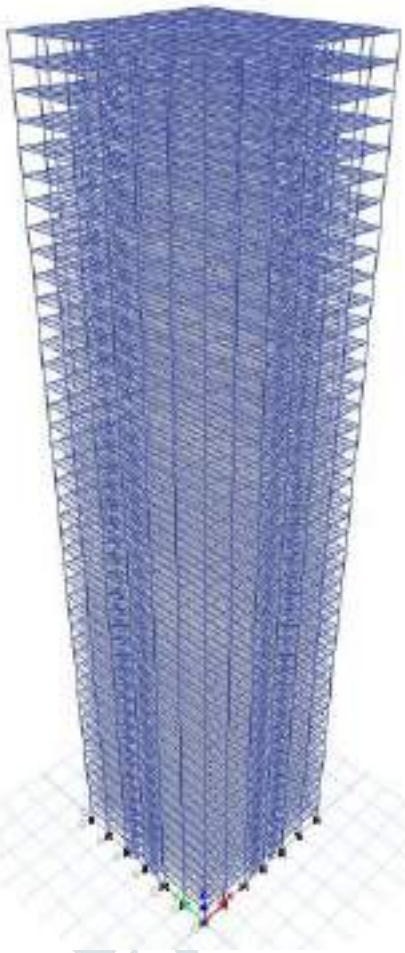

ANALYSIS AND RESULTS

Time period

The natural period (Tn) of a building is the time it takes to go through a complete vibration cycle. This is the inherent nature of the building controlled by its mass "m" and stiffness "k". These three astrological signs are interconnected.

$$Tn = 2\pi\sqrt{m/k}$$

Its unit is second. Buildings that are heavy and flexible have more natural period than light and stiff buildings.

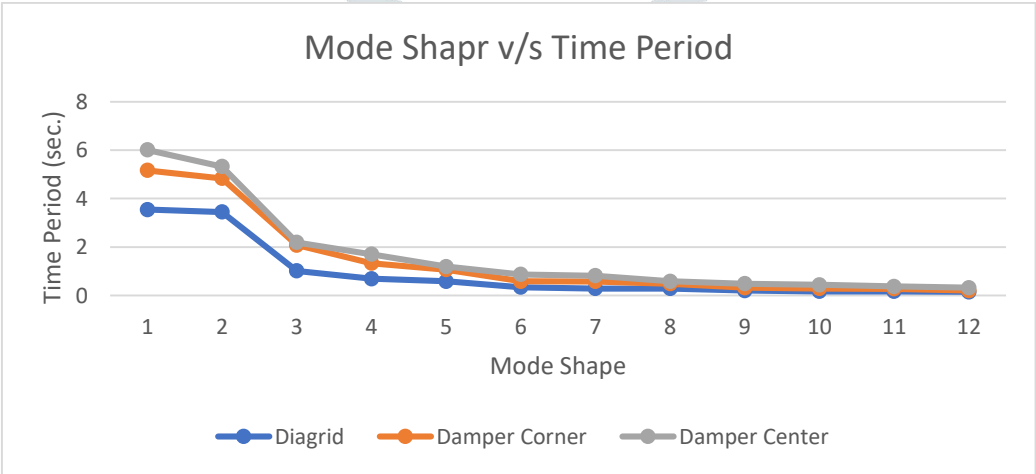

Graph:1 Fundamental natural time period

STORY DRIFT

It is the displacement of one story relative to the other story above or below. The story drift in any story due to the minimum specified design lateral force, with partial load factor of 1, shall not exceed 0.004 times the story height or (h/250).

In Eurocode 8:2004 Part 1 specifies allowable maximum story drift is 1% of story height therefore as per Eurocode permissible limit of drift will be 0.01 X 3000 = 30 mm.

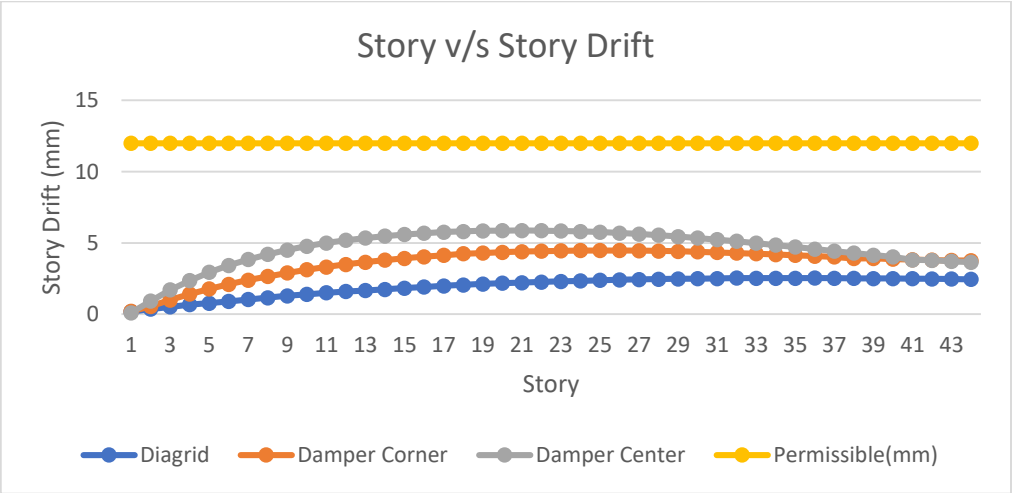

Graph:2 Story v/s Story drift

STORY DISPLACEMENT

It is total displacement of the story with respect to ground. According to IS 1893:2016 Clause deformations, the maximum allowable deflection is calculated as H/250, where h is the height of the story from the ground level. In Eurocode 8:2004 specifies allowable maximum story displacement is H/100.

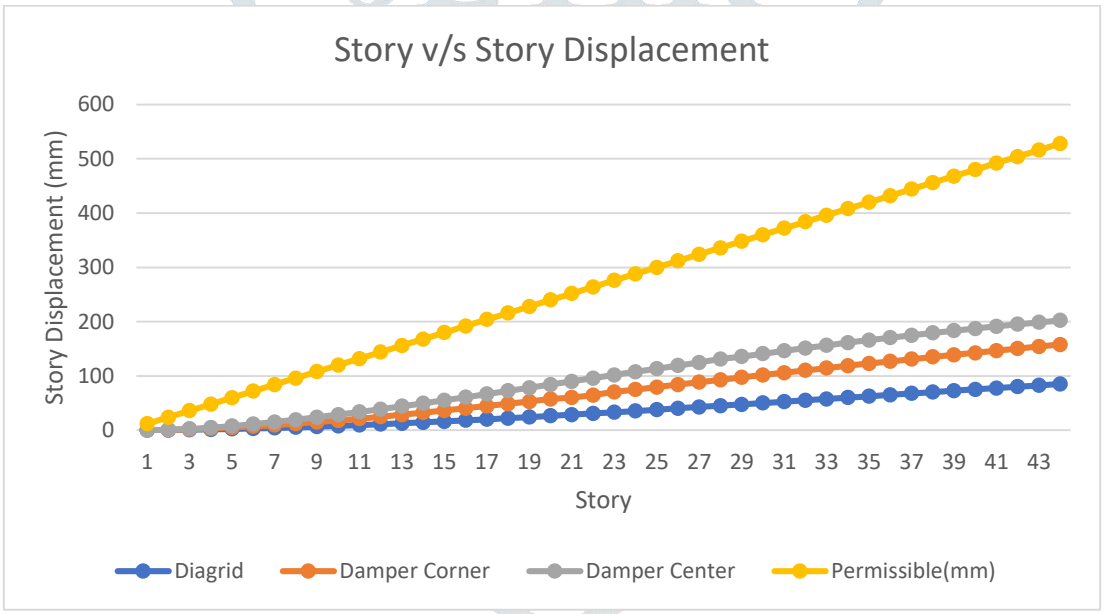

Graph:3 Story v/s Story displacement

BASE SHEAR

IS 1893:2016 (Part I) Auto Seismic Load Calculation:

This calculation presents the automatically generated lateral seismic loads for load pattern EQ-X and EQ-Y according to IS 1893:2016.

$$V_b = A_h \times W$$

Where, Ah= Design horizontal seismic coefficient for structure

W= Seismic weight of the building.

Where, R=response reduction factor.

Z= zone factor.

I= importance factor.

Sa/g=average acceleration response coefficient.

Model	Base Shear (kN)
Model-1	2103.8416
Model-2	2523.47
Model-3	2520.6485

STORY STIFFNESS

The term story stiffness is defined as capability of resisting force/load acting on any story. It is depending on material property, if the story is stiffer it means less flexible.

Story	Diagrid	Damper Corner	Damper Centre
1	23603049.1	989255.573	1192357
2	13287922.4	911726.623	1100669
3	9522098.36	880606.49	1012978
4	7504123.74	847875.789	982994
5	5324271.12	813968.332	953670
6	4430119.54	785484.175	925661
7	3798572.67	755676.824	897729
8	3341870.9	727736.724	869698
9	3088971.22	701896.915	841696
10	2716787.78	677241.584	814024
11	2430655.13	653650.968	787047
12	2233859.77	630998.566	761102
13	1866444.25	609273.233	736439
14	1634880.38	588471.647	713176
15	1452989.15	568593.547	691306
16	1357128.11	549627.73	670728
17	1327309.21	531555.69	651296
18	1221582.59	514357.33	632868
19	1122504.59	498017.136	615337
20	1077200.9	482526.738	598642
21	904764.791	467883.201	582761
22	808354.258	454084.044	567685
23	752267.657	441121.499	553393
24	744096.249	428978.817	539838
25	852749.619	417630.567	526945
26	837264.079	407047.19	511624
27	843980.429	397202.083	500798
28	876017.702	388077.944	490431
29	712401.081	379668.634	480137
30	697105.807	371973.598	470177
31	703746.579	364984	460422
32	731613.417	358662.533	451299
33	805657.926	352922.043	442720
34	796796.367	347608.976	434428
35	796906.861	342500.69	425963
36	805834.033	337313.838	416679
37	702683.862	331749.244	405798
38	652501.375	325497.091	392510

39	598673.57	318438.539	376107
40	536677.112	310297.374	356175
41	470952.78	302023.768	332795
42	338329.857	292442.806	307553
43	213556.812	282322.309	276509
44	198817.56	270715.809	261980

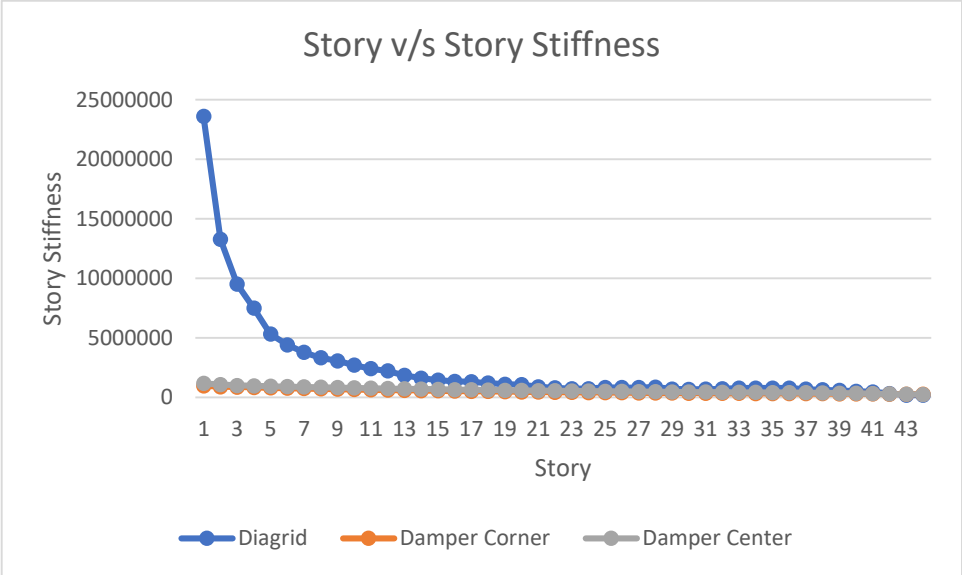

Graph:4 Story v/s Stiffness

CONCLUSION

1. Among all the diagrid model analysed, gives least value in considered parameter. And more in story stiffness.

2. Time taken in first mode is minimum in diagrid structure and in other all with respect to diagrid structure, 49.78% more in Damper in corner and 74.25% more in Damper in centre.

3. Drift is minimum in diagrid overall comparisons shows with respect to diagrid structure, 73.77% more in Damper in corner and 128.16% more in Damper in centre.

4. Displacement is minimum in diagrid structure and in other all with respect to diagrid structure, 85.36% more in Damper in corner and 137.64% more in Damper in centre.

5. Base shear is minimum in diagrid structure cause of less weight of structure and in other all with respect to diagrid structure, 19.94% more in Damper in corner and 19.81% more in Damper in centre.

6. Story stiffness is maximum for Diagrid structure from all models.

From above all I can say, Diagrid structure is much better than other all considered models. And also, in diagrid structure using 20-25% less building material by which weight of building is reduces. For seismic effect one of the major factors is weight of building.

REFERENCES

[1] Ali, M.M. and Moon, K.S., 2007. Structural developments in tall buildings: current trends and future prospects. *Architectural science review*, *50*(3), pp.205-223.

[2] Moon, K.S., 2008. Practical Design Guidelines for Steel Diagrid Structures. In *AEI 2008: Building Integration Solutions* (pp. 1-11).

[3] Kim, J. and Lee, Y.H., 2010. Seismic performance evaluation of diagrid system buildings. *The Structural design of tall and special buildings*, *21*(10), pp.736-749.

[4] Jani, K. and Patel, P.V., 2013. Analysis and design of diagrid structural system for high rise steel buildings. *Procedia Engineering*, *51*, pp.92-100.

[5] MOON, K., 2013, September. Optimal structural configurations for tall buildings. In *Proceedings of the Thirteenth East Asia-Pacific Conference on Structural Engineering and Construction (EASEC-13)* (pp. G-4). The Thirteenth East Asia-Pacific Conference on Structural Engineering and Construction (EASEC-13).

[6] Yadav, S. and Garg, V., 2015. Advantage of steel diagrid building over conventional building. *International Journal of Civil and Structural Engineering Research (ISSN)*, *3*(01), pp.394-406.

[7] Bhale, P. and Salunke, P.J., 2016. Analytical Study and Design of Diagrid Building and Comparison with Conventional Frame Building. *International Journal of Advanced Technology in Engineering and Science*, (4).

[8] Shah, M.I., Mevada, S.V. and Patel, V.B., 2016. Comparative study of diagrid structures with conventional frame structures. *Int. J. Eng. Res. Appl. (IJERA)*, *6*(5), pp.22-29.

[9] Asadi, E., Li, Y. and Heo, Y., 2018. Seismic performance assessment and loss estimation of steel diagrid structures. *Journal of Structural Engineering*, *144*(10), p.04018179.

[10] Meghna, Singh V. K. (2019) Structural Performance of Four Storey Diagrid Tall Building. JETIR, 2019 May, Volume 6, Issue 5 (ISSN-2349-5162)

[11] Radmard Rahmani, H. and Könke, C., 2019. Seismic control of tall buildings using distributed multiple tuned mass dampers. *Advances in Civil Engineering*, *2019*.

[12] Dadkhah, H. and Mohebbi, M., 2019. Performance assessment of an earthquake-based optimally designed fluid viscous damper under blast loading. *Advances in Structural Engineering*, *22*(14), pp.3011-3025.

[13] S. Lakshmi Shireen Banu, Kothakonda Ramesh (2019). Seismic Response Study and Evaluation of Vibration Control of Elevated RCC Structure using Friction Damper. IJITEE, 2019.

[14] S.lakshmishireenbanu, pathaushasri,(2019). Study of Seismic Energy Dissipation and Effect in Multistory RCC Building with and Without Fluid Viscous Dampers. IJITEE, 2019.

[15] De Domenico, D. and Ricciardi, G., 2019. Earthquake protection of structures with nonlinear viscous dampers optimized through an energy-based stochastic approach. *Engineering Structures*, *179*, pp.523-539.

[16] Dadkhah, H. and Mohebbi, M., 2019. Performance assessment of an earthquake-based optimally designed fluid viscous damper under blast loading. *Advances in Structural Engineering*, *22*(14), pp.3011-3025.

[17] De Domenico, D., Ricciardi, G. and Takewaki, I., 2019. Design strategies of viscous dampers for seismic protection of building structures: a review. *Soil Dynamics and Earthquake Engineering*, *118*, pp.144-165.

[18] Del Gobbo, G.M., 2019, June. Placement of fluid viscous dampers to improve total-building seismic performance. In *Proceedings of the CSCE Annual Conference, Laval, Montreal, QC, Canada* (pp. 12-15).

[19] Patle, Y.Z., Gajghate, V. and Manchalwar, A., Seismic Response Control of Adjacent Building Using Fluid Viscous Damper.

[20] Sahu, G. and Sahu, P., 2019. COMPARATIVE ANALYSIS OF EFFECTS OF BASE ISOLATOR & FLUID VISCOUS DAMPER ON RESPONSE OF A RCC STRUCTURE.

[21] Koshti, A., Shinde, S., Yamagar, K. and Shegunshi, S., Seismic Response of Structure with Fluid Viscous Damper (FVD).

[22] IS: 800:2007 General Construction of Steel- Code of Practice.

[23] IS: 456:2000 Plain and Reinforced Concrete- Code of Practice.

[24] IS: 1893(Part-1):2016 Criteria for Earthquake Resistant Design of Structures.

[25] IS: 875 (Part 2) - 1987, Code of Practice Design Loads (Other Than for Earthquake) For Buildings and Structures.

[26] IS: 13920:2016 Ductile Design and Detailing of Reinforced Concrete Structures Subjected to Seismic Forces- Code of Practice.

[27] Eurocode 8: Design of structures for earthquake resistance, 2004.

Journal of Emerging Technologies and Innovative Research
An International Open Access Journal Peer-reviewed, Refereed Journal
www.jetir.org | editor@jetir.org An International Scholarly Indexed Journal

Certificate of Publication

The Board of

Journal of Emerging Technologies and Innovative Research (ISSN : 2349-5162)

Is hereby awarding this certificate to

VIKASH YADAV

In recognition of the publication of the paper entitled

SEISMIC STUDY OF DIAGRID STRUCTURE WITH DAMPER OF DIFFERENT ARRANGEMENT

Published In JETIR (www.jetir.org) ISSN UGC Approved (Journal No: 63975) & 7.95 Impact Factor

Published in Volume 7 Issue 6 , June-2020 | Date of Publication: 2020-06-18

Parisa P
EDITOR

EDITOR IN CHIEF

JETIR2006265 Research Paper Weblink http://www.jetir.org/view?paper=JETIR2006265 Registration ID : 234347

International Journal of All Research Education and Scientific Methods (IJARESM), ISSN: 2455-6211
Volume 9, Issue 1, January-2021, Impact Factor: 7.429, Available online at: www.ijaresm.com

Mold Flow Simulation of "Car Door Handle" for Optimization of warpage by Using Different Gate System

Gajanan G Khirao[1], Prof. R. R. Kulkarni[2], Prof. B B Kedar[3], Prof. Dr. P A Makasare[4]

[1]PG Scholar, Department of Mechanical Engineering, Siddhant College of Engineering, Pune
[2,3,4]Professor, Department of Mechanical Engineering, Siddhant College of Engineering, Pune

----------**********----------

ABSTRACT

Mold flow simulation helps designers to see how their designs will be resulted after injection molding process without needing to do the Injection molding process. The use of simulation programs saves time and reduces the costs of the Molding system design. Injection molding design simulation holds an important role in analyzing the outcome of the design. In this paper plastic Car door handle is analyzed and studied to solve the problems war page by using different gate system with different dimensions of gate like Edge gate & Fan gate etc. All the designs were simulated with Autodesk Mold flow Insight & Adviser. Autodesk Simulation Mold flow effectively eliminates the use of trial and error method by validating and optimizing the Design of plastic before production. This not only improves the quality but also help us to guide about the selection of machines and the production planning.

Keywords: Injection molding, Mold design, Mold flow simulation, Optimization Plastic Injection Mold, Mold Flow Plastic.

1. INTRODUCTION

Injection Molding is one of the common methods to do the mass-production of plastic product. Thermoplastics are science's gift to the toy industry. They can be melted at fairly low Temperatures, molded in colors with fine detail, and stand up well to play wear because of their Resilience.. Injection molding is the most commonly used manufacturing process for the Fabrication of plastic parts. A wide variety of products are manufactured using injection molding, which vary greatly in their size. Complexity and application. Injection Molding is the way most of our plastic toys are created. The material is injected under pressure into a two-part mold. The material is allowed to cool, The mold is opened, and the solid product inside is ejected into a collection hopper. Common Problems associated with injection molding are numerous.

Nowadays, Computer Aided Design is not limited to sketching and drafting, but also helps to create analyzable models as needed for computer based process simulation. Mold flow Software, used solution for Digital Prototyping, provides injection molding simulation tools for use on digital prototypes. Providing in-depth validation and optimization of plastic parts and associated injection molds, Mold flow software helps study the injection molding processes in use today. The Autodesk Simulation Mold flow results help to identify the main problem areas before the part is manufactured that are particularly difficult to predict with traditional Methods. In conventional optimization process includes actual shop floor trials in which pattern, feeder size, shape and location cores, mold layout, gating etc are required to be changed in each iteration which is associated with machining cost, tooling cost, modification cost, melting cost, fettling and transportation cost as well as energy, materials, time are wasted in each trial until and unless the required results are obtained.

Analysis is essential for designing and mold making through simulation step-up and result interpretation to show how changes to wall thickness, gate location, material and geometry affects manufacturability and also experiments with "what-if" scenarios before finalizing a design. Injection Molding simulation software into the mold design process in order to analyze the product, foresee the possible defects, and optimize the design to achieve the maximum outcome of the products with minimum cycle time in each production cycle . Door handles are the only hardware used for opening and closing of doors. Doors are used by every individual and for its functionality door handles are used. Doors are used for security purposes of our belongings and automobiles. There are many kinds of doors like passage; closet, dummy doors etc. similarly there are various kinds of door handles used for variety of doors and their functionality. Door handles are installed on doors to simply open and close the door with minimum effort. Sometimes door handles are equipped with locks for

better sense of security and safety. Lockless door handles are also available in the market. In this project we have classified door handles into three categories such as (i) pull handles (ii) door knobs and (iii) lever handles..

2. LITERATURE REVIEW

Lyd´eric Bocquet1 , Annie Colin2, Armand Ajdar [1] , have did research to design A kinetic model for the elasto-plastic dynamics of a flowing jammed material is proposed, which takes the form of a non-local – Boltzmann-like – kinetic equation for the stress distribution function. Coarse-graining this equation yields a non-local constitutive law for the flow, introducing as a key dynamic quantity the local rate of plastic events. This quantity, interpreted as a local fluidity, is spatially correlated, with a correlation length diverging in the quasi-static limit, i.e. close to yielding. We predict finite size effects in the flow behavior, as well as the absence of an intrinsic local flow curves. These features are supported by recent experimental and numerical observation.

Soft amorphous materials such as foams, emulsions, granular systems or colloidal suspensions display complex flow properties at high enough concentrations, intermediate between that of a solid and a liquid: at rest they behave like an elastic solid, but are able to flow "like a liquid" under sufficient applied stress . This mixed fluid/solid behavior occurs above a threshold volume fraction associated with the appearance of a yield stress σd. The yielding behavior makes such systems particularly interesting for applications – from tooth paste, coatings to cosmetic and food emulsions –,but fundamentally difficult to describe. Furthermore, it has been recognized over the recent years that this yielding behavior is, in most cases, associated with peculiar spatial features. This takes the form of inhomogeneous flow patterns, such as shear-bands, or cooperativity in the flow or deformation response, potentially associated with non-locality in the constitutive rheological law and dependence of the flow on the nature of the boundaries. While such features appear to be generic for this class of materials, suggesting a underlying common flow scenario, a consistent framework linking the global rheology to the local microscopic dynamics is still lacking.

I. Marchenko & Chaouqi Misbah [2] Starting from known kinematic picture for plasticity, we derive a set of dynamical equations describing plastic flow in a Lagrangian formulation. Our derivation is a natural and a straight forward extension of simple fluids, elastic and viscous solids theories. These equations contain the Maxwell model as a special limit. We discuss some results of plasticity which can be described by this set of equations. We exploit the model equations for the simple examples: straining of a slab and a rod. We find that necking manifests always itself (not as a result of instability), except if the very special constant-velocity stretching process is imposed. This will work towards bringing the sprung to unsprung mass ratio closer to the original value, and therefore allow for further reduction of the unsprung mass as well as sprung mass.

Pierre Le Doussal1, M. Cristina Marchetti2, Kay Jorg Wiese ¨ 1 [3]l, Studied model of two layers, each consisting of a d-dimensional elastic object driven over a random substrate, and mutually interacting through a viscous coupling. For this model, the mean-field theory (i.e. a fully connected model) predicts a transition from elastic depinning to hysteretic plastic depinning as disorder or viscous coupling is increased. A functional RG analysis shows that any small inter-layer viscous coupling destabilizes the standard (decoupled) elastic depinning FRG fixed point for $d \leq 4$, while for $d > 4$ most aspects of the mean-field theory are recovered. A one-loop study at non-zero velocity indicates, for $d < 4$, coexistence of a moving state and a pinned state below the elastic depinning threshold, with hysteretic plastic depinning for periodic and non-periodic driven layers. A 2-loop analysis of quasi-statics unveils the possibility of more subtle effects, including a new universality class for non-periodic objects. We also study the model in $d = 0$, i.e. two coupled particles, and show that hysteresis does not always exist as the periodic steady state with coupled layers can be dynamically unstable. It is also proved that stable pinned configurations remain dynamically stable in presence of a viscous coupling in any dimension d. Moreover, the layer model for periodic objects is stable to an infinitesimal commensurate density coupling. Our work shows that a careful study of attractors in phase space and their basin of attraction is necessary to obtain a firm conclusion for dimensions $d = 1, 2, 3$

F. Boulogne & S.J. Cox [4] We simulate quasistatic flows of an ideal two-dimensional monodisperse foam around different obstacles, both symmetric and asymmetric, in a channel. We record both pressure and network contributions to the drag and lift forces, and study them as a function of obstacle geometry. We show that the drag force increases linearly with the cross section of an obstacles. The lift on an asymmetric aerofoil-like shape is negative and increases with its arc length, mainly due to the pressure contribution.

Jie Lin & Matthieu Wyart [5] , Failure and flow of amorphous materials are central to various phenomena including earthquakes and landslides. There is accumulating evidence that the yielding transition between a flowing and an arrested phase is a critical phenomenon, but the associated exponents are not understood, even at a mean-field level where the validity of popular models is debated. Here we solve a mean-field model that captures the broad distribution of the mechanical noise generated by plasticity, whose behavior is related to biased L´evy flights near an absorbing boundary. We compute

the exponent θ characterizing the density of shear transformation $P(x) \sim x\theta$, where x is the stress increment beyond which they yield. We find that after an isotropic thermal quench, $\theta = 1/2$. However, θ depends continuously on the applied shear stress, this dependence is not monotonic, and its value at the yield stress is not universal. The model rationalizes previously unexplained observations, and captures reasonably well the value of exponents in three dimensions. Values of exponents in four dimensions are accurately predicted. These results support that it is the true mean-field model that applies in large dimension, and raise fundamental questions on the nature of the yielding transition..

Akira Onuki [6] discussed that a phenomenological time- dependent Ginzburg-Landau theory of nonlinear plastic deformations in solids. Because the problem is very complex, we first give models in one and two dimensions without vacancies and interstitials, where large strains produce densely distributed slips but the mass density deviations remain small except near the tips of slips. Next we set up a two-dimensional model including a vacancy field (or local free-volume fraction), where relevant is the sensitive dependence of the elastic shear modulus on the vacancy density. In our simulation, if strains are applied to nearly defect less solids but in the presence of such elastic inhomogeneity, the vacancy density and the mass density can become considerably heterogeneous for large strains on spatial scales much longer than the atomic size. These strain-induced disordered states are metastable or long-lived once they are created.

Akira Onuki [7] A time-dependent Ginzburg-Landau model of plastic deformation in two-dimensional solids is presented. The fundamental dynamic variables are the displacement field u and the lattice velocity $v = \partial u/\partial t$. Damping is assumed to arise from the shear viscosity in the momentum equation. The elastic energy density is a periodic function of the shear and tetragonal strains, which enables formation of slips at large strains. In this work we neglect defects such as vacancies, interstitials, or grain boundaries. The simplest slip consists of two edge dislocations with opposite Burgers vectors. The formation energy of a slip is minimized if its orientation is parallel or perpendicular to the flow in simple shear deformation and if it makes angles of $\pm\pi/4$ with respect to the stretched direction in uniaxial stretching. High-density dislocations produced in plastic flow do not disappear even if the flow is stopped. Thus large applied strains give rise to metastable, structurally disordered states. We divide the elastic energy into an elastic part due to affine deformation and a defect part. The latter represents degree of disorder and is nearly constant in plastic flow under cyclic straining.@ PACS numbers: 62.20.Fe, 61.72.Lk, 81.40.Lm, 83.20.Jp

By B. Dollet , A Scagliarini and M. Sbragaglia [8], In order to understand the flow profiles of complex fluids, a crucial issue concerns the emergence of spatial correlations among plastic rearrangements exhibiting cooperativity flow behavior at the macroscopic level. In this paper, the rate of plastic events in a Poiseuille flow is experimentally measured on a confined foam in a Hele-Shaw geometry. The correlation with independently measured velocity profiles is quantified. To go beyond a limitation of the experiments, namely the presence of wall friction which complicates the relation between shear stress and shear rate, we compare the experiments with simulations of emulsion droplets based on the lattice-Boltzmann method, which are performed both with, and without, wall friction. Our results indicate a correlation between the localization length of the velocity profiles and the localization length of the number of plastic events. Finally, unprecedented results on the distribution of the orientation of plastic events show that there is a non-trivial correlation with the underlying local shear strain. These features, not previously reported for a confined foam, lend further support to the idea that cooperativity mechanisms, originally invoked for concentrated emulsions (Goyon et al. 2008),have parallels in the behavior of other soft- glassy materials

Kamran Karimi [9] , We report on a particle-based numerical study of sheared amorphous solids in the dense slow flow regime. In this framework, deformation and flow are accompanied by critical fluctuation patterns associated with the macroscopic plastic response and single particle kinematics. The former is commonly attributed to the collective slip patterns that relax internal stresses within the bulk material and give rise to an effective mechanical noise governing the latter particle-level process. In this work, the avalanche-type dynamics between plastic events is shown to have a strong relevance on the self-diffusion of tracer particles in the Fickian regime. As a consequence, strong size effects emerge in the effective diffusion coefficient that is rationalized in terms of avalanche size distributions and the relevant temporal occurrence.

Violeta Karyofylli, Loïc Wendling, Michel Make, Norbert Hosters and Marek Behr [10] The quality of plastic parts produced through injection molding depends on many factors. Especially during the filling stage, defects such as weld lines, burrs, or insufficient filling can occur. Numerical methods need to be employed to improve product quality by means of predicting and simulating the injection molding process. In the current work, a highly viscous incompressible non-isothermal two-phase flow is simulated, which takes place during the cavity filling. The injected melt exhibits a shear-thinning behavior, which is described by the Carreau-WLF model. Besides that, a novel discretization method is used in the context of 4D simplex space-time grids [2].

This method allows for local temporal refinement in the vicinity of, e.g., the evolving front of the melt [10]. Utilizing such an adaptive refinement can lead to locally improved numerical accuracy while maintaining the highest possible

computational efficiency in the remaining of the domain. For demonstration purposes, a set of 2D and 3D benchmark cases, that involve the filling of various cavities with a distributor, are presented.

G Ashif S. Iquebal, Dinakar Sagapuram, and Satish Bukkapatnam [11] We report electron microscopy observations of the surface plastic flow in polishing of rough metal surfaces with a controlled spherical asperity structure. We show that asperity–abrasive sliding contacts exhibit viscous behavior, where the material flows in the form of thin fluid-like layers. Subsequent bridging of these layers among neighboring asperities result in progressive surface smoothening. Our study provides new phenomenological insights into the long-debated mechanism of polishing. The observations are of broad relevance in tribology and materials processing.

M.-Carmen Miguel1 & Stefano Zapperi [12] , A new class of artificial atoms, such as synthetic nanocrystals or vortices in superconductors, naturally self-assemble into ordered arrays. This property makes them applicable to the design of novel solids, and devices whose properties often depend on the response of such assemblies to the action of external forces. Here we study the transport properties of a vortex array in the Corbino disk geometry by numerical simulations. In response to an injected current in the superconductor, the global resistance associated to vortex motion exhibits sharp jumps at two threshold current values. The first corresponds to a tearing transition from rigid rotation to plastic flow, due to the reiterative nucleation around the disk center of neutral dislocation pairs that unbind and glide across the entire disk. After the second jump, we observe a smoother plastic phase proceeding from the coherent glide of a larger number of dislocations arranged into radial grain boundaries.

D M Nuruzzaman1, N Kusaseh2, S Basri2, A N Oumer3 and Z Hamedon [13] observed In the production of complex plastic parts, injection molding is one of the most popular industrial processes. This paper addresses the modeling and analysis of the flow process of the nylon (polyamide) polymer for injection molding process. To determine the best molding conditions, a series of simulations are carried out using Autodesk Moldflow Insight software and the processing parameters are adjusted. This mold filling commercial software simulates the cavity filling pattern along with temperature and pressure distributions in the mold cavity. In the modeling, during the plastics flow inside the mold cavity, different flow parameters such as fill time, pressure, temperature, shear rate and warp at different locations in the cavity are analyzed. Overall, this Moldflow is able to perform a relatively sophisticated analysis of the flow process of pure nylon. Thus the prediction of the filling of a mold cavity is very important and it becomes useful before a nylon plastic part to be manufactured.

S. D. Sonawane* & S. K. Dahake [14] , In Past, Mold Design process was time-consuming as well as hectic. At first, Manual Drawing and then 2D software were used; after which patterns were made. But the results were not convincing most of the times. Thus the design to market time increased immensely and also project cost required was on a higher side. Due to the technological advancements, the process of Mold Design has fastened and also the results are convincing. With the help of 3D software, Parametric Designs can be created, which are editable. Also we can look at number of possibilities for designing a mold. In a 3D software, Visualization of our creation is easy possible. Thus the design to market time get shrink immensely also the project cost required is on lower side. Using CAD/CAM/CAE Software, companies can be very much assured that their product will be of a good aesthetics, it will be more durable, more accurate, and will launched in time. They can actually view and modify the product on computer before actually manufacturing it. 3D CAD Technology in Mold Design helps in Heavy Reduction in Design Time and Design Cost in Long term, also Optimization in Designing. We can work out multiple options and choose the efficient one. Better Visualization of objects before actual production is achieved. Mold flow Analysis makes it easy to judge the flow of material in the mold. CAD data can be used for creating manufacturing program using CAM i.e. Computer Aided Manufacturing .

Holger Mensler ,1 Shujun Zhang,2 Thomas Win2 [15], During the filling phase of an injection molding process, the flow front velocity of the plastics melt has a decisive influence on the form part quality. It has been believed that a constant flow front velocity of the melt leads to distortion free and residual stress-free form parts. A process control strategy based on a constant flow front velocity of the melt, however, requires the full understanding of the flow front position as a function of the screw position of the injection molding machine. With current methods, this can only be achieved by direct measurements using a number of sensors inside the mold, which leads to complicated structure, great efforts, and high cost for the tooling equipment. This article proposes, designs, and develops an innovative method for determining the flow front velocity of a plastic melt in an injection molding using only one pressure sensor at the front of the screw and based on the idea of mapping a simulated filling process to a real injection molding process. The mapping ensues that the characteristic event points are identified and matched for both the simulated and real filling process. The results of the simulation analysis and experimental evaluation show that the proposed method can be used to determine the flow front position and the resulting flow front velocity of the melt within the cavity of the mold and provide evidence that the new method offers great potential to process control strategies based on machine independent parameters. POLYM. ENG. SCI., 00:000–000, 2019.

3. PROBLEM STATEMENT

As warpage is common found in every plastic material here case is Door Handle, The part should be completely fill in injection molding process and sufficient package pressure should be provided. But practically it is not possible to predict the warpage, filling time, package pressure so mold flow analysis software is used. The main aim of this project is to mold flow analysis of ‘ car door handle ’ for filling, packing, warp and cool analysis, and optimizing process parameters for warpage by using different feed systems.

4. OBJECTIVES:

To optimize warpage value in door Handle by using different gate system with different dimensions like edge gate & Fan Gate etc.

5. METHODOLOGY

Methodology used in the Mold flow analysis of the Handle

Research Paper:
For This Project We were focusing on finding research papers for prediction of research gap and the idea to find new concept with mind-set of project development regarding injection molding process and their defect . The research papers were gave us the domains and works which were already completed and provided lots of information regarding mold flow analysis of plastic handle and other plastic components for optimization of process parameters and warpage value.

Collection of Data:
From research papers and resources we were collect the data for mold flow analysis used for different plastic component. We were come to know the different material used for handle and plastic component. The all collected data was used for getting proper path for development of plastic component.

Catia Part Data Arrangement:
For our project the next step to arrange the standard design of handle. I have taken the standard handle 3D CAD model. Design of actual bumper to crash analysis of wheel rim with approximate calculations of different forces acting on wheel rim. For Catia modeling we have taken the help of some of the research papers and car catalogue we developed the 3D model of our project that is wheel rim design in CATIA v5 software

Mold Flow Simulation:
In this step we will perform following two step 5.4.1.FEA Modeling
In this step we will do the meshing of 3D CAD model of handle to meet criteria for Mold Flow Analysis .It is available in Autodesk Simulation Mold Flow Insight Ultimate Software

Feed System Design:
Analysis Run for
Analysis of the gate location
Analysis of cavity filling (Fill)
Analysis of filling and packing pressure
Analysis of runner balance (runner balance)
Analysis of cooling (cool)
Analysis of warpage and shrinkage h)

Result and Conclusion:
In This step result of Gate Location, Filling Analysis, and Final Result of Warpage Analysis is interpreted. Based on result of all analysis conclusion is made.

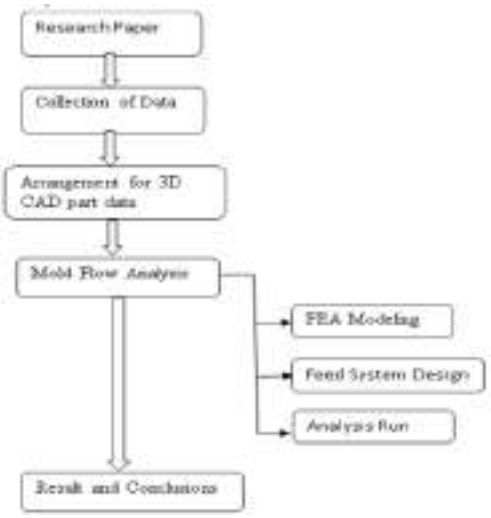

Figure 1: Methodology of current work

6. PLASTIC MATERIAL

Practically stated, a plastic is an organic polymer, available in some resin form or some form derived from the basic polymerized resin. These forms can be liquid or paste like resins for embedding, coating, and adhesive bonding, or they can be molded, laminated, or formed shapes, including sheet, film, or larger-mass bulk shapes. The number of basic plastic materials is large, and the list is increasing. In addition, the number of variations and modifications to these plastic materials is also quite large. The methods by which these materials are processed, finished, and prepared for final use is also immense. Together, the resultant quantity of materials and processes available is just too large to be completely understood and correctly applied by anyone other than those whose day-to-day work puts them in direct contact with a diverse selection of materials. The practice of mixing brand names, tradenames, and chemical names of various plastics only makes the problem of understanding these materials more troublesome. Although there are numerous minor classification schemes for polymers, depending on how one wishes to categorize them, nearly all polymers can be placed in one of two major classifications— thermosetting materials (or thermosets) and thermoplastic materials. Likewise, foams, adhesives, embedding resins, elastomers, and so on, can be subdivided into thermoplastic and thermoset-ting classifications.

Thermosetting Plastics As the name implies, thermosetting plastics or thermosets are cured, set, or hardened into a permanent shape. Curing is an irreversible chemical reaction known as cross-linking, which usually occurs under heat. For some thermosetting materials, curing is initiated or completed at room temperature. Even here, however, it is often the heat of the reaction or the exotherm that actually cures the plastic material. Such is the case, for instance, with a room-temperature-curing epoxy or polyester compound. The cross- linking that occurs in the curing reaction is brought about by the link-ing of atoms between or across two linear polymers, resulting in a three-dimensional rigidized chemical structure. One such reaction is shown in Fig. IN.1. Although the cured thermoset part can be softened by heat, it cannot be re melted or restored to the flowable state that existed before curing. Continued heating for long times leads to de gradation or decomposition. In general, unfilled thermosetting plastics tend to be harder, more brittle, and not as tough as thermoplastics. Thus it is common practice to add filler to thermosetting materials. A wide variety of fillers can be used for varying product properties. For molded products, usually compression or transfer molding, mineral or cellulose fillers are often used as lower-cost, general-purpose filler and glass fiber fillers are often used or optimum strength or dimensional stability. There are also many product and processing trade- offs, but a general guide to the application of filler can be found in several major texts on the subject. It should be added that filler form and filler surface treatment could also be major variables. Thus it is important to consider fillers along with the thermosetting material, especially for molded products. Other product forms may be filled or unfilled, depending on requirements.

7. CAD DESIGN AND MOLDFLOW SIMULATION WORKBENCH

The objective of the experimentation to assess the developed system for showing time domain plots for particular response and temperature variation. Experimentation carried on a heat exchanger device for temperature monitoring and

on mobile phone for vibration monitoring. The temperature recording is continued till steady state temperature is achieved which can be verified by plotting Time Vs Temperature graph.

It is a multi-platform CAD/CAM/CAE commercial software suite developed by the French company Dassault Systems and marketed worldwide by IBM. Written in the C++programming language, CATIA is the cornerstone of the Dassault Systems product lifecycle management software suite. The software was created in the late 1970s and early 1980s to develop Dassault's Mirage fighter jet, then was adopted in the aerospace, automotive, shipbuilding, and other industries.

8. STEPS IN MOLD FLOW SIMULATION

- Import CAD Model into Autodesk Mold flow
- Pre-Processor or Auto Meshing Part
- Cooling System Design
- Gate System Design
- 8.5. Run Gate location Analysis
- Auto Run Fill Analysis
- Set Machine parameters
- Run Fill + Pack + Warp Analysis + Cooling Analysis
- Result

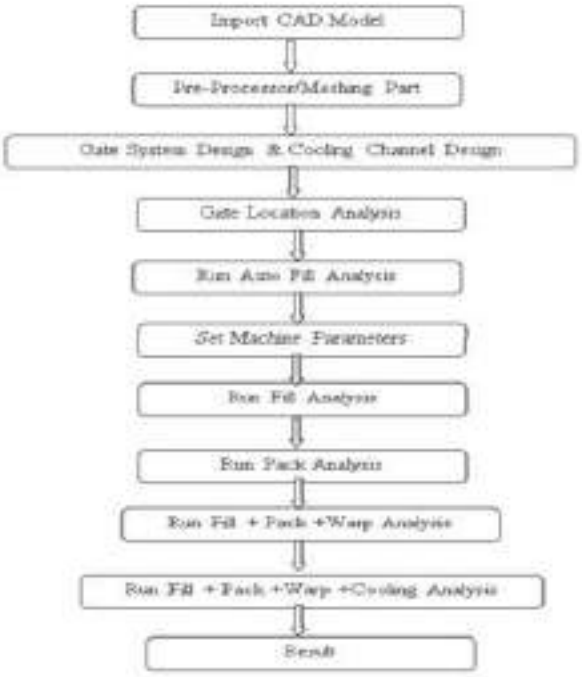

Figure 2: Autodesk Moldflow Simulation Analysis Flow Chart

9. IMPORT CAD MODEL INTO AUTODESK MOLDFLOW INSIGHT SOFTWARE

Figure 3: Door Handle CAD Model

10. COOLING SYSTEM DESIGN

(Cooling channel positions & dimensions are considered as in given tool layout)

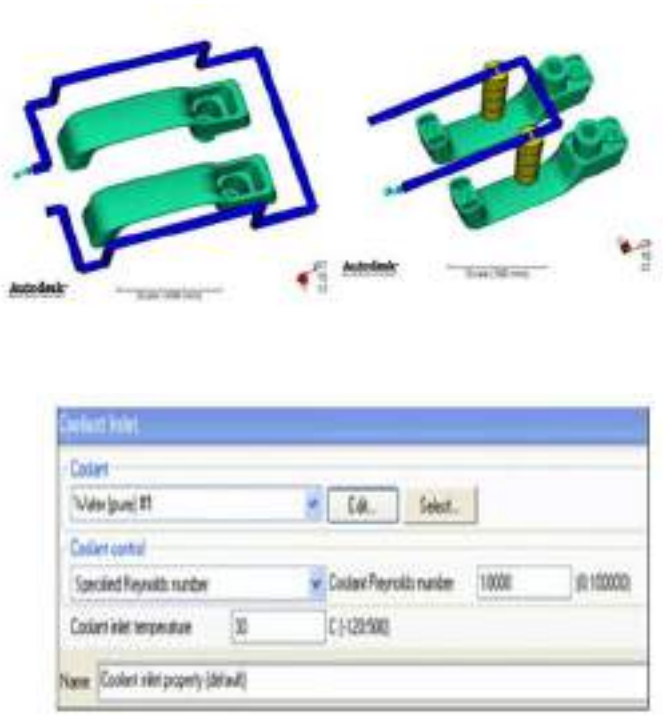

Figure 4: Cooling System & Parameters

Cooling channel - Dia 10 mm Baffle Diameter -24 mm

11. MATERIAL DETAILS

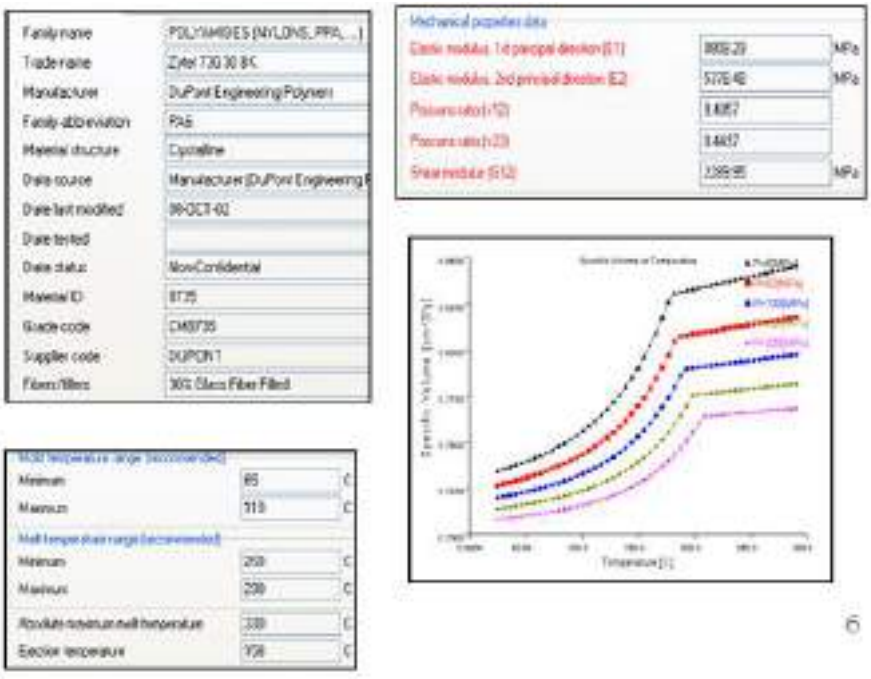

International Journal of All Research Education and Scientific Methods (IJARESM), ISSN: 2455-6211
Volume 9, Issue 1, January-2021, Impact Factor: 7.429, Available online at: www.ijaresm.com

12. PROCESS PARAMETERS

Cycle Time: injection time + Packing time + cooling time
Cycle Time: 3.4 + 10+ 320 ~ 334 s.
Cooling time is time to freeze the part 100%, but it can cooled outside the part also after ejected from mold.
It may need cooling fixture or quenching in water is necessary.

13. GATE SYSTEM DESIGN

Gate System Option 01

Feed system details:- Cold runner as shown below (All dimensions are considered as in given tool layout Edge type gate with Start Width =3.0mm, Start Thik =1.8mm End width = 2.5mm, End Thik = 2.5mm

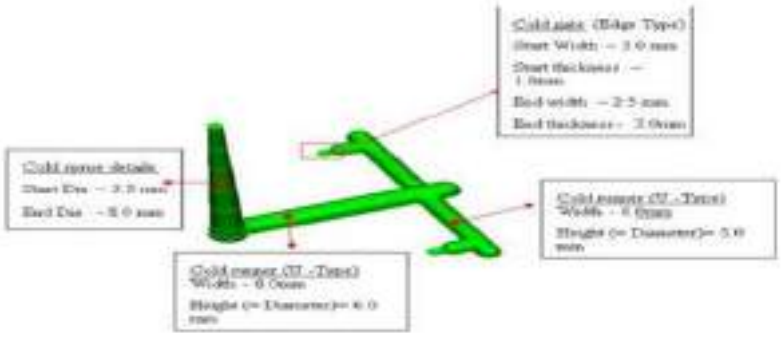

Gate System Option 02

Feed system design with Fan type gate
Start Width =20mm, Start Thik =2.0mm
End width = 15mm, End Thik = 4mm

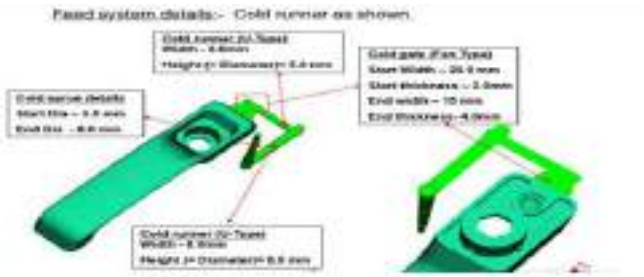

Gate System Option 03
Feed system design with Edge type gate
Start Width =3.0 mm, Start Thik =1.8 mm
End width = 3.0 mm, End Thik = 2.5mm

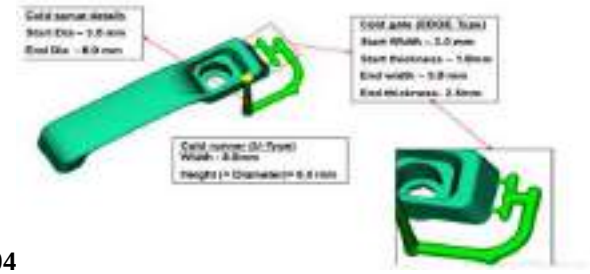

Gate System Option 04
Feed system design with Edge type gate
Start Width =20mm, Start Thik =2.0mm
End width = 15mm, End Thik = 4mm

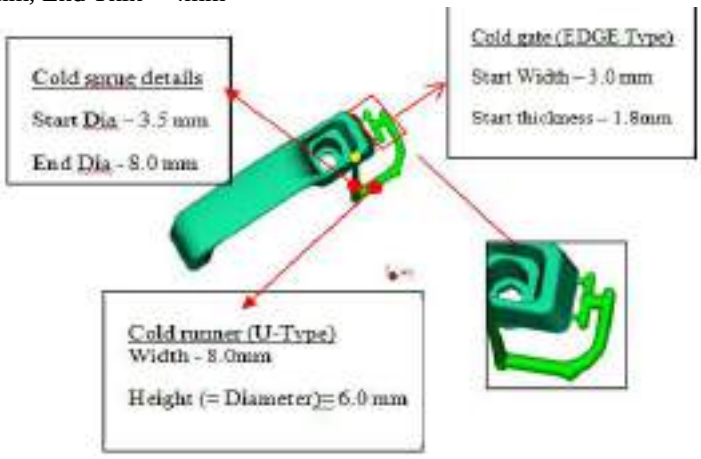

14. MOLD FLOW GATE LOCATION ANALYSIS

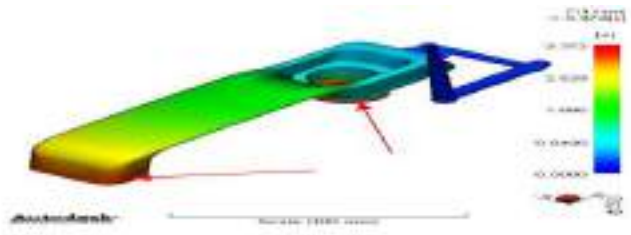

Figure 11 : Fill Time (Gate System Option 02 Analysis) Part is filling completely in 3.37s & with flow rate 70CC/s.

15. GATE SYSTEM OPTION 01 ANALYSIS RESULT

Full Time Plot

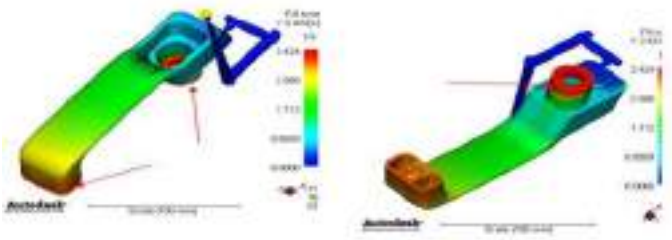

Figure 6 : Fill Time (Gate System Option 01 Analysis) Part is filling completely in 3.42s & with flow rate 70CC/s

Warpage Analysis Result :

(Deflection pattern is **scaled 5 to 10 times** to understand the shape of the component after deflection)

Deflection All Effect :

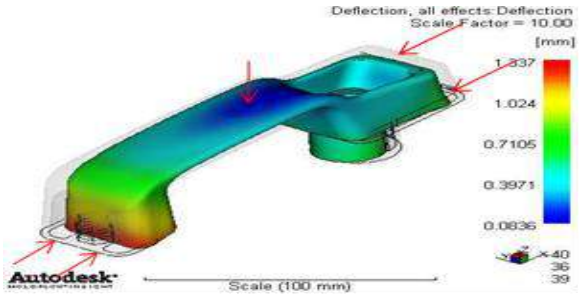

Figure 7 : Deflection All Effect (Gate System Option 01 Analysis)

Deflection In X-Direction :

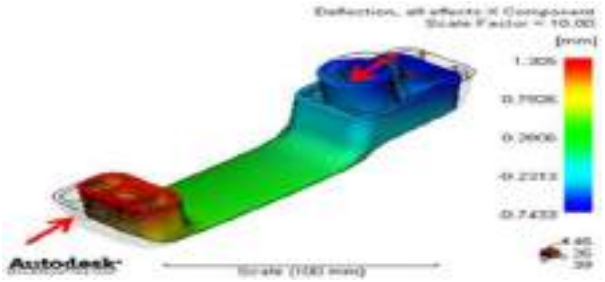

Figure 8 : Deflection in X- direction (Gate System Option 01 Analysis)

Maximum shrinkage observed in X- direction is (+1.30mm,-0.74mm). Shrinkage observed is 1.05%

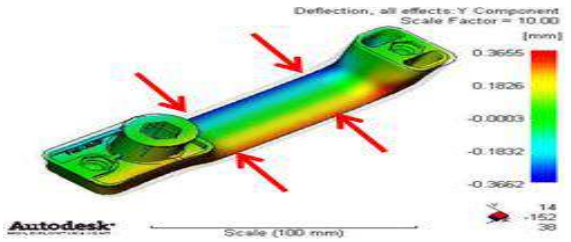

Deflection In Y-Direction

Figure 9: Deflection in Y- direction (Gate System Option 01 Analysis) Maximum shrinkage observed in Y- direction is (+0.36mm,-0.36mm). Shrinkage observed is 1.52%

Deflection In Z-Direction

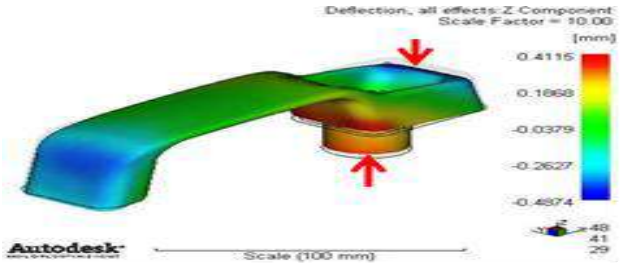

Figure 10: Deflection in Z- direction (Gate System Option 01 Analysis) is (+0.414mm,-0.48mm)

16. GATE SYSTEM OPTION 02 ANALYSIS RESULT

Full Time Plot

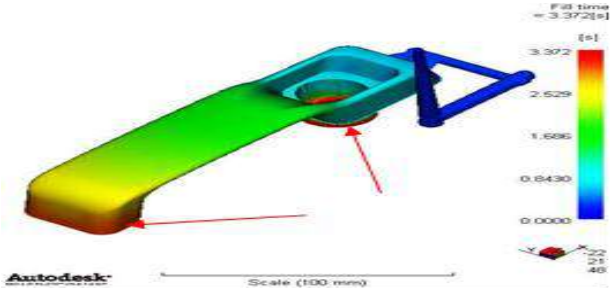

Figure 11 : Fill Time (Gate System Option 02 Analysis) Part is filling completely in 3.37s & flow rate 70CC/s.

Warpage Analysis Result :

(Deflection pattern is **scaled 5 to 10 times** to understand the shape of the component after deflection)

Deflection All Effect :

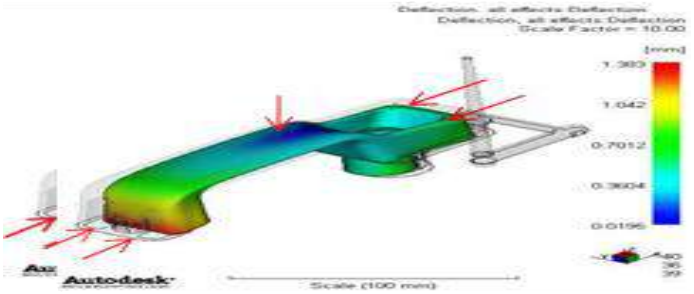

Figure 12 : Deflection All Effect (Gate System Option 02 Analysis)is 1.38 mm

Deflection In X-Direction :

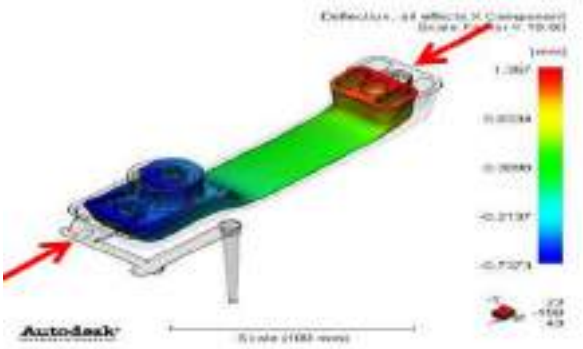

Figure 13 : Deflection in X- direction (Gate System Option 02 Analysis)
Maximum shrinkage observed in X- direction is (+1.35mm,-0.73mm). Shrinkage observed is 1.07%

Deflection In Y-Direction

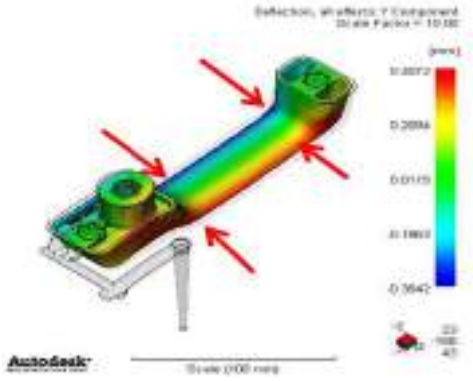

Figure 14 : Deflection in Y- direction (Gate System Option 02 Analysis) is (+0.40mm,-0.38mm) Shrinkage observed is 1.44%

Deflection In Z-Direction

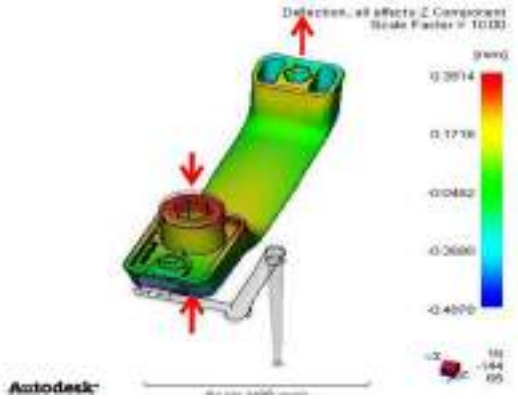

Figure 15 : Deflection in Z- direction (Gate System Option 02 Analysis) is (+0.39mm,-0.48mm)

17. GATE SYSTEM OPTION 03 ANALYSIS RESULT

Full Time Plot

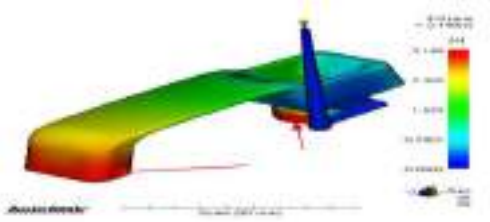

Figure 16 : Fill Time (Gate System Option 03 Analysis) Part is filling completely in 3.14s & with flow rate 70CC/s.

Warpage Analysis Result:

(Deflection pattern is **scaled 5 to 10 times** to understand the shape of the component after deflection)

Deflection All Effect :

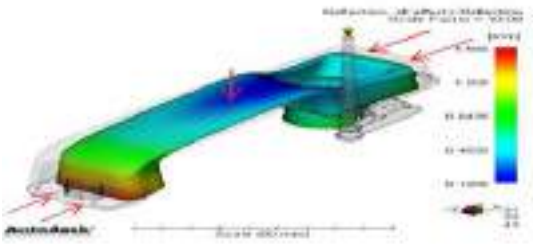

Figure 17 : Deflection All Effect (Gate System Option 03 Analysis)

Deflection In X-Direction

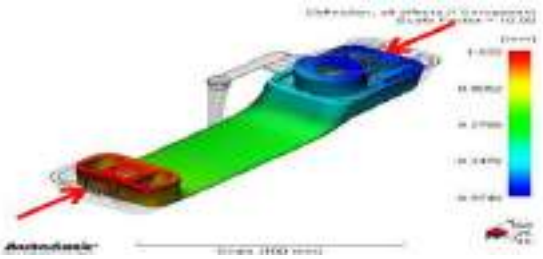

18 : Deflection in X- direction (Gate System Option 03 Analysis) Max Deflection Observed is (+1.53mm,-0.97mm).Shrinkage observed is 1.21%)

Deflection In Y-Direction

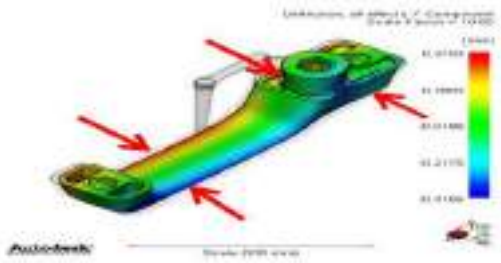

Figure 19 : Deflection in Y- direction (Gate System Option 03 Analysis) is (+0.37mm, -0.41mm). Shrinkage observed is 1.48%)

Deflection In Z-Direction

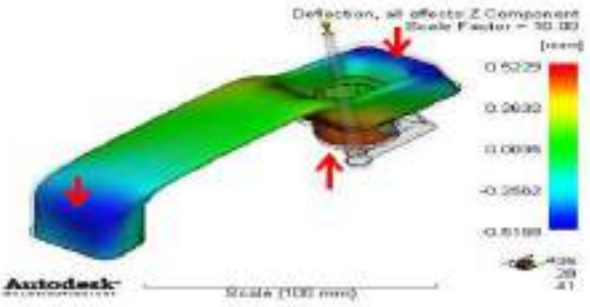

Figure 20: Deflection in Z- direction (Gate System Option 03 Analysis) is (+0.52mm,-0.51mm)

18. GATE SYSTEM OPTION 04 ANALYSIS RESULT

Full Time Plot

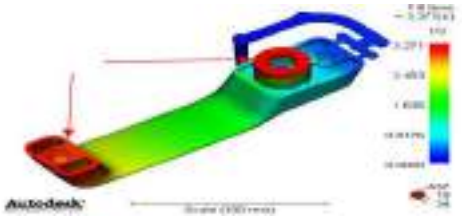

Figure 21 : Fill Time (Gate System Option 04 Analysis) Part is filling completely in 3.27s & with flow rate 70CC/s

Warpage Analysis Result: (Deflection pattern is scaled 5 to 10 times to understand the shape of the component after deflection)

Deflection All Effect:

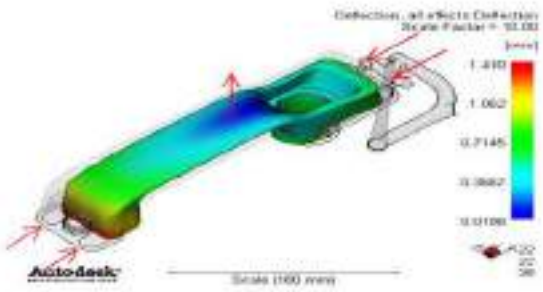

Figure 22 : Deflection All Effect (Gate System Option 04 Analysis) is 1.41 mm

Deflection In X-Direction

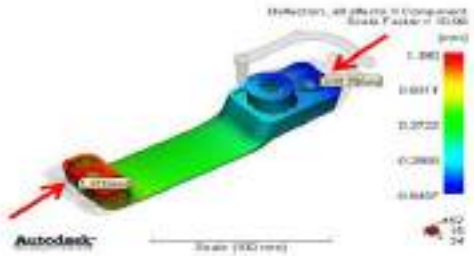

Figure 23: Deflection in X- direction (Gate System Option 04 Analysis) is (+0.37mm, -0.41mm). Shrinkage observed is 1.17%)

Deflection In Y-Direction

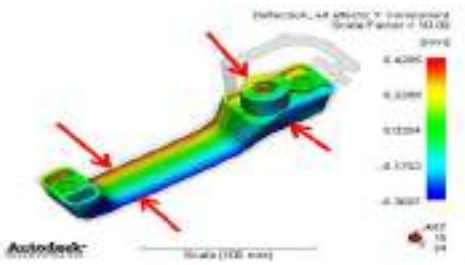

Figure 24 : Deflection in Y- direction (Gate System Option 04 Analysis) is (+0.42mm,-0.36mm). Shrinkage observed is 1.95%

Deflection In Z-Direction

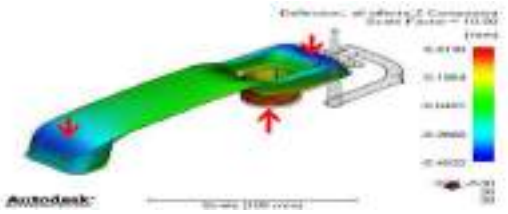

Figure 25 : Deflection in Z- direction (Gate System Option 04 Analysis) is (+0.41mm,-0.49mm)

19. RESULT AND CONCLUSIONS

1. Part is filling completely in all the 4 options with flow rate of 70cc/sec
2. As per mold flow gate location analysis, gate is preferable at one end, where higher thicknesses are observed.
3. Further gate option of fan type gate at extreme end & gate at side edge of size of 2.0x20mm is analyzed.
4. There is no much difference is observed with all 4 options, it is up +0.2 variation.
5. We have observed more X-deflection at other end, where gate is not provided. Further we may need to add one more gate at other end, but it will add bigger weld line at center of part
6. It may be shrinkage after part is being ejected from mold. it should fixed to cooling fixture immediately after ejection from mold and quenched in water to arrest the dimension.

Option	All direction	X-deflection	Y-deflection	Z-deflection
Option -1	1.33mm	+1.30mm,-0.74mm	+0.36mm,-0.36mm	+0.41mm,-0.48mm
Option -2	1.38mm	+1.35mm,-0.73mm	+0.40mm,-0.38mm	+0.39mm,-0.48mm
Option -3	1.56mm	+1.53mm,-0.97mm	+0.37mm,-0.41mm	+0.52mm,-0.51mm
Option -4	1.41mm	+1.39mm,-0.84mm	+0.42mm,-0.36mm	+0.41mm,-0.49mm

20. REFERANCES

[1] Auto desk Mold-Flow Insight material data warehouse
[2] Manmit Salunke “Casting methods design,simulation and optimization of circular plate” 3rd 3.International Conference on “Emerging Trends & Reasearch in Engineering “at Amaravati M.S. in I.J.P.A.E.T.(ISSN:2319- 507X).
[3] Manmit Salunke “Injection molding methods design, optimization, Simulation of plastic toy building block by mold Flow analysis” International Journal of Mechanical Engineering and Technology, ISSN 0976 – 6340 (Print) ISSN 0976 – 6359 (Online)Volume 6, Issue 6, June (2015), pp. 33-41 Article ID: 30120150606004
[4] Wikimedia Foundation, Inc, 2010. Injection Moulding. [online] Availableat:<http://en.wikipedia.org/wiki/Injection_mo ulding> [Accessed 28 August 2010]
[5] Bryce, D. M., ‘Plastic injection molding: Manufacturing process fundamental’.Society of Manufacturing Engineers, (1996)
[6] Moldflow Plastic Insight, 2014. Moldflow Tutorial. [Software tutorial] Mold-flow Corporation
[7] Tang, S.H., Kong, Y.M.,Sapuan, S.M., Samin, R., and Sulaiman, S., “Design and thermal analysis of plastic injection mold” , Journal of Materials Processing Technology, Vol. 171, pp. 259-267, 2006.
[8] http://www.engineersedge.com/injection_m olding,.htm, 2006
[9] http://www.efunda.com/DesignStandards/plastic_design/plastic_intro.cf m, 2006
[10] Hariyanto Gunawan and Willyanto Anggono **“** Improving quality of injection mold using moldflow software simulationcase study: new design plastic cup” ISBN 979-15577-0-5, proceeding of international seminar on product design and development 2006 yogyakarta-indonesia, december 13 – 14, 2006

IJARESM

ISSN: 2455-6211, New Delhi, India

International Journal of All Research Education & Scientific Methods

An ISO & UGC Certified Peer-Reviewed Multi-disciplinary Journal

Certificate of Publication

Prof R. R. Kulkarni

Project Guide, Department of Mechanical Engineering, Siddhant College of Engineering, Pune

TITLE OF PAPER

Mold Flow Simulation of "Car Door Handle" for

Optimization of warpage by Using Different Gate System

has been published in

IJARESM, Impact Factor: 7.429, Volume 9 Issue 1, Jan.- 2021

Paper Id: IJARESM/Jan.21

Date: 09-01-2021

Website: www.ijaresm.com
Email: editor.ijaresm@gmail.com

Authorized Signatory

International Journal of All Research Education and Scientific Methods (IJARESM), ISSN: 2455-6211
Volume 9, Issue 5, May -2021, Impact Factor: 7.429, Available online at: www.ijaresm.com

Study of Vibration Signature Monitoring on FSW Process and Verification with FEA

Mr. Nitin Digambar Bure[1], Prof. R. R. Kulkarni[2]

[1]ME Student, Department of Mechanical Engineering Siddhant College of Engineering, Pune, India
[2]Professor, Department of Mechanical Engineering, Siddhant College of Engineering, Sudumbare Pune, India

----------**********----------

ABSTRACT

The Experimental study conducted during joining butt weld in FSW process on Al 6061 alloy of size 50 mm width X 100 mm length X 8 mm thickness of two plates wherein the effect of the interaction between the plates, tool and the vibration that occurs during the process are investigated, are reported. In this study, joining sides of the workpiece samples are artificially induced with air gaps of drilled holes in 2mm, 3mm, 5 mm diameter holes and 3mm width X 4 mm depth of slots in random distances. The vibration behaviour of the tool and workpiece joining system are characterized by a frequencies arrived in modal analysis using Finite Element Analysis (FEA), each mode corresponds to tool and workpiece system. Variations in the amplitudes of vibration signals in the particular range of frequencies from 6.0 to 7.0 kHz are proportional to workpiece and significant changes in linear pattern indicate the defective and steady joining area of workpiece. So, this method is effective in monitoring of workpiece joining in FSW process. The Fast Fourier Transform (FFT) analysis of vibration signal shows the changes in individual frequencies and is used for identifying the frequency range of monitoring workpiece with gap and without gap conditions. The steady joining portions cause the vibration which corresponds to 4th region frequencies of workpiece.

INTRODUCTION

The friction stir welding process is a solid state combined that uses a non-expendable tool to link two non-melting material. This method can progress the mechanical properties of the joint, such as the strength and hardness etc. The heat will be created due to friction and plastic distortion between the tool and the work pieces. This friction and plastic distortion result in the mixing and agitation of the materials around the pin from the front to the rear. The heat generated by friction leads to the softening of metals, especially near the friction welding tool. This means that mechanical energy is converted into thermal energy in the contact areas, without the need for heat from other sources. The main function of the friction welding tool is to heat the parts, and then to induce the materials to flow and restrict under the shoulder and Impression action will generate friction between two surfaces and relative motion between two part. People are studying to optimize process parameters for active connection of materials.[2]

LITERATURE REVIEW

Premature failure of the welding tool can lead to unacceptable welding joint quality and loss of welding productivity. Friction welding is a completely machined process. The forces and vibration generated by the process are high enough that manual operation is not possible, except possibly for very fine materials. Therefore, for online monitoring of vibration is therefore in demand.

Lambiase et al. (2018) have investigated force variation, temperature and torque distribution in process with an al-Si-Mg aluminium alloy that varies the tool's rotation speed and welding speed. Temperature measurements were made using an IR camera. *Prasanna et al. (2010)* have observed the experimental and numerical evaluation with aluminium alloy aa6061. Temperature variation and simulation model is tested parameter with experimental results. *Buffa. G et al (2008)* have developed the distribution of temperature and tension in welding nugget was investigated. Projected the relationships between the forces of the tool and the variation in the parameters. Temperature profile almost symmetrical in the welding area was found. *Reza-E-Rabbya et al (2013)* have found pin characteristics in the flow of material and the weldability by stirring by friction of two aluminium alloys (AA 7050 and AA6061) with a pin tool cylinder, including the pin smooth / without thread attached to a geometry of shoulder displacement single invariant. Welds were made under a range of process parameters (welding and rotation speed). *Sadeesh Pa et al (2014)* conducted with plates of aluminium AA2024 and AA6061 dissimilar, and obtained the optimal parameters of the process. Different tool designs have been used to analyze the properties. Investigated the effect of welding speed on the microstructure hardness and tensile properties of the welded joints. As the process parameters varied, seamless, high-efficiency welded joints were produced. *Jalay Shukla et al (2016)* have observed mechanical and metallurgical properties by changing various parameter that FSW can be used to study the parameters on the process in laboratory. Experiments have been conducted to validate some of the simulation results of the ANSYS software. *Ramesh et al (2016)* have investigated (FSW)

of aluminium alloy 6082 to study the tensile strength and hardness by changing the process parameter Speed of rotation and welding of the tool. And different weld condition. They found the effect of tool design on mechanical properties in FSW of AA6061. *Sakala Ramya Sree et al (2018)* studied the double-sided agitation friction welding of aa6061 plates using a hexagonal tool and process parameters was the speed of rotation and the welding speed. The resistance analysis is carried out on the welded joints AA6061. They used technique of order preference by similarity to ideal solution is used to identify the process parameters. In this paper, modal analysis of workpieces and hard tool using Finite Element Analysis (FEA) are compared with the range of frequency occurring during experiments in the fast Fourier transform (FFT) analysis of vibration signals. The fact of this approach is presented from friction stir welding (FSW) experiments using hard tool and an aluminium alloy workpiece.

MATERIALS AND METHODS

Experimental Procedure: The workpiece materials used for experimental study are commercially available Al 6061. The size of the samples of workpiece plates are 100 mm length X 50 mm width X 8 mm thickness. The chemical compositions and material properties are tabulated in Table 1 &2[9][10]. The two plates were mounted using a clamp and retrofitted on a CNC milling machine which is shown in Fig.1 (photograph of the experimental set-up used to study friction stir process). Tool pin was made with D/d ratio (Shoulder/pin) of 3 in which Tool shoulder and pin made up of diameter 16 mm X height 60 mm pin diameter of 6 mm X height 7.5 mm respectively. The chemical composition and material properties are given in Table 3 & 4[11]. Joining of workpiece samples were performed on a 3-axis CNC milling machine which has 3-axis movement and carried using a special CNC program which was run at speed 800 rpm and feed 33 mm/min [Ref]. Both workpieces are properly secured using a clamp. The vibration signals were measured using a (Kistler model- 8702B50) accelerometer sensor which is positioned on the clamp, used for holding dynamometer. A data acquisition card (NI 9133) used to convert analog output signals into digital signals. Among four of its channels, single analog input channel was used to collect the data by sampling the signals at 25 kHz and interfaced with a personal computer and simultaneously processed and recorded by LabVIEW software 8.5 (Sound and Vibration assistant).

Table 1: Chemical composition of AA6061

Fe%	Si%	Mn%	Cu%	Ni%	Cr%	Ti%
0.244	0.741	0.095	0.157	0.01	0.125	0.007

Sn%	V%	Co%	Zn%	Pb%	Mg%	Al%
0.006	0.006	0.002	0.020	0.005	0.901	97.699

Table 2: Mechanical properties of AA6061

Yield Strength	Ultimate Tensile Strength	Elongation	Shear Strength	Fracture Strength
276 MPa	310 MPa	12%	207 MPa	94 MPa

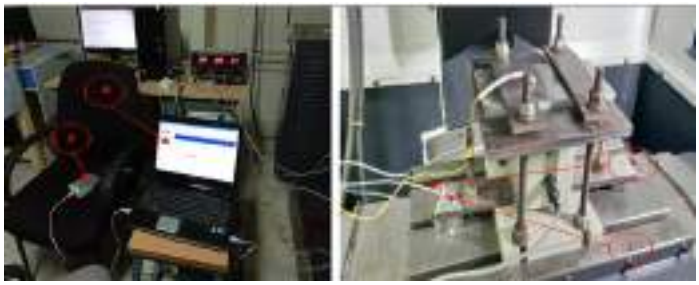

Fig. 1. Photograph of experimental set-up with vibration monitoring system

1. Accelerometer
2. Data Acquisition card
3. Connecting cable (iv) Laptop

Table 3: Chemical composition of H13

Cr%	Mo%	Si%	V%	C%
4.75-5.5	1.1-1.75	0.80-1.2	0.80-1.2	0.32-0.45

Ni%	Cu%	Mn%	P%	S%
0.3	0.25	0.2-0.5	0.03	0.03

Table 4: Properties of H13

Density	7800 kg/m3
Melting point	1427°C
Tensile strength (Ultimate)	1.2 to 1.5 GPa
Tensile strength (Yield)	1 to 1.3 GPa
Modulus of elasticity	215 GPa
Poisson's ratio	0.3
Thermal conductivity	28.6 W/mK

Methodology and experimental procedure:

Fig. 3 shows the flow diagram of methodology followed for comparison through extracting the features from Fast Fourier Transform (FFT) of the sub module of Sound and Vibration software in the LabVIEW and modal anlysis of FEA. First step, it was planned to record vibration signals for beginning of the plate joining to ending of the plate joining for the size of 100mm length X 50 mm width X 8 mm thickness. Once the vibration signals were recorded through data acquisition card of converted analog to digital signal then further signal processing was carried in LabVIEW for feature extraction from time domain and frequency domain. In this project Vibration characteristics such as amplitude and frequencies are extracted in the FFT and used for comparison of frequencies arrived through modal analysis of free vibration in ANSYS 18.1.

Fig. 2. Flow chart of describing feature extraction from FFT and comparison with FEA

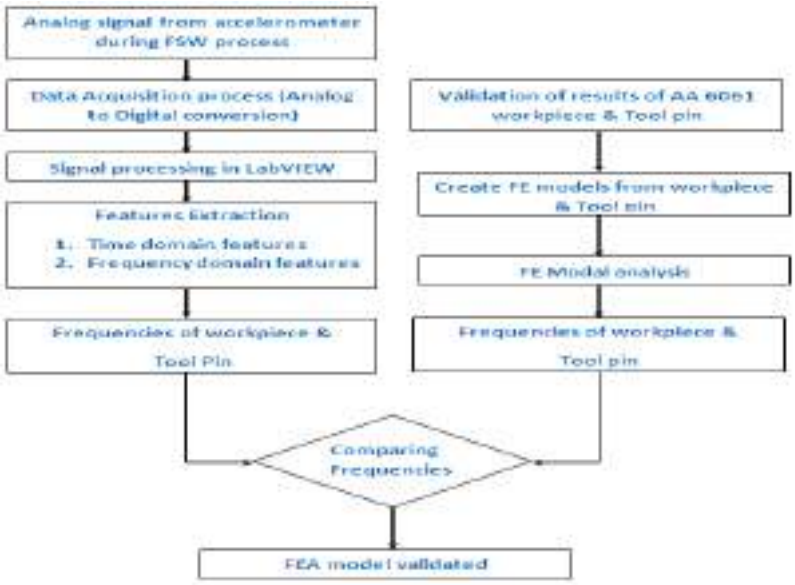

RESULTS AND DISCUSSIONS

FEA analysis: The workpiece with the size of 100 mm length X 50 mm width x 8 mm thickness of two plates have been modeled together and outer perimeters are arrested to the dimensions equal to the dimensions of clamp of 20 mm on both sides which is used for holding the workpiece and input parameters are given such as mass density is 2710 kg/m^3 Young's modulus is 68.9 X10^9 N/m^2 and Poisson's Ratio is 0.3. Entire model is meshed and allowed to run the rectangular plate in free vibration, arrived modal values for 30 modes. Table 5 shows that first 4 modal values of the rectangular plate. Figure 3 (a) shows the meshing model of two workpieces and Fig. 3 (b) shows the modal analysis result of rectangular plates which are performed by FEA software (ANSYS 18.1) and shown for the first mode.

Table 5: Modal values of workpiece in free vibration

Component	Modes of free vibration	I mode	II mode	III mode	IV mode
Workpiece	By FEA, F_n (Hz)	6674.8	12960	13213	18614
Tool pin	By FEA, F_n (Hz)	3051.9	3052.2	13533	15817

Tool pin is modeled for size of diameter 16 mm X height 60 mm of tool shoulder and diameter of 6 mm X height 7.5 mm of tool pin. Top surface of tool pin is arrested and input parameters are given such as mass density, Young's modulus and Poisson's Ratio of 7800 kg/m^3, 2.15 X10^{11} N/m^2 and 0.3 respectively. Entire model is meshed and is showed in Fig. 4 (a). Meshing model is used to run for free vibration and 1st mode result of tool pin is shown in Fig. 4 (b).

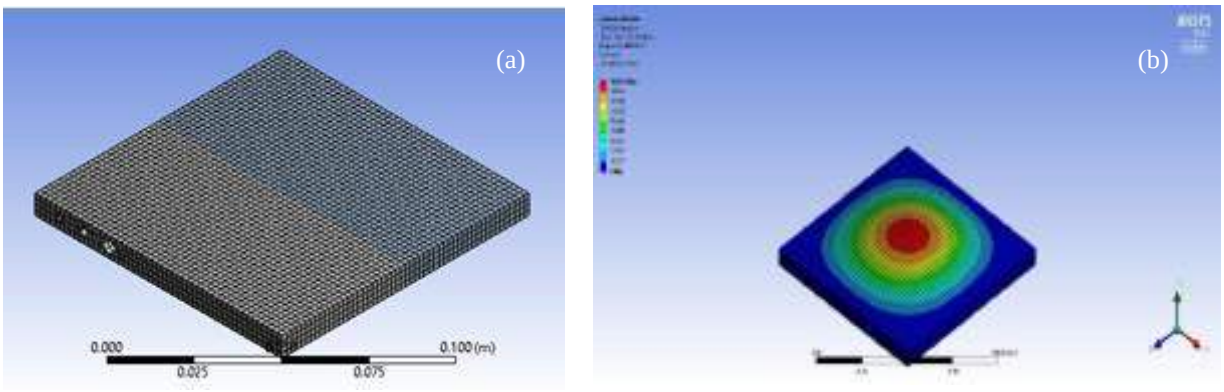

Fig.3. (a) Meshing model of two workpieces (b) 1st mode result of rectangular plates

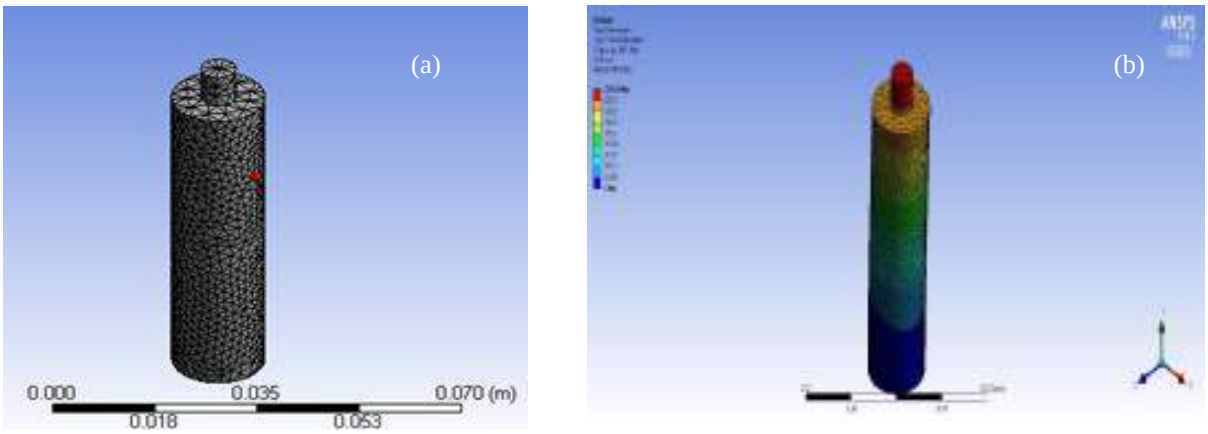

Fig.4. (a) Meshing model of Tool pin (b) 1st mode result of Tool pin

Power Spectrum Analysis: Joining operations on plates have been performed using spindle speed of 800 rpm, feed of 71.2 mm/min. Fig. 5 shows that the plates are joined with defects and the joined plates are separated into three segments such as metal joining at entry, steady joining and exit. Segmented areas are monitored through FFT and used for analysis. During entire process of joining, sensor was positioned at the fixture of the base plate. While joining plates, accelerometer sensor measured the vibration signal and LabVIEW software used to store the information in the computer. Totally 2 plates were used for joining up to 100 mm length. Time domain and corresponding frequency domain signals of three segments are shown in Fig.6. The amplitude was measured 4.5 X 10^{-3} m/s^2 at entry and exit of joining. While the metal in steady joining the amplitude level was 6.6 X 10^{-3} m/s^2. This is captured in the frequency range between 6000 to 7000 Hz. The variation in the amplitude level occurs because of friction between the contacting materials, due to which temperature also raises to solidification stage for joining metal. The results of the experiments conducted are shown in Fig. 6, which provides time domain and corresponding power spectrum graph. Power spectrum indicates the corresponding frequencies (Hz) arrived in the FEA analysis. The figure 7 shows the bar graph of amplitude level against the various stages of plates.

Figure 5: Plate segmented at three stages

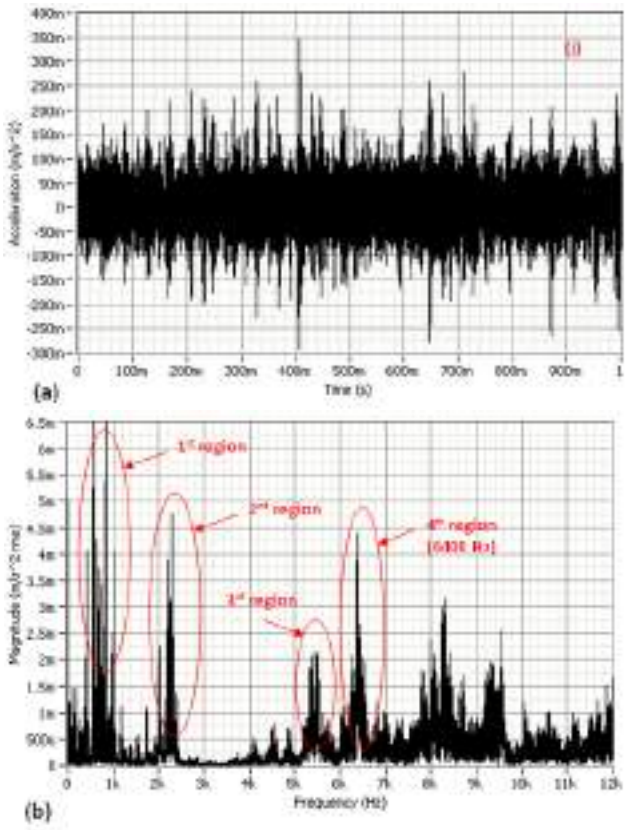

Fig. 6.(i) (a) Time domain and (b) corresponding FFT during entry

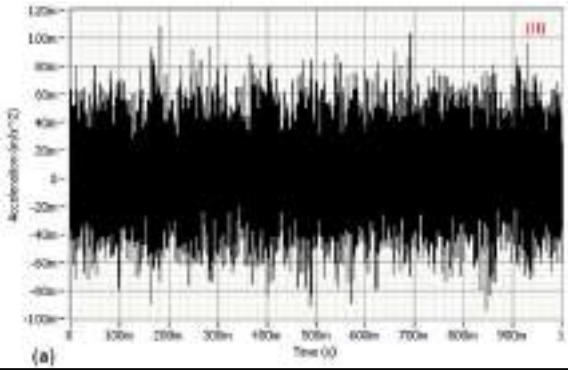

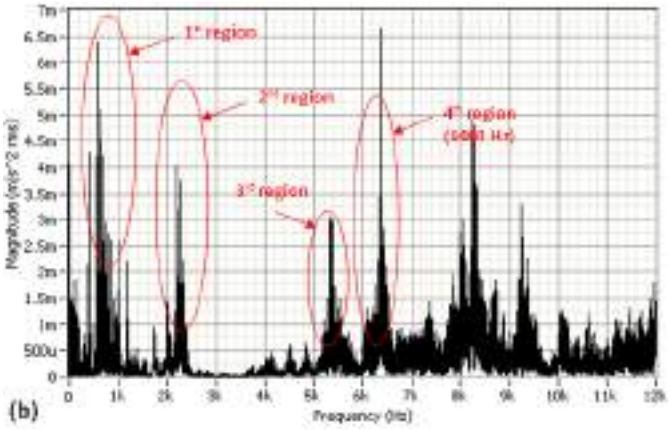

Fig.6.(ii) a) Time domain signal and (b) corresponding FFT during steady joining

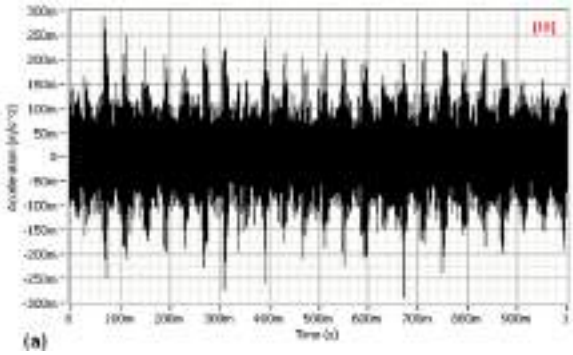

Fig.6: iii) (a) Time domain signal and (b) corresponding FFT during exit of FSW process

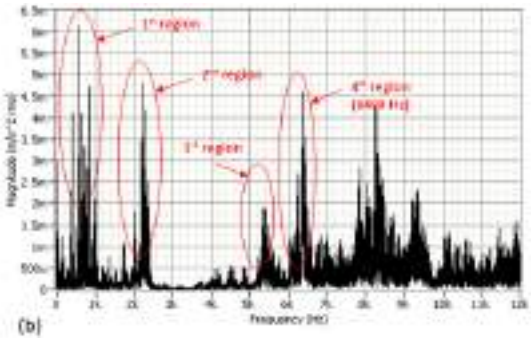

Fig. 6. Comparison of Power spectra for different stage joining of workpiece

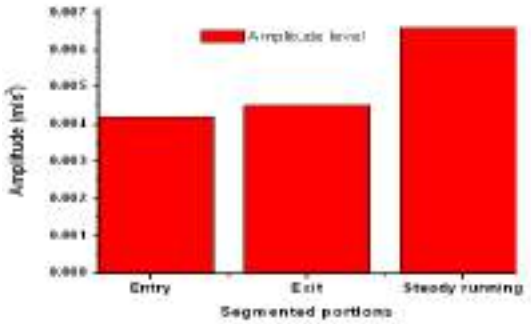

Figure 7: Effect of friction on amplitude

CONCLUSION

In this study, a relation between the workpiece, tool stiffness and the vibration signals in joining process are reported. The stiffness of the workpiece is the most influencing parameter causes high frequency components in FSW process. The friction with temperature raise also causes notable changes in high frequency components of power spectrum. It was found that 4^{th} region of frequency 6400 Hz of workpiece frequency is affected by changes in metal joining pattern. This increases the vibration amplitude in the range of frequencies from 6.0 to 7.0 kHz. The increases in the vibration amplitude are observed in this frequency band and that are most sensitive during the metal process. This significant increase of amplitude by two times indicates the friction increases between tool and workpiece. It is concluded that the monitoring of 4^{th} region frequency of the workpiece can be utilized for effectively monitoring of defects during FSW process.

ACKNOWLEDGMENT

I gratefully acknowledge Mechanical engineering department of SCOE Pune for technical support and providing the research facilities. I would also like to thank to Dr. D. K. Chavan, Principal (SCOE, Pune) and Prof. Nitin Bagal, (Mechanical department) for their help and dedication toward my research and related research, also my friends for their directly & indirectly help, support and excellent cooperation.

REFERENCES

[1] F. Lambiase & A. Paoletti & A. Di Ilio “Forces and temperature variation during friction stir welding of aluminum alloy AA6082-T6”
[2] Sudhir Kumar and Pardeep Kumar “Study the Effect of Parameters of Friction Stir Welding 0n the Impact Strength of Aluminium 6063”
[3] G. Buffa, L. Fratini, F. Micari, R. Shivpuri “Material Flow in FSW of T-joints “Experimental and Numerical Analysis ”
[4] P. Prasann1, B. Subba Rao, G. Krishna Mohana Ra “EXPERIMENTAL AND NUMERICAL EVALUATION OF FRICTION STIR WELDS OF AA6061-T6 ALUMINIUM ALLOY”
[5] Md. Reza-E-Rabby “Effect of tool pin thread forms on friction stir weldability of different aluminum alloys”
[6] Sadeesh Pa,Venkatesh Kannan “Studies on friction stir welding of AA 2024 and AA 6061 dissimilar metals”
[7] Jalay Shukla ,Raghu Echempati “INVESTIGATION AND THERMAL ANALYSIS OF FRICTION STIR WELDING PROCESS PARAMETERS OF AA6061 PLATES”
[8] A.Ramesh,M Indira Rani, A.Pransanth “INFLUENCE OF TOOL DESIGN ON THE MECHANICAL PROPERTIES IN FRICTION STIR WELDING OF ALUMINIUM ALLOY AA 6082-T6”
[9] Mukhopadhyay Prantik “Alloy Designation Processing,and Use of AA6XXX SeriesAluminiumAlloys”
[10] Azomaterial https://www.azom.com/article.aspxArticleID=9107

IJARESM

ISSN: 2455-6211, New Delhi, India
International Journal of All Research Education & Scientific Methods
An ISO & UGC Certified Peer-Reviewed Multi-disciplinary Journal

Certificate of Publication

Prof. R. R. Kulkarni

Professor, Department of Mechanical Engineering, Siddhant College of Engineering, Sudumbare Pune, India

TITLE OF PAPER

Study of Vibration Signature Monitoring on FSW Process and Verification with FEA

has been published in

IJARESM, Impact Factor: 7.429, Volume 9 Issue 5, May- 2021

Paper Id: IJARESM/May21

Date: 21-05-2021

Website: www.ijaresm.com
Email: editor.ijaresm@gmail.com

Authorized Signatory

International Journal of All Research Education and Scientific Methods (IJARESM), ISSN: 2455-6211
Volume 9, Issue 5, May -2021, Impact Factor: 7.429, Available online at: www.ijaresm.com

FEM Based Crack Analysis in Metal Powder Compaction

Megha G. Marewad[1], Prof. R. R. Kulkarni[2]

[1]ME Student, Department of Mechanical Engineering Siddhant COE, Sudumbare, Pune India
[2]Prof, Department of Mechanical Engineering Siddhant COE, Sudumbare, Pune India

----------**********----------

ABSTRACT

This paper presents a preliminary assessment and qualitative analysis on fracture criterion and crack growth in metal powder compact during the cold compaction process. Based on the fracture criterion of granular materials in compression a displacement based finite element model has been developed to analyze fracture initiation and crack growth in metal powder compact. Approximate estimation of fracture toughness variation with relative density is established in order to provide the fracture parameter as compaction proceed. A single crack initiated from the boundary of a multi-level component made of iron powder is considered in this work. The finite element simulation of the crack propagation indicates that shear crack grows during the compaction process and propagates in the direction of higher shear stress and higher relative density. This also implies that the crack grows in the direction where the compaction pressure is much higher, which is in line with the conclusion made by previous researchers on shear crack growth in materials under compression. In agreement with reported work by previous researchers, high stress concentration and high density gradient at the inner corner in multi-level component results in fracture of the component during preparation. Powder metallurgy (PM) is widely applied to produce mainly automotive parts such as bearings, cams, and toothed components. Manufacturing parts using PM involves four major steps: powder and lubricant mixing, compacting powders into appropriate shapes in closed dies to produce green compacts, sintering the green compacts at elevated temperature and finally, post-sintering secondary operations. In modeling the compaction process, the macro-mechanical modeling approach is used in this work, which provides information on the macroscopic behavior of the powder assembly such as powder movement, density distribution, stress state and the shape of the compact during and after compaction.

INTRODUCTION

Powder compaction is a production method commonly used in the manufacturing industry today such as those in the ceramic forming, pharmaceutical and detergent industries. The granulated material is consolidated by the application of pressure. Artifacts of the granule structure often persist as pores and laminations after compaction, and may persist as defects in the sintered microstructure. Such defects can be detrimental to the properties of the final part called “green body”. The fracture and deformation behavior of particles under impact loading is important in many industrial processes. For example, impact commination is widely used to modify the size distribution of a population of particles.

On the other hand, unintentional attrition by impact can degrade particles, and the resulting fragments may cause serious problems elsewhere in the system. Thus, it is desirable to eliminate the granule structure as completely as possible during the compaction. In cold uniaxial powder compaction, the powder is formed into a desired shape with rigid tools and a die. A critical property in the powder pressing process is the mechanical properties of the formed piece. Beyond a defect-free green body, the desired properties are high strength and a uniform density. The compression induces a tensile stress perpendicular to the compressed diameter. Understanding breakage in granulation could lead to a better control of product quality and improved manufacturing efficiency. In either case, it is important to understand the mechanisms of failure under impact conditions so that these attrition and commination processes can be appropriately controlled.

Powder metallurgy (PM) is widely applied to produce mainly automotive parts such as bearings, cams, and toothed components. Manufacturing parts using PM involves four major steps: powder and lubricant mixing, compacting powders into appropriate shapes in closed dies to produce green compacts, sintering the green compacts at elevated temperature and finally, post-sintering secondary operations.

In modeling the compaction process, the macro mechanical modeling approach is used in this work, which provides information on the macroscopic behavior of the powder assembly such as powder movement, density distribution, stress state and the shape of the compact during and after compaction. Thus the powder medium is considered as a continuum that undergoes large elastic plastic deformation. In order to describe the effect of loading state on the response of the powder, constitutive model based on granular material is used since it was found in the literature that powder behaves similarly to a frictional granular material with regard to militancy and densification behavior. Details on cold compaction process can be found, where the numerical modeling of the compaction, relaxation, ejection and emergence phases have been developed, and validated by experiments.

LITERATURE REVIEW

Review of Papers

S.M. Tahir, A.K. Ariffininvestigated that a preliminary assessment and qualitative analysis on fracture criterion and crack growth in metal powder compact during the cold compaction process. Based on the fracture criterion of granular materials in compression, a displacement based finite element model has been developed to analyse fracture initiation and crack growth in metal powder compact.

Approximate estimation of fracture toughness variation with relative density is established in order to provide the fracture parameter as compaction proceed. A single crack initiated from the boundary of a multi-level component made of iron powder is considered in this work. The finite element simulation of the crack propagation indicates that shear crack grows during the compaction process and propagates in the direction of higher shear stress and higher relative density. This also implies that the crack grows in the direction where the compaction pressure is much higher, which is in line with the conclusion made by previous researchers on shear crack growth in materials under compression. In agreement with reported work by previous researchers, high stress concentration and high density gradient at the inner corner in multi-level component results in fracture of the component during preparation

Mohamed Bouaziz1, Said Abid, HatemKsibiinvestigated that The compaction of granulated powder is a common forming process used in ceramic and pharmaceutical industries. Argillaceous particles are used as a model system to investigate granule failure during cold compaction. In this work both experimental and numerical investigations have been focused on the fracture in powder compacts. This includes studies of crack propagation and determination of operating conditions to avoid the green body fracture. In fact, axial compaction tests have been performed to determine material parameters for hardening. The numerical modeling is implemented using a finite element method based on the Von Mises criterion. Simulation examples are presented to dem- onstrate the ability of the model to compute the distribution of the relative stresses in porous media.

Sydney H. Luk, Frank Y. Chan, Alan B. Davala, Thomas F. Murphy Hoeganaes Corporation investigated that Green strength enhanced material systems have been developed for iron and Low alloy as well as stainless powder metallurgy applications. Relative to normal processing, the increase in green strength is 50-100%. The nature of green strength with respect to both materials and processing conditions is reviewed. The processing variations designed to meet target properties such as apparent density, flow and compressibility are compared with conventional material systems. Manufacturing experience with a mechanical press is presented.

Thomos F. Murphy and Bruce Lindsleyinvestigated that preliminary assessment and qualitative analysis on fracture criterion and crack growth in metal powder compact during the cold compaction process. Based on the fracture criterion of granular materials in compression, a displacement based finite element model has been developed to analyse fracture initiation and crack growth in metal powder compact. Approximate estimation of fracture toughness variation with relative density is established in order to provide the fracture parameter as compaction proceed.

A single crack initiated from the boundary of a multi-level component made of iron powder is considered in this work. The finite element simulation of the crack propagation indicates that shear crack grows during the compaction process and propagates in the direction of higher shear stress and higher relative density. This also implies that the crack grows in the direction where the compaction pressure is much higher, which is in line with the conclusion made by previous researchers on shear crack growth in materials under compression. In agreement with reported work by previous researchers, high stress concentration and high density gradient at the inner corner in multi-level component results in fracture of the component during preparation.

Young-Sam Kwon and Suk-Hwan Chung. Seonjin-ri, Yonghyeon-myon, Sacheon, Kyongnam, investigated that

The optimization program is developed to analyze and optimize the powder compaction.
The optimization program has the capability to predict
(1) The formation of cracks in the green compact,

(2) The tooling forces required to achieve these densities,
(3) The density distribution in the compact and
(4) provide the optimum processing variables during powder compaction.

The optimization program is applied to predict the density distribution and tooling forces. Based on the verification of the program, loading schedule is optimized to achieve uniform density distribution in the Hub shaped green part during die compaction. This part had been previously analyzed by several compaction simulation models through the European consortium MODNET. A new concept to predict crack formation during powder compaction is proposed. The numerical simulation results show excellent agreement with experimental data and the process conditions obtained by the optimization procedure remarkably improve the quality of prod

Joaqu´ın A. Hern´andez Ortega, Xavier Oliver Olivella, Juan Carlos investigated that Powder metallurgy (P/M) is an important technique of manufacturing metal parts from metal in powdered form. Traditionally, P/M processes and products have been designed and developed on the basis of practical rules and trial-and-error experience. However, this trend is progressively changing. In recent years, the growing

efficiencies of computers, together with the recognition of numerical simulation techniques, and more specifically, the finite element method, as powerful alternatives to these costly trial-and-error procedures, have fueled the interest of the P/M industry in this modeling technology. Research efforts have been devoted mainly to the analysis of the pressing stage and, as a result, considerable progress has been made in the field of density predictions. However, the numerical simulation of the ejection stage, and in particular, the study of the formation of *cracks* caused by elastic expansion and/or interaction with the tool set during this phase, has received less attention, notwithstanding its extreme relevance in the quality of the final product.

The primary objective of this work is precisely to fill this gap by developing a constitutive model that attempts to describe the mechanical behavior of the powder during both pressing and ejection phases, with special emphasis on the representation of the cracking phenomenon. The constitutive relationships are derived within the general framework of rate-independent, isotropic, finite strain elasto plasticity. The yield function is defined in stress space by three surfaces intersecting non smoothly, namely, an elliptical cap and two classical Von Mises and Drucker-Prager yield surfaces.

The distinct irreversible processes occurring at the microscopic level are macroscopically described in terms of two internal variables: an internal hardening variable, associated with accumulated compressive (plastic) strains, and an internal softening variable, linked with accumulated (plastic) shear strains. The innovative part of our modeling approach is connected mainly with the characterization of the latter phenomenological aspect: strain softening. Incorporation of a softening law permits the representation of macroscopic cracks as high gradients of inelastic strains (strain localization). Motivated by both numerical and physical reasons, a parabolic plastic potential function is introduced to describe the plastic flow on the linear Drucker-Prager failure surface.

Outcome of Review papers

Generally, crack can grow in three different manners:

i. Under low pressure, crack grows via incipient kink by opening mode, at an angle from the original crack plane,
ii. Under increasing pressure, crack grows as a combination of open (mode I) and shear (mode II) crack, iii) Under substantially high pressure, crack grows as a shear (mode II) crack, straight ahead or at a small angle from the original crack plane.

BASIC THEORY

Working procedure of Metal powder compaction.

The tooling equipment consists of the upper punch, the lower outer punch, the lower inner punch and die. Even though the lower outer punch was the fixed component, three process parameters such as the upper punch, the lower inner punch and die have to be controlled. They used five different conditions for the upper punch, the lower inner punch and die. But, there can be a number of processing conditions since the three independent process parameters make many combinations. Recently, developed the optimization program to provide the optimum process conditions to achieve the most uniform density distribution inside the powder compact.

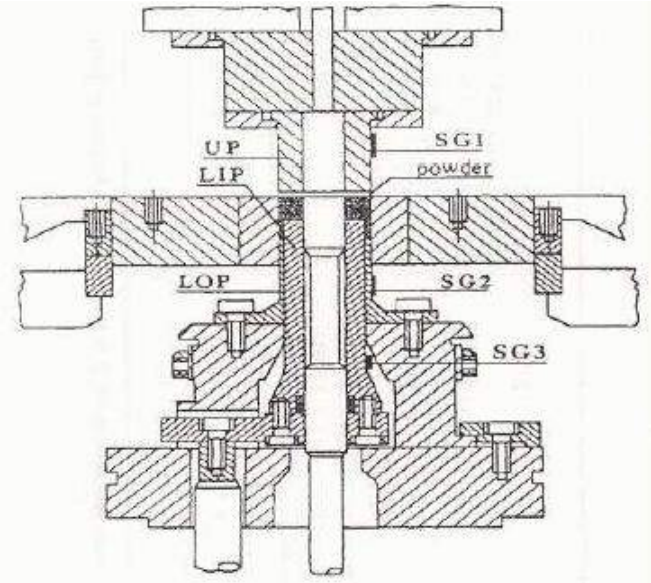

Die set of a general compaction machine

The metal powders are placed in a die cavity and compressed to form a componentshaped to the contour of the die. The pressure used for producing green compact of the component vary from 80 Mpa to 1400 Mpa, depending upon the material and the characteristics of the powder used. Mechanical presses are used for compacting objects at low pressure. Hydraulic presses are for compacting objects at high pressure.

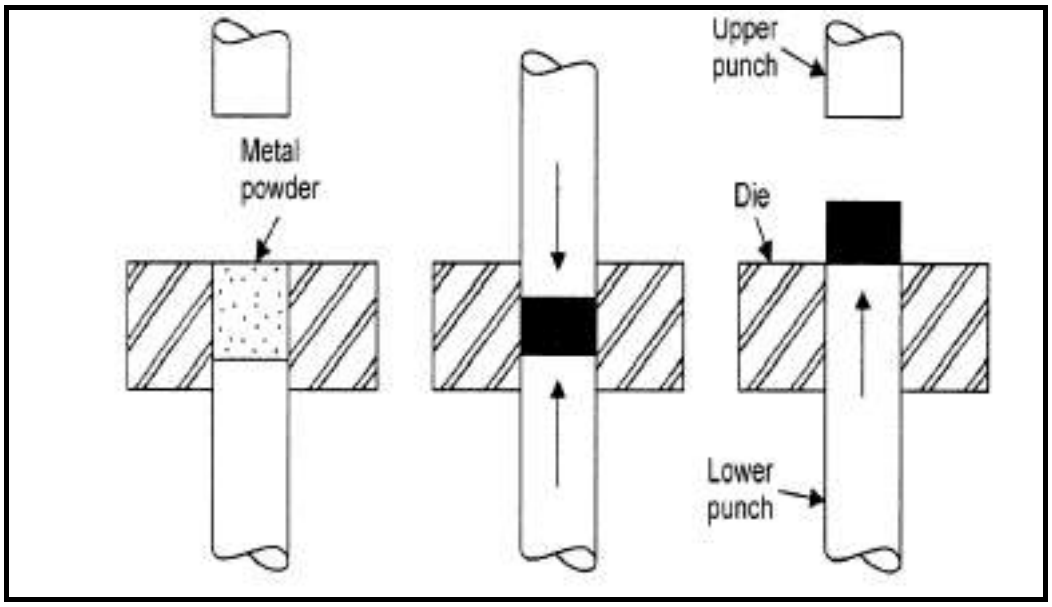

Steps in Pressing Operation

Causes of Cracks in green P/M Compaction.
Inter particle Shifting.
Another mechanism of cracks is inter particle side shifting. The inter particle bonds are formed primarily by plastic deformation and bulk movement of the powders. In an ideal condition, densification is bilateral, symmetrical and simultaneous, and inter particle side shifting does not take place. This particle motion after the onset of densification can prevent the inter particle bonds from forming and generate a crack.

Improper Elastic Strain Release.
Improper elastic strain release is another mechanism of crack formation. During compaction an unrecoverable plastic deformation of the particles occurs. Additionally a recoverable elastic deformation is also present. When the tooling elements reach their final required positions, the related pressures are reduced and during ejection will eventually go to zero. At the moment of release from compaction pressures, the compressive stresses relax and the green compact will

change abruptly from a plastic to a purely elastic stage. If the internal stresses are beyond the compact's strength Limit, cracks will form.

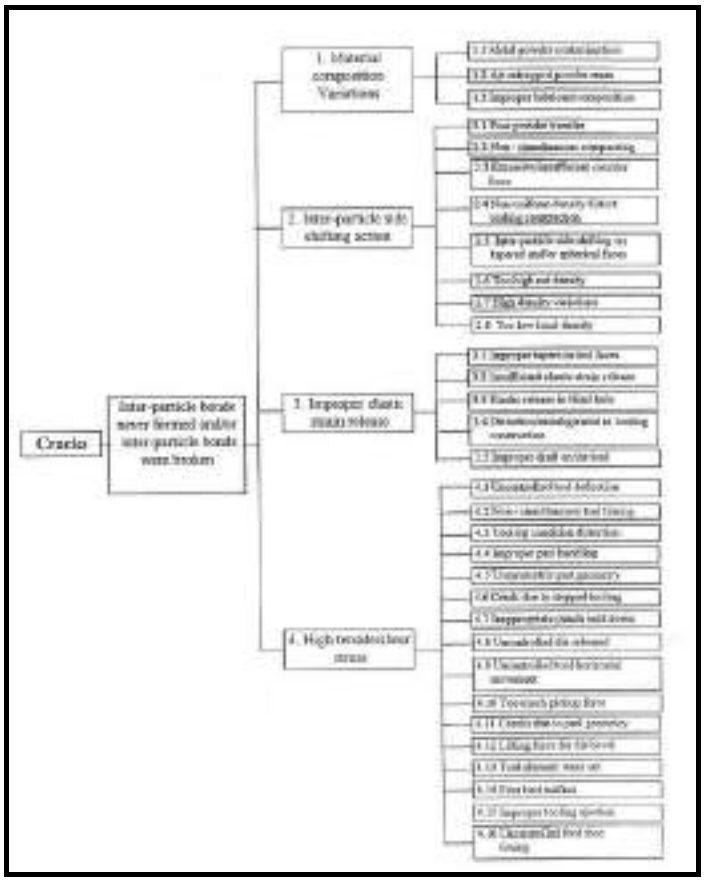

General Causes of cracks in green P/M Compacts

High Tensile/Shear Stress.

In the green P/M state, if the tensile/shear stress which can be generated by external or internal factors in a compact exceeds its green strength, which usually ranges between 10- 30 MPa for most P/M green compacts, then a crack could be formed

FINITE ELEMENT ANALYSIS

Fracture criteria.

Even though it is believed that failure in metal powder compaction is due to shear fracture (mode II), the fracture criterion in need must not neglect the possibility of fracture due to opening mode (mode I). Classical mixed mode fracture criteria have always been used to find the crack initiation angle (or direction) where crack extension depends on a specific fracture parameter. However, based on three basic criteria, namely the maximum circumferential stress criterion (rh-criterion), the maximum strain energy release rate criterion (Gcriterion) and the minimum strain energy density criterion (S-criterion) reveals that these criteria fail to predict the occurrence of mode II fracture even when pure shear load is applied. The crack initiation angle obtained from all three criteria is between 70 and 80 from the original crack plane when pure shear load is applied, while the true mode II crack should be in the direction of the maximum shear stress intensity factor, that is in the original crack plane or at a small angle from the original crack plane. In other words, the analysis proved that a more robust fracture criterion is needed to predict the occurrence of mode II crack.

Adaptive mesh and crack mechanism.

An adaptive finite element mesh is applied to accommodate large displacement changes in geometry of the domain. Error estimator based on stress error norm is used, where automatic re meshing is calculated at each step during the compaction process. Crack initiation and propagation have been developed and implemented in the model, without having to predefine the direction of crack. Initially, a three nodes triangle element is used. After the first stage of re meshing, the three nodes elements are automatically converted into six nodes triangle elements.

In finite element modeling using advanced re meshing technique, crack propagation can be modeled by inter-element or intra-element in the mesh. while the node release mechanism is used to provide two adjacent crack faces when the criteria is fulfilled. Using an adaptive mesh, the maximum and minimum element size can always be chosen such that the smallest element will be generated around the crack tip. As crack propagates, elements with appropriate size are generated around the crack tip, while the mid node of an element will become a new crack tip in order to ensure that the crack extension is within the process zone.

Geometry and boundary conditions of finite element model.

A multi-level component, in this case a rotational flanged component, is modelled by an axisymmetric representation as shown in. Iron powder with material properties obtained from experimental work inas listed in, is compacted by bottom and top punch movements. Total displacement of the bottom punch, db = 7.69 mm while the top punch displacement, dt = 6.06 mm at the end of compaction process. In this work, the compaction is performed in 20 steps movement of bottom and top punch, respectively, band in turn as shown in. This mean that a total displacement of 7.69 mm is first achieved when the bottom punch had finished a 20 steps movement, followed by a total displacement of 6.06 mm by the top punch after a 20 steps movement.

Material properties	
Young_s modulus, E	40 MPa
Poisson ratio,	0.35
Cohesion, C	2.5
Angle of internal friction	33
Coulombs friction coefficient	0.3332
Initial relative density	0.327

Material properties of iron powder

Fracture toughness.

The fracture criterions require values of the critical stress intensity factors, KIC and KIIC which are the material parameters and also called fracture toughness. Standard procedures exist for determination of fracture toughness for solids, such as three-point bending test or four-point bending test. However, the fracture toughness of the powder compact during the compaction process is not as simple as fully dense solids due to continuous rapid change of density and other material properties at each compaction step. Hence variation of fracture toughness with relative density must be obtained in order to provide these fracture parameters as compaction proceeds.

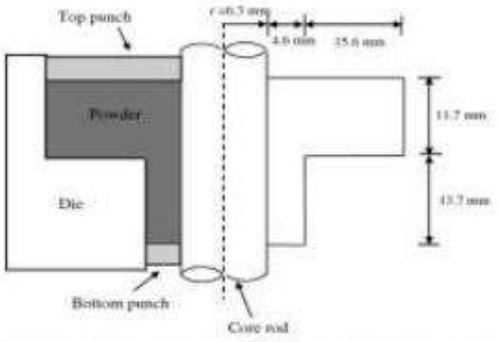

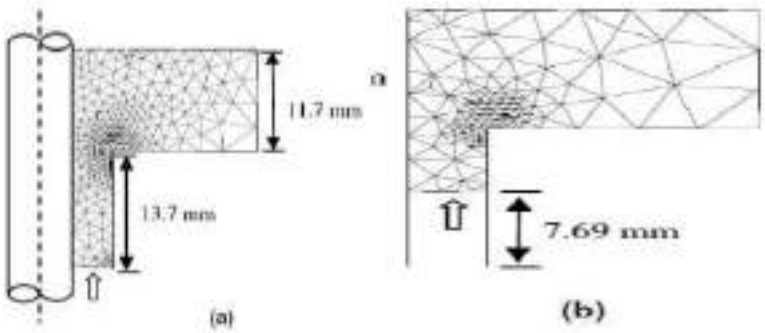

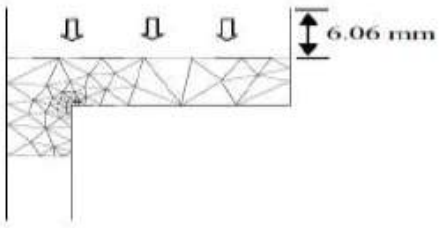

(c)

Axisymmetric representation of compaction process with tool path and position during compaction process. (a) Step begins, (b) end of step and (c) end of final step

RESULT AND DISCUSSION

Crack initiation

Since no pre-crack is present in this case, the direction of maximum shear stress is used as the original crack direction, in the calculation of KI(h) and KII(h) for the first crack formation. This is acceptable because the same conclusions regarding the crack path are achieved in materials under compression, by assuming that crack grows along the plane of maximum shear stress as by assuming that crack follows the direction of maximum KII. Without pre crack in this work, the point with maximum shear stress is taken as the point where the crack starts.

A single crack propagating inward from the boundary surface is considered in this work. It is found that the point with the maximum shear stress is always generated around the sharp corner. Shear crack starts at the end of compaction step 9, and the shear stress distributions as well as the relative density distributions at step 10 are shown in respectively. These two figures indicate that crack starts in the region with high shear stress but low relative density.

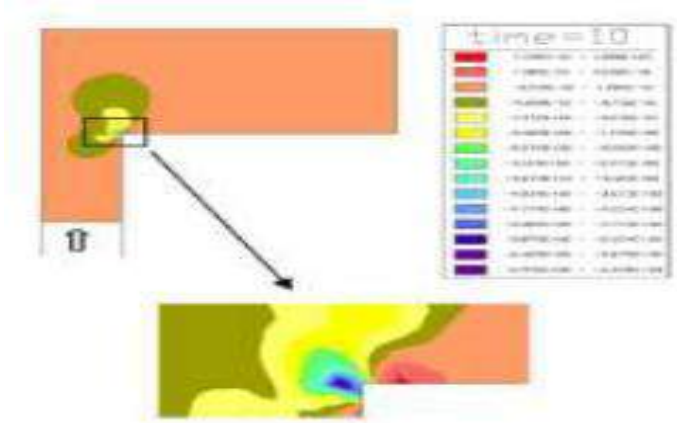

Shear stress distribution

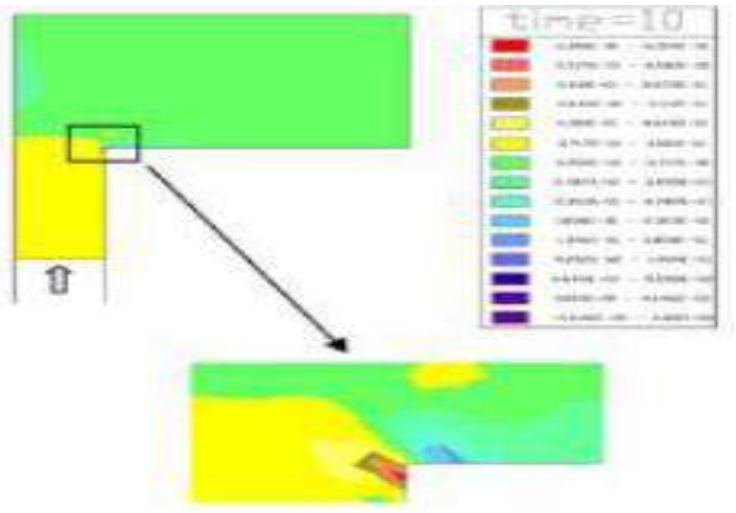

Relative Density distribution

Crack propagation

As compaction proceeds, the crack propagates as shear crack at step 17, 18 and 20, where the crack propagation directions, h. No further propagation occurs after step 20, until compaction is completed at step 40. The shear stress distributions and relative density distributions at step 21 are shown in. Due to the small angle of propagation direction, a smooth curve of crack propagation is formed at the inner corner, showing the behaviour of shear crack growth. Neglecting the sign convention that indicates the direction of stresses, it can be seen from that the crack propagates towards the region with higher shear stresses. that the crack also propagates in the direction where the relative density is much higher. Since relative density increases as compaction pressure increases, it can be deduced that the crack grows in the direction of higher compaction pressure. This is in line with the conclusion made byarguing that crack grows in the direction of higher confininghydrostatic pressure, which is equivalent to the compaction pressure in this case.

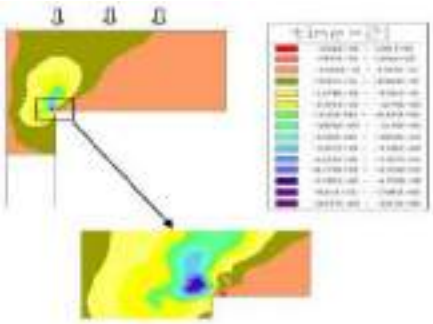

Shear stress distribution

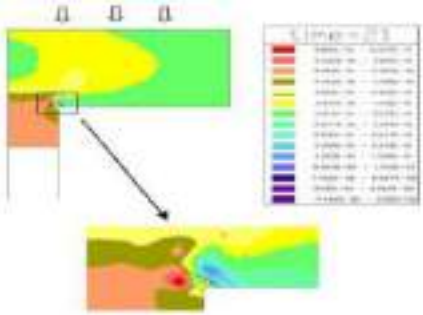

Shear stress distribution

CONCLUSION

- A displacement based finite element model has been developed to simulate the crack initiation and propagation in a rotational flanged component made of iron powder.
- A fracture criterion based on fracture of granular materials in compression has been successfully used to model the crack propagation process.
- Simulation of the crack propagation process in the iron compact shows that shear crack starts in the region with the highest shear stress and the lowest relative density distributions.
- As compaction proceeds, the crack propagates in shear mode in the direction where the shear stress and the relative density are much higher.
- Propagation of the crack towards the region of much higher relative density distribution also implies that the crack grows in the direction of higher compaction pressure, which is in line with the conclusion made by previous researchers on crack growth in materials under compression.
- In addition, simulation of crack growth at inner corner in multi-level component due to high stress concentration and high density gradient around the corner is indeed in line with reported fracture in multilevel component during preparation by previous researchers.
- This useful preliminary assessment on fracture behavior in metal powder during the compaction process can be further developed for prediction of crack growth in multi-level components with more complex geometrical shape and by using more accurate material fracture parameters.

ACKNOWLEDGMENT

I gratefully acknowledge Mechanical engineering department of Siddhant COE, Sudumbare, Pune. for technical support and providing the research facilities. I would also like to thank to Prof. U.V. Shinde, Principal (SCOE, Pune), Dr. P.A. Makasare, HOD (Mechanical department) and Prof. R. R. Kulkarni for their help and dedication toward my research and related research, also my friends for their directly & indirectly help, support and excellent cooperation.

REFERENCES

[1]. D. C. Zenger and H. Cai, J. McNeill and R. Ludwig ,"Classification stratergy to identify and classify common cracks" Review ofProgress in Quantitative Nondestructive Evaluation, Vol. 16Edited by D.O. Thompson and D.E. Chimenti, Plenum Press, New York, 1997

[2]. Mohamed Bouaziz1, Said Abid1,2, Hatem Ksibi2 **,"**Effect of Pressure on the Fracture of Compacted Argillaceous Particles" Received May 27, 2011; revised July 1, 2011; accepted July 10, 2011

[3]. Young-Sam Kwon and Suk-Hwan Chung, Howard I. Sanderow, KiTae Kim," Numerical Analysis and Optimization of Die Compaction Process", TIC, 296-3, Seonjin-ri, Yonghyeon myon, Sacheon, Kyongnam, 664-953, Korea

[4]. Suk Hwan Chung, Hyundai Steel CompanyYoung-Sam Kwon, CetaTech, Inc.," Modeling and Simulation of Press and Sinter Powder Metallurgy", ASM Handbook, Volume 22B, Metals Process SimulationD.U. Furrer and S.L. Semiatin, editors

[5]. Sydney H. Luk, Frank Y. Chan, Alan B. Davala, Thomas F. Murphy Hoeganaes Corporation," Processing Experience Of Green Strength Enhanced Material Systems",Presented at PM2 TEC '97 International Conference on Powder Metallurgy & Particulate Materials June 29-July 2, 1997 - Chicago, IL USA

[6]. Par Jonsen,"Fracture and Stress in Powder Compacts," Luleå University of TechnologyDepartment of Applied Physics and Mechanical Engineering Division of Solid Mechanics2006:29-1544 -06/29

[7]. S.M. Tahir a, A.K. Ariffin b ,"Fracture in metal powder compaction"

[8]. Joaqu´ın A. Hern´andez Ortega, Xavier Oliver Olivella, Juan Carlos CanteTer´an,"Numerical Modeling Of Crack Formation In Powder Compaction Processes"

[9]. Luleå University of Technology Luleå Division of Solid Mechanics, "Powder Mechanics" 2010-06-06

[10]. Thomas F. Murphy and Bruce Lindsley, "Metallographic analysis of PM Fractured Surfaces"

[11]. Dr. Keith J. Bowman, Nathan J. Smith, School of Materials Engineering Purdue University, " Fracture and Mechanical Properties of Porous Body Compacts"

[12]. MaterialsSean Garner, Jerry Klinzing, AntoniosZavaliangosDepartment of Material Science and Engineering. Drexel

IJARESM

ISSN: 2455-6211, New Delhi, India

International Journal of All Research Education & Scientific Methods

An ISO & UGC Certified Peer-Reviewed Multi-disciplinary Journal

Certificate of Publication

Prof. R. R. Kulkarni

Prof, Department of Mechanical Engineering Siddhant COE, Sudumbare, Pune India

TITLE OF PAPER

FEM Based Crack Analysis in Metal Powder Compaction

has been published in

IJARESM, Impact Factor: 7.429, Volume 9 Issue 5, May- 2021

Paper Id: IJARESM/May21

Date: 24-05-2021

STES's

Smt. Kashibai Navale College of Engineering

Sinhgad Institutes

S.No. 44/1, Vadgaon (Bk), Off Sinhgad Road, Pune – 411 041, Maharashtra, India

4th INTERNATIONAL CONFERENCE ON IDEAS, INNOVATIONS, IMPACT IN SCIENCE AND TECHNOLOGY

Organized By

Department of Mechanical Engineering

&

Department of Electronics and Telecommunication Engineering

Certificate

This is to certify that

Prof. Rahul R. Kulkarni

Participated / Presented the Paper entitled

Design and Optimization Process of Press Tools using Forming Analysis, for Cross Member Rear Floor Automobile Panel

in the "4th International Conference on Ideas, Innovations, Impact in Science and Technology" organized by Smt. Kashibai Navale College of Engineering, Pune, held on 17th June 2021

Dr. S.K. Jagtap	Dr. N. P. Shelje	Dr. K.R. Borole	Dr. A.V. Deshpande
Convener & Head, E&TC Dept	Convener & Head, Mech Dept	Vice Principal	Principal

Design and Analysis of Wheel Rim for Mass Optimization by Using Composite Material

Mr. Ranjeet R Bhalerao[1] Prof. R. R. Kulkarni[2]
[1]M.E. Student [2]Project Guide
[1,2]Department of Mechanical Engineering
[1,2]Siddhant College of Engineering, Sudumbre Pune, India

Abstract— The purpose of the passenger Vehicle wheel rim provides a firm base on which to fit the tire. Its dimensions, shape should be suitable to properly accommodate the particular tire required for the vehicle. In this study we are focusing on the optimization of weight by using FEA method. The wheel rim is designed by using modeling software catiaV5R19 by reverse engineering procedure. In modeling the time spent in producing the 3-D models and the risk involved in design and manufacturing process can be easily minimized. For better design results this CATIA model is imported to ANSYS for analysis work. ANSYS software is the latest used for simulating the different forces acting on the component and also for calculating and viewing the results. A solver mode in ANSYS software calculates the stresses, deflections and their relations without manual interventions, reduces the time compared with the method of mathematical calculations by a human. Also in the weight of component is display by density and size of material. ANSYS static analysis work is carried out by considered four different materials namely aluminum alloy, Mg alloy, mild steel and Composite material. Also their relative performances have been observed respectively. In addition to this rim is subjected to FEA analysis. In this paper by observing the results of both FEA static analysis and testing results obtained by comparing weight of all selected material and find the best material in that all material.

Keywords: ANSYS, Wheel Rim, aluminum alloy, Mg Alloy, Carbon Fibre, and mild steel

I. INTRODUCTION

Automotive wheels have been developed over the periods from early spoke designs of wood and steel, flat steel discs and lastly to the stamped metal configurations and structural steel and aluminum alloys rims of today's modern vehicles. Historically, successful designs reached after years of experience and widespread field testing. In the latest years, the procedures have been enhanced by a variety of experimental and analytical methods used for structural analysis (strain gauge and finite element methods). Within the past 10 years, durability analysis (fatigue life predication) and reliability methods for dealing with the differences inherent in engineering structures has been applied to the automotive wheel. Wheels are clearly safety allied components and hence fatigue performance and the state of stress in the rim under various loading conditions are major concerns. Further, wheels carry on obtaining a considerable amount of attention as a part of industry efforts to reduce weight through material replacement and down gauging. Even though wheels are loaded in a complex manner and are highly stressed in the course assumed multiple choices in respect of material, cross section for rim and arm connecting hub and rim. The newer car is supposed to have lesser weight without compromising the strength. Consequently, there is a scope for optimization of wheel design in respect of geometry of car rim, geometry of arm, material etc. The car rim is subjected to static loading condition. It undergoes Pressure, Tensile, circumferential loading and also impact loading. Consequently, it is justified to have a detailed analysis using the technique like FE for the stresses developed during used. It is proposed to analyze the car rim using FE approach for varied geometry parametric parameter for optimization of its weight. Of their rolling duty, lightweight is one of the major requirements hence cast and forged aluminum alloys are essential in the design. So, the current generation automobile have the alloy wheel. This technology ups gradation has wheeled is the one of the most important components of an automobile. It supports and bears the entire vehicle load. It suffers not only the vertical force but also the irregular forces resulting from the car's ride, braking, cornering, road bumps, and all uneven shocks in the process of moving on road. Due to high speed rotation, its quality has a massive impact on wheel stability, handling and other characteristics. Cornering Fatigue Test and Radial Fatigue Test are performed on any road wheel. It is observed that the FEA result of the above two tests shows that the maximum stress being induced in the wheel is much less than the allowable stress of aluminum alloy. Here comes the scope for further optimization of these wheels. Structural optimization is aimed at to minimize the mass of wheel without compromising the strength of wheel

II. PROBLEM DEFINITION

The failure of rim wheel is due to crack initiated near the hole which further gets propagated. To improve the strength of wheel rim, material optimization and design optimization is necessary for which the best material has to be selected by conducting design of experiments to find parametric design which gives higher strength of wheel rim. So I am doing the analysis of wheel rim with materials are magnesium alloy, Aluminium alloy, Carbon fiber+ Kevlar, mild steel. After testing the material in ansys software its material samples will be tested to check better material to reduce the wheel rim weight and improve the strength

A. Images of failure:

Fig. 1: Crack near the hub hole

Fig. 2: Bend due to impact:

III. AIM AND OBJECTIVE

The failure of the wheel rim can be avoided by changing the design of the wheel rim cross section. The alternate design option provides the strength and stiffness to the wheel rim. To prevent the failure of wheel rim due to crack initiated near the hole which further gets propagated throughout the rim which leads to fatigue failure.

1) To improve material optimization.
2) To improve design optimization is necessary for which best material has to be selected by conducting design of experiments.

IV. DESIGN METHODOLOGY

Methodology used in the analysis and design of the wheel rim

A. Research Paper

For This Project We were focusing on finding research papers for finding the research gap and the idea to find new concept with focus of project development regarding design and manufacturing. The research papers were gave us the domains and works which were already completed and provided lots of information and research data regarding design and analysis of wheel rim for weight optimization by using composite material.

B. Collection of Data

From research papers and resources we were collect the data for actual design of bumper and to overcome the bugs and challenges. We were come to know about many material used for wheel rim. The all collected data was used for getting proper path for development

C. CATIA design for Arrangement

For our project the next step to design of actual wheel rim with dimension and approximate calculations of different forces acting on wheel rim. For Catia modeling we have taken the help of selection of the research papers and car catalogue we created the 3D model of our project that is wheel rim design in CATIA v5 software.

D. Analysis

For our project we are doing analysis on Ansys Workbench 16. With modal analysis and static structural analysis workbench for solving procedure.

E. Testing

In this step we did the testing of wheel rim material plates with different forces acting on it. This will give us data regarding different parameter which help us to improve the design of wheel rim and for selection of better material.

F. Result comparison, Conclusion and report writing

In this last step we are comparing the result of theoretical and practical method and finding the better material by minimum weight, high strength and low deflection. By using this result we are concluded the best material.

V. LITERATURE SURVEY

Karthi et al studied the design of motor cycle alloy wheel using the PRO-E and Analyzed with the ANSYS. Analysis a tool used for the evaluation of systems and structures. It is needed to analyze complex structures, whereas very simple ones. There are three processes involved which are reprocessing, analysis and visualization. The chosen material was an Aluminum alloy, magnesium alloy, titanium alloy. The aluminum alloy is well to the conventional steel wheels in strength and durability. It has excellent wear resistance, anticorrosion properties and longer service life as estimated by the stress frequency distribution. The analysis is done with the extreme load can be applied on rim. The rear wheel and front wheel have their maximum load that can be sustained. It was found that the stress of the analysis is still in the range of the yield strength of Aluminum alloy. The Displacement is at the low value. This design is still in the safe condition.

Choudhury & Dipesh Rohan discussed about vehicle mass effect. Mass can be categorized as sprung-mass and unsprung-mass. A lower value of unsprung mass leads faster response time. There will be steady vertical load acting through the tyres and therefore a consistent level of friction acts between the car and road. Acceleration, braking and cornering performance of the vehicle is better. This paper goals to develop a composite wheel rim to be used with a lightweight aluminum center to reduce the unsprung mass of the vehicle and thus decrease the suspension response time for a better control of the vehicle. This will work towards bringing the sprung to unsprung mass ratio closer to the original value, and therefore allow for further reduction of the unsprung mass as well as sprung mass

H. N. Kale et al, studied about Wheel rim design. Rim is a central part of wheel above which a rubber tyre is mounted. In wheel assembly tyre fixed on the rim in between the left and right board flange over the bead seat area. Wheel convert axle torque into the rotational motion that rotating tyre comes in contact with road surface and rotational motion gets converted into the linear motion of a vehicle, that means the wheel assembly is very important part of any automobile without it vehicle cannot displace from one position to another. Well build road surfaces are not available everywhere in the world. On the road there are so many up and downs as well as pot holes which are responsible for impact load on the wheel and rim directly. Wheel is exposed to the loads of passenger, goods in addition with self-weight of vehicle itself, such load act as an alternating load and responsible for induction of irregular stresses into the rim and resulted fatigue failure of rim. Distinctly from above load wheel rims come in contact with environmental conditions which adversely affects on the rim. This paper presents

reasonable study of various types of wheel rim materials in comparison to wide varieties of aspects. Right material for right design acts as an important role in the life of any mechanical components. Relative study will help any designer while selecting materials for wheel rims of any type of ground vehicles. Deformation of lightweight alloy wheel is additional than the steel and forged steel, which means forged steel, can be used for light as well heavy duty vehicles such as trucks, tractors, trolley, scooter, bikes etc. Heat dissipation and corrosion resistance of Mg and Al alloy is well as compared to Steel C1008 and forged steel. All materials presented in table-1 are strong yet durability is also dependent on the manufacturing method employed for rim, dimensional design of rim.

S. Ganesh &Dr. P. Periyasaamy research on Aluminium Alloy wheels of automobiles. Wheels which are manufactured from an alloy of aluminum, magnesium metals or sometimes a mixture of both Alloy wheels vary from normal steel wheels because of their lighter weight which improves the steering and the speed of the car. Alloy wheels will decrease the unstrung weight of a vehicle compared to one fitted with standard steel wheels. The benefit of decreased unsprung weight is more precise steering as well as a nominal reduction in fuel consumption. Alloy is an excellent conductor of heat, refining heat dissipation from the brakes, reducing the risk of brake failure under demanding driving conditions. At latest design four wheeler wheels are made of Aluminum Alloys. In this project a parametric model is designed for Alloy wheel used with four wheeler by collecting data from reverse engineering process from current model. Design is valued by analyzing the model by altering the design of rim styles to be strong and balanced. Its material should not deteriorate with weathering and corrosion.

P. Meghashyam et al has motive study about car rim wtth Catia & Ansys Tool. The car wheel rim provides a firm base on which to fit the tire. Its dimensions, shape required as appropriate to effectively accommodate the particular tire required for the vehicle. In this study a tire of car wheel rim fitting to the disc wheel category is considered. Design in important industrial activity which affects the quality of the product. The wheel rim is designed by using modeling software catiav 5 r18. In modeling the time spent in creating the complex 3-D models and the risk involved in design and manufacturing process can be easily minimized. So, the modeling of the wheel rim is completed by using CATIA. Later this CATIA model is imported to ANSYS for analysis work. ANSYS software is the newest used for simulating the different forces, pressure acting on the component, and also for calculating and viewing the results. A solver mode in ANSYS software calculates the stresses, deflections, bending moments and their relations without manual interventions, reduces the time compared with the method of mathematical calculations by a human. ANSYS static analysis work is conceded out by deliberating two different materials namely aluminium and forged steel and their virtual performances have been observed respectively. In addition to this rim is exposed to vibration analysis (modal analysis), a portion of dynamic analysis is carried out its performance is observed. In this paper by detecting the results of both static and modal analyses obtained forged steel is recommended as best material.

VI. CALCULATIONS OF LOAD AT WHEELS

Average Vehicle Weight considered in Indian SUV vehicle segment = 2225 Kg.

Loading conditions for the wheel rim: Below are forces acting on the wheel rim while driving the vehicle.

- The Vehicle at the instant of braking: The braking force transferred to wheel rim is calculated as below,

Bump Force calculated below:-

For bumping force value first we required to calculate below values.

1) Brake Pedal Force
   The Brake applied on the pedal is assumed to be 300 N (30.6 Ksp)
2) Pedal ratio of every 4 wheeler is 6:1
3) Fmax = Force X Pedal Ratio
   = 300 X 6
   = 1800 N

Hence, $P = Fmax / \Pi / 4 \times d^2$

∴ P = Hydrostatic Pressure d = dia of master cylinder

Fmax = P X Π /4 X D^2 by Pascal Law Fmax = Force acting on each cylinder D = Dia of piston cylinder in caliper

By Solving,

Fmax = fmax X $(D/d)^2$

= 1800 X $(0.3 / 0.19)^2$

= 4487.5346 N

4) Now we calculate the torque acting on the disc,

T = Fmax X u X Re X no. of Piston per caliper

= 4487.6346 X 0.3 X 0.097 X 3

T = 391.7671

Where, u = Coefficient of friction between the brake pad and disc with thus = 0.3

Re = Radius of disc.

Max velocity of vehicle = 156 kmph Mass of Vehicle = 2225 kg

Newton's law of motion,

F= m x ag = 9.31 m/s

Here,

= 2225 X 9.81

= 21827.25 Kg.m

S^2

F = 21827.25 N

∴ Force applied on each wheel

= F / 4

= 21827.25 / 4

F = 5456.8125 N Units

Bump force calculated with reference of paper no. 11 mentioned in reference list.

VII. MATERIAL PROPERTIES

To optimize weight of the wheel rim and ensure its durability three new different materials considered.

Al alloy is existing material. And Carbon fibre, Mg alloy, Mild steel are new materials.

	Al Alloy	Carbon fiber	Mg alloy	Mild steel
Young's Modulus	7.1e+4 Mpa	70 e3Mpa	4.6 e5 Mpa	140 e3 Mpa
Poisson's Ratio	0.33	0.10	0.35	0.290
Density	2770 kg/m3	1600 Kg/m3	1800 kg/m3	7850 kg/m3
Ultimate tensile strength	310Mpa	1200Mpa	230Mpa	440 Mpa
Yield Strength	280Mpa	945Mpa	130 Mpa	250 Mpa

Table 1: Material Properties

VIII. FINITE ELEMENT ANALYSIS AND CATIA DESIGN

CATIA &ANSYS Workbench Simulation11.0 (also known as ANSYS Workbench Meshing 11.0) is used in this research work.

A. Building and Importing CAD model in ANSYS

The baseline Wheel rim model is prepared in CATIA using Sketcher and Part Design workbench. The model prepared in CATIA is as shown in the below figure.

Fig. 3: Al Wheel rim CAD model in CATIA

1) Meshing

Baseline Wheel rim is meshed with meshed with solid 187 elements for better accuracy and results.
Number of nodes = 201888
Number of elements = 1114332
Mesh element size - 8 mm
Element Type = Higher order Solid 187 elements

Fig. 4: Mesh model of Al wheel rim

2) Boundary Conditions

The pressure generated from the action of bumping pressure is applied at the region where top of the wheel rim Section are touching to wheel rim. Following boundary conditions are applied on the wheel rim

Total downward direction pressure-9806.6 mm/s² as a worst loading scenario. Bump force 5456.81N is considered as impact force during bump analysis in FEA.

Boundary conditions for baseline wheel rim model

3) Analysis of Al alloy Wheel Rim

1st analysis Al alloy tube pressure:

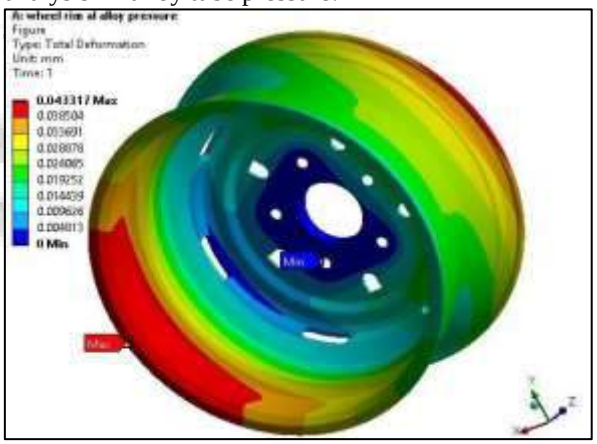

Fig. 5: Total deformation contour plot for baseline Al Wheel rim

The maximum displacement shown by the baseline wheel rim design is 0.043317 mm.

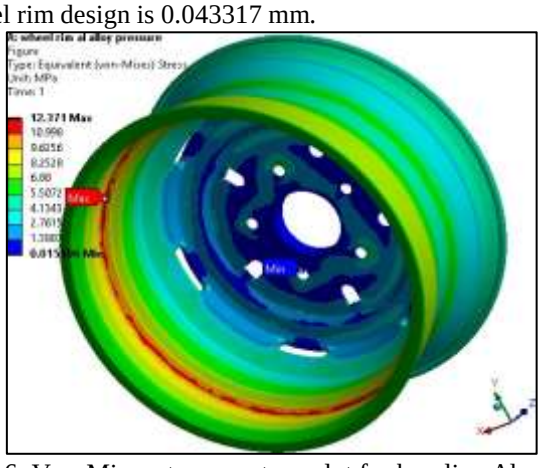

Fig. 6: Von-Mises stress contour plot for baseline Al wheel rim by tyre tube pressure

4) 2nd Analysis Tube pressure + bump

Fig. 7: Wheel rim al alloy pressure + bump gravity force downward direction

The maximum equivalent stress observed in the baseline wheel rim is 12.371 MPa.

The yield strength of the material is 280 MPa. According to the results, the von-Mises stress 280 MPa is less but nearer to the yield strength of the material. The sudden or impact braking action can cause the failure of the wheel rim at weakest cross sectional area of the wheel rim. The Field failure of the disc is caused due to sudden and dynamic load acting on the bumper. The same location of the failure is detected in finite element analysis study which is shown in the Figure.

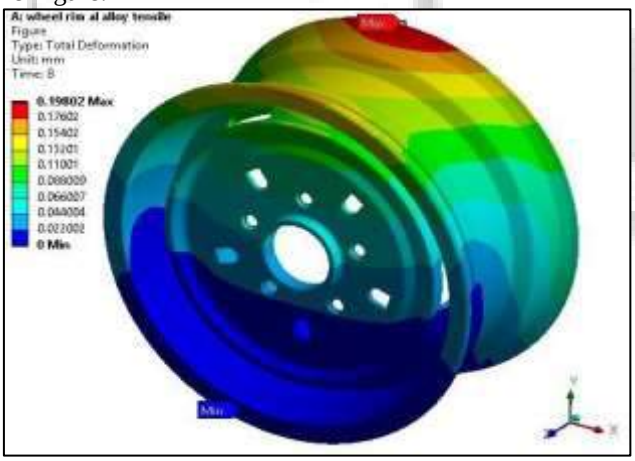

Fig. 8: Total deformation of al alloy rim by tensile loading

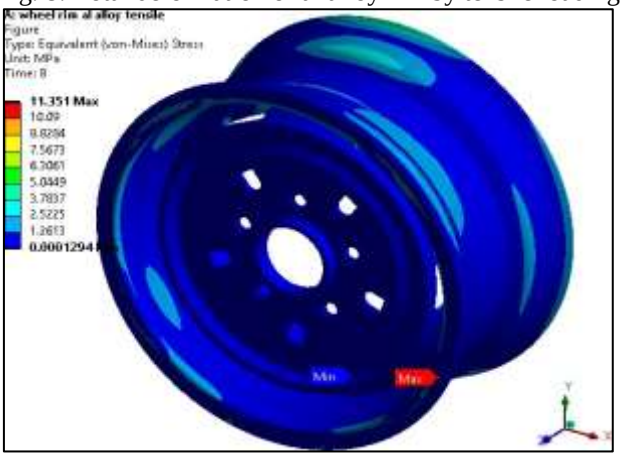

Fig. 9: Equivalent von mises stress of al alloy rim by tensile loading

5) Analysis of Wheel rim with Carbon Fiber material:

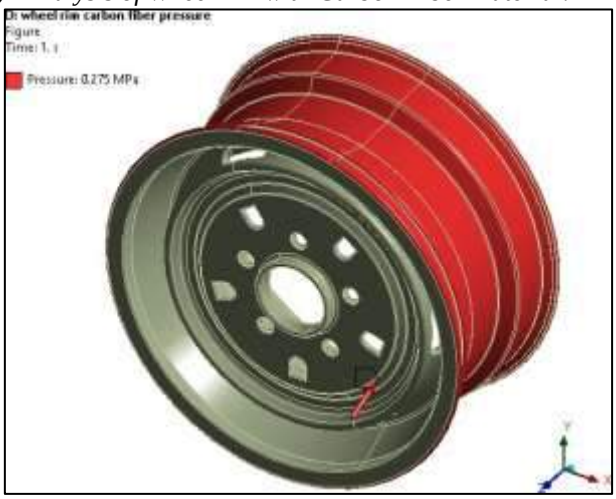

Fig. 10: Tyre tube pressure on rim surface

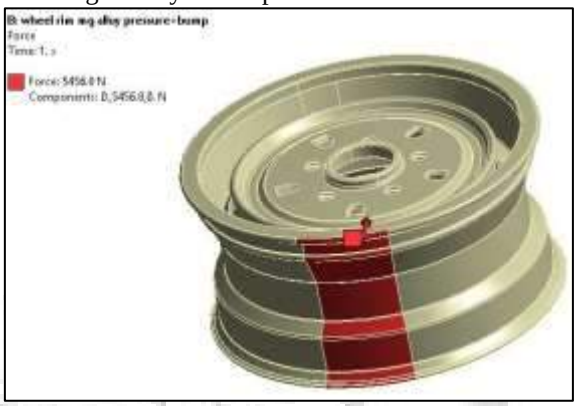

Fig. 11: Bump force 5456.8 N applied at carbon fibre rim

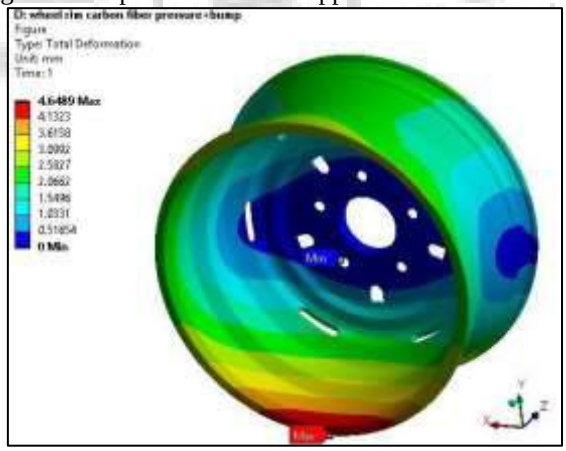

Fig. 12: Total deformation on carbon fiber rim by bump

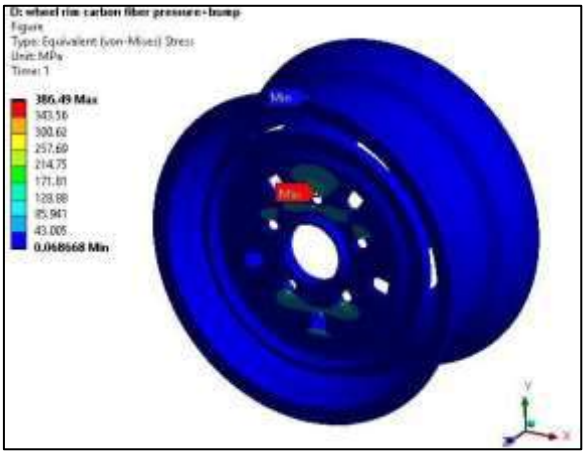

Fig. 13: Von Mises stresses on carbon fiber rim by bump

6) Analysis of wheel rim Magnesium alloy material:

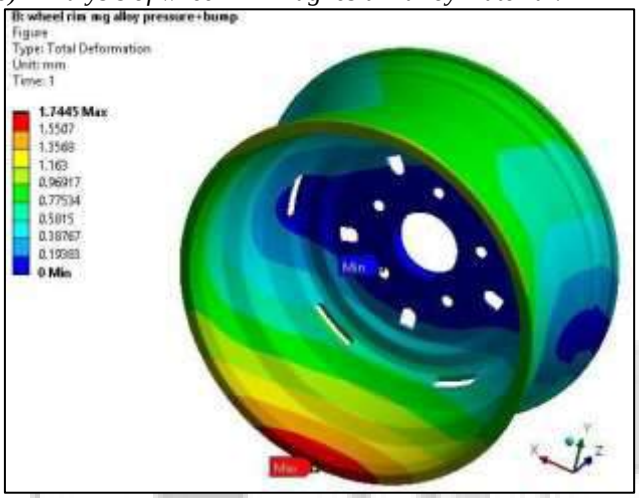

Fig. 14: Total deformation on Mg alloy rim by bump

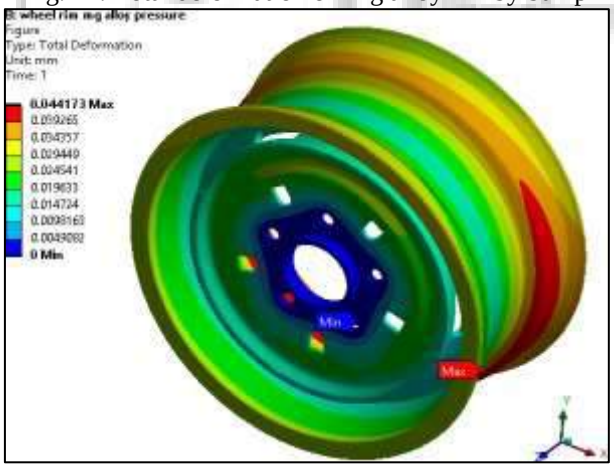

Fig. 15: Total deformation on Mg alloy rim by tyre tube pressure

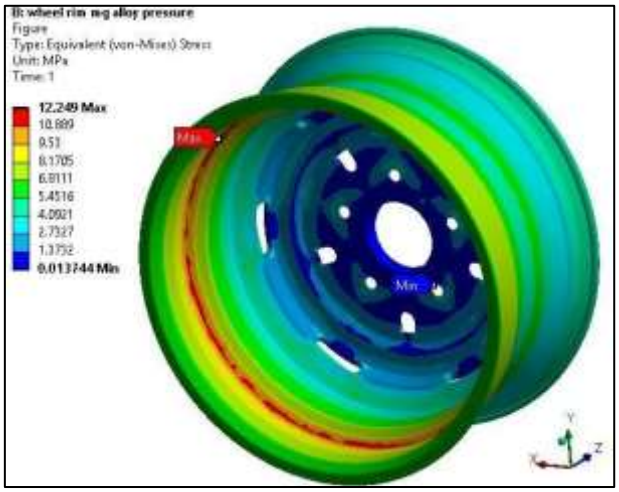

Fig. 16: Von Mises stresses on Mg alloy rim by tyre tube pressure

7) Analysis of wheel rim with Steel material:

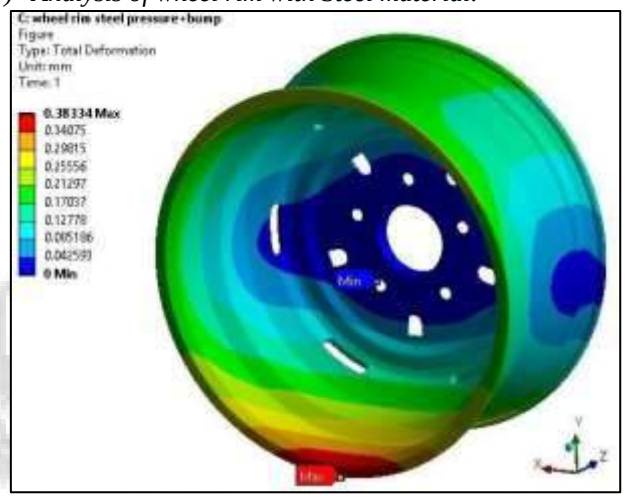

Fig. 17: Total deformation on steel rim by bump

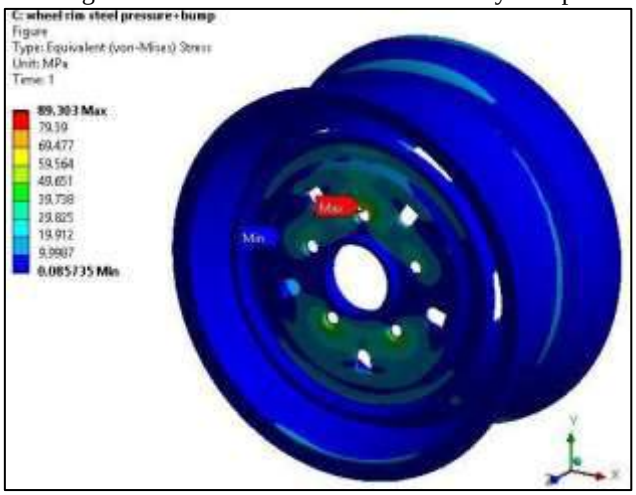

Fig. 18: Von Mises stresses on steel rim by bump

IX. RESULTS AND DISCUSSION

Results summarized after Design, FEA and Testing of respective material samples.

Sr. No.	Description	Mass (kg)	Deflection (mm)	Von- Mises stress (MPa)	FOS	Yield strength of material
1	Aluminium alloy Tube pressure Tube Pressure +Bump	12.2 12.26	0.04331 1.1056	12.371 93.793	25.05 3.30	280Mpa
2	Carbon Fiber Tube pressure Tube	6.596	0.20334	27.495	34.55	945Mpa

	Pressure + Bump	6.596	0.46489	386.49	2.45	
3	Magnesium alloy Tube pressure Tube Pressure + Bump	7.968 7.968	0.04417 1.7445	12.249 97.041	10.61 1.3396	130 Mpa
4	Mild steel Tube pressure Tube Pressure + Bump	34.75 34.75	0.38334 0.01911	89.303 12.542	2.799 19.93	250 Mpa

Table 2: FEA results for various samples

Results for compressive, tensile and impact strength of Aluminium alloy, Magnesium alloy, Stainless Steel & Carbon fibre composites in Praj Lab, Kothrud Pune represented in following table.

Sr No.	Defl-ectio	Load at Various Deflection (N)			
		Comp-osite	Mg	SS	Al
1	0.15	555.6	1136.8	984.9	940.80
2	0.30	1989.4	3322.2	3400.6	2195.2
3	0.45	4449.2	6027.0	6365.1	3777.9
4	0.60	7173.6	8859.2	9476.6	5566.4
5	0.75	10230.1	11686.5	12940.9	7389.2
6	0.90	13916.0	14709.8	16640.4	9192.4
7	1.05	17742.9	17836.o	20570.2	8879.8
8	1.20	21746.2	20981.8	24764.6	7918.4
9	1.40	26783.4	25666.2	26420.8	----

Table 3: Compressive strength of various samples
(As per ASTM D – 695-2002)

Sr. No.	Sample Identification	Tensile Strength Mpa
1	Carbon Fibre	349.34
2	MS sample	697.28
3	SS Sample	790.62
4	Al Sample	267.48

Table 4: Tensile strength of various samples
(As per ASTM D 638 - 2003)

Sr.No.	Sample Identification	Impact Value (J)	Izod Impact Strength
1	Composite Sample	17.20	252.29 Kj/m2

Table 5: Impact strength of Carbon fibre sample
(As per ASTM D 256 - 2003)

UTM – 4 Ton capacity Izod Impact machine-300Kj

Tensile and compression testing is carried out by using UTM machine and Impact testing is carried out by using Izod Impact test machine at Praj Lab, Kothrud, Pune

X. Conclusion

It is observed from the results that, Maximum stresses are developed in the various type material and its tube pressure, tube pressure + Bump and precisely matches with the test sample failure. A comparison of maximum total deformation and equivalent stress values of the wheel rim are calculated. By comparing the ansys results and material sample test results with respect to the value of factor of safety of various materials and their weight comparison. It is resulted that Carbon Fiber is better material. And it can be used for modified wheel rim design.

Acknowledgment

I would like to thank my Guide for their valuable support and guidance to me and Head of Department for Support. I also thankful to PG Coordinator.

References

[1] V.Karthi, N. Ramanan, J. Justin Maria Hillary."Design and Analysis of Alloy Wheel Rim", International Journal of Innovative Research in Science, Engineering and Technology, Volume 3, Special Issue 2, April 2014, ISSN (Online): 2319-8753 ISSN(Print): 2347 – 6710.

[2] Choudhury Dipesh Rohan,"Design and Analysis of a Composite Wheel Rim", Journal of Material Science and Mechanical Engineering (JMSME) Online ISSN: 2393-9109; Volume 2, Number 6; April – June, 2015 pp 50 – 56.

[3] H. N. Kale,Dr. C. L. Dhamejani, Prof. D. S. Galhe,"Comparative Study of Wheel Rim Materials", IJARIIE, ISSN -2395-4396, Vol-1 Issue-5 2015.

[4] S.Ganesh, Dr.P.Periyasamy, "Design and Analysis of Spiral Wheel Rim for Four Wheeler", The International Journal Of Engineering And Science (IJES), Volume 3; Issue : 4 , Pages 29- 37 – 2014, ISSN (e): 2319 – 1813 ISSN (p): 2319– 1805.

[5] P. Meghashyam, S. Girivardhan Naidu and N. Sayed Baba, "Design and Analysis of Wheel Rim using CATIA & ANSYS", International Journal of Application or Innovation in Engineering &Management (IJAIEM).Volume 2, Issue 8, August 2013 ISSN 2319 – 4847.

[6] S. Chaitanya, B.V.RamanaMurty, "Mass Optimization of Automobile Wheel Rim", International Journal of Engineering Trends and Technology (IJETT) – Volume 26 Number 3- August 2015.

[7] MayurKhule, P. Baskar, "Stress analysis and shape optimization of wheel rim", International Journal for Research in Applied Science & Engineering Technology (IJRASET), www.ijraset.com Volume 4 Issue V, May 2016, IC Value: 13.98 ISSN: 2321-9653.

[8] MI Guo-fa , NAN Hong-van, LID Yan-leF , ZHANG Bin, ZHANG Hong , SONG Guo- xiang, "Influence of Inclusion on Crack Initiation in Wheel Rim", Science Direct, Journal Of Iron And Steel Research, International. 2011, 49-54.
[9] Yee-Pien Yang, Member, IEEE, Yih-Ping Luh, and Cheng-Huei Cheung, "Design and Control of Axial-Flux Brushless DC", IEEE, VOL. 40, NO. 4, JULY 2004.
[10] J. Jürgens, A. Brune, B. Ponick, "Electromagnetic Design and Analysis of a Salient-Pole Synchronous Machine with Tooth- Coil Windings for Use as a Wheel Hub Motor in an Electric Vehicle", IEEE 4799-4389.
[11] Basavaraj Sajjan, Adithya Parthasarathy, Sai Kiran P, Varun Kumar K N , "Product Design and Development of Wheel Hub for an All-Terrain Vehicle (ATV)", International Journal of Engineering Research & Technology (IJERT), ISSN: 2278-0181 IJERT Vol. 5 Issue 08, August- 2016.
[12] Material Properties Taking from Material design Data Book.
[13] Mr. Sushant K. Bawne, Prof. Y.L. Yenarkar, "Optimization of Car Rim"International Journal of Engineering Research & Application (IJERT), ISSN: 2248-9622, Vol 05, Issue 10, October- 2015.

ISSN (ONLINE) : 2321 0613

IJSRDV8I100152

No: 379916

IJSRD

INTERNATIONAL JOURNAL FOR SCIENTIFIC RESEARCH & DEVELOPMENT

CERTIFICATE OF PUBLICATION

is here by awarding this certificate to

Prof. R. R. Kulkarni

in recognition of the publication of the paper entitled

Design and Analysis of Wheel Rim for Mass Optimization by Using Composite Material

published in e-journal

Volume 8, Issue 10, in Dec 2020

EDITOR-IN-CHIEF

EXECUTIVE-EDITOR

- Visit us @ www.ijsrd.com or call us @ +91 8866191212

STES's

Smt. Kashibai Navale College of Engineering

Sinhgad Institutes

S.No. 44/1, Vadgaon (Bk), Off Sinhgad Road, Pune – 411 041, Maharashtra, India

4th INTERNATIONAL CONFERENCE ON IDEAS, INNOVATIONS, IMPACT IN SCIENCE AND TECHNOLOGY

Organized By

Department of Mechanical Engineering

&

Department of Electronics and Telecommunication Engineering

Certificate

This is to certify that

Swapnil Gangane

Participated / Presented the Paper entitled

Gear Cutting Cost Optimization by Hob Tool Communization Through Simulation

in the "4th International Conference on Ideas, Innovations, Impact in Science and Technology" organized by Smt. Kashibai Navale College of Engineering, Pune, held on 17th June 2021

Dr. S.K. Jagtap	Dr. N. P. Sherje	Dr. K.R. Borole	Dr. A.V. Deshpande
Convener & Head, E&TC Dept	Convener & Head, Mech Dept	Vice Principal	Principal

Sinhgad Institutes

STES's

Smt. Kashibai Navale College of Engineering

S.No. 44/1, Vadgaon (Bk), Off Sinhgad Road, Pune – 411 041, Maharashtra, India

4th INTERNATIONAL CONFERENCE ON IDEAS, INNOVATIONS, IMPACT IN SCIENCE AND TECHNOLOGY

Organized By

Department of Mechanical Engineering

&

Department of Electronics and Telecommunication Engineering

Certificate

This is to certify that

Rahul Kulkarni

Participated / Presented the Paper entitled

Gear Cutting Cost Optimization by Hob Tool Communization Through Simulation

in the "4th International Conference on Ideas, Innovations, Impact in Science and Technology" organized by Smt. Kashibai Navale College of Engineering, Pune, held on 17th June 2021

Dr. S.K. Jagtap	Dr. N. P. Sherje	Dr. K.R. Borole	Dr. A.V. Deshpande
Convener & Head, E&TC Dept	Convener & Head, Mech Dept	Vice Principal	Principal

International Journal of Trend in Scientific Research and Development (IJTSRD)
Volume 4 Issue 6, September-October 2020 Available Online: www.ijtsrd.com e-ISSN: 2456 – 6470

Integrated ERP & E-Commerce for Medicines

Shivmalhar Bhise, Anushri Wali, Payal Pingale, Rohit Gupta, Dr. Brijendra Gupta

Department Computer Engineering, Siddhant College of Engineering, Sudumbre, Pune, Maharashtra, India

ABSTRACT

In Medicals and medicine is very essential and most required thing in the world .so here is the resource to reach to everyone i.e. Medical solution for all the roles required in the main purpose of this integrated system is to keep the expire medicines record as well as to notify with its need and expire date . It is an cloud based so that the system could act as a online warehouse, which will be secured as well. So that every store could refill their stock and would get notify by the expire date for each medicine. In integrated ERP we get details of medicines from medical store owner and stored details using the medicine batch number. Using this batch number of medicine check for its expiry.

KEYWORDS: *ERP, e-commerce security, distributed algorithm, random forest, commodity trading, batch no*

How to cite this paper: Shivmalhar Bhise | Anushri Wali | Payal Pingale | Rohit Gupta | Dr. Brijendra Gupta "Integrated ERP & E-Commerce for Medicines" Published in International Journal of Trend in Scientific Research and Development (ijtsrd), ISSN: 2456-6470, Volume-4 | Issue-6, October 2020, pp.696-699, URL: www.ijtsrd.com/papers/ijtsrd33485.pdf

IJTSRD33485

I. INTRODUCTION

An ERP system integrated with e-commerce is attempt to provide all function across a single company .With these system all those functions "specific needs" Integration is the key word for ERP & E-commerce. Issues gathered while communicating with the medical store owner.

1. Maintains of stock information
2. It listing expire inventory
3. It couldn't recognize whether the stock is finished or not. According to analysis we understand the issue faced by medical store owners now we providing them and ERP system. It Collecting the information from medical Store owner's using our ERP system and store all the information in a database we providing them the stock information. Get the detail information from owner of medical store and store it into the database. Using search method we find about the expiry details of the age inventory. Recognize the details of product which have to get referral and send a message to the owner. Distributed database is the term we are using to integrate the databases which we will get from different ERP systems. In particular areas multiple medical stores are present about nervous system we are providing for a single medical store and if we consider a particular area there are multiple medical stores thus the database will be in the distributed format. Now we have separate the database of each medical store and we are going to integrate the data maintain the medical inventory properly.

II. LITERATURE SURVEY

In e-commerce, the security involves two areas: hard security and soft security. Hard security includes cryptography, information hiding, while soft security is associated with the methods which are based on trust. Integrated means combining more than two data bases and working on them at the same time to implement this are thinking to implement one ERP system and one E-Commerce application so it will get the information through ERP and process those data base through e-commerce.

Following are the papers we have surveyed to get the detailed information of ERP system and e-commerce application.

1. Proposing a Distributed Algorithm to Finding Malevolent Entities and Improving Security in E-Commerce Environments.
2. Developing an E-Commerce Website.
3. A Role Oriented Requirements Analysis for ERP Implementation in Medical Service Organizations.
4. An Ad Hoc-based ERP for Medical Treatment Provision in Crisis Conditions.

Enterprise resource planning is the integrated management of main business processes, often in real time and mediated by software and technology. ERP system is easy to design and easy to maintain the data. E-Commerce is a business firms that used to sell anything on internet. And e-commerce is hard to design but easy to collaborate or to integrate with the data created by ERP system.

Since we were thinking to integrate these two systems with each other we get to know the problem of the shop owner of medical are having the problem which may have this solution hence we started to collect the knowledge about ERP system and e-commerce application integration of database and processing it.

Integrating ERP and E-Commerce it is easy to maintain all the database and expiry dates of medicine. Integrating systems that helps to maintain data easily and ERP has own databases means no loss of data occurs. Database designs emphasis on relation connectivity. The entire development process is based on 2 processes Front End and Back End

In the context of e-commerce, the concept of security involves two areas: hard security and soft security. Hard security includes cryptography, information hiding and other standards, while soft security is associated with the methods which are based on trust. finding malevolent entities or malevolent agents are one of the most important concepts in e-commerce. Thus, sufficient attention should be paid to their security. Since the centralized security management architecture in e-commerce environment and cannot have enough effectiveness nor be implemented, with the aim of overcoming the limitations of centralized architectures, a distributed and dynamic algorithm is proposed to finding malevolent entities and improving security. This algorithm uses a distributed network. The results of this study indicate that the proposed algorithm is capable of finds malevolent entities and improves security in a fast and efficient manner.

III. SOFTWARE AND HARWARE REQUIREMNETS

Software Requirements:

1. Androd Studio/Visual studio 19
2. MySQL/XAMPP Server
3. Windows 7/8/10.

Hardware Requirements:

1. Intel core i7, 2 GHz

IV. ARCHITECTURE DIAGRAM

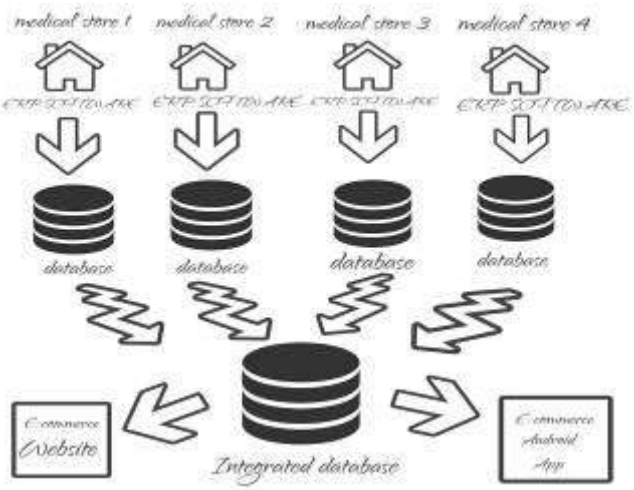

Figure 1: Architecture Diagram

V. UML DIAGRAMS

1. Activity Diagram

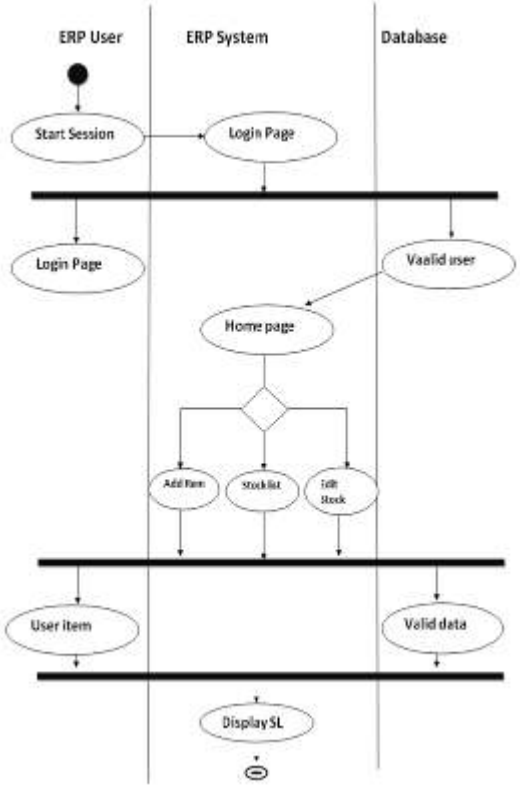

Figure 2: Activity diagram

2. Sequence Diagram

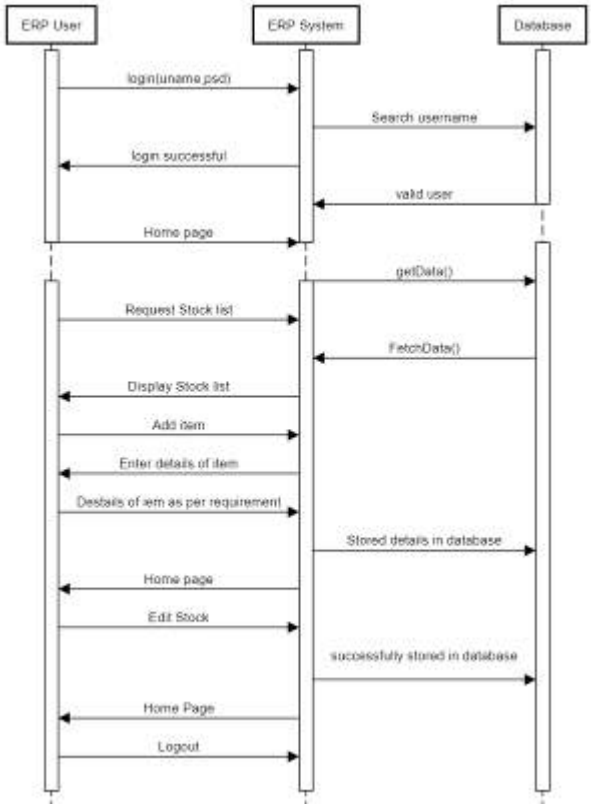

Figure 3: Sequence Diagram

VI. COMPONENT DIAGRAM

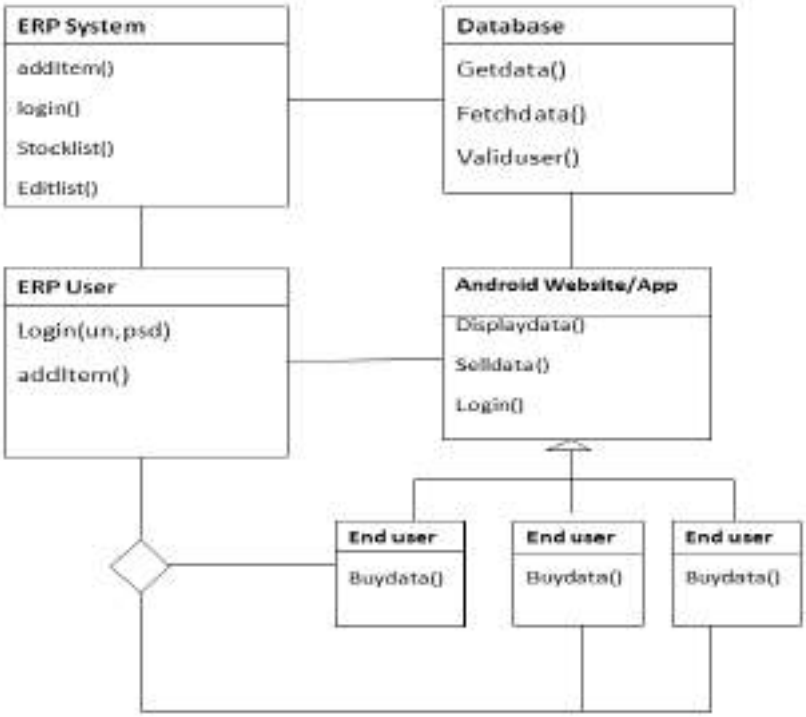

Figure 4: Class digram

VII. ADVANTAGES AND DISADVANTAGES

Advantages:

1. Provide security.
2. Efficient to handle big data.

Disadvantages:

1. Specified detail information.
2. While asking for high dosage doctor consultation is must.

VIII. RESULT AND DISSCUSSION

Application provides the detailed information and detail of medicines to maintain the medical owner the detail of medicine which helps to to give the correct information of medicines.

City medical connect to each other using our erp software If anyone want medicine which is in another city. Then he can easily get it using our own e commerce app they order also Medicine Or medical product.

Through which the medical owner easily supply the medicines hence the user whomever using using a where application will get nearest location where his or her all medicines he or she can purchase.

Collecting the information from medical Store owner's using our ERP system and store all the information in a database we providing them the stock information. Get the detail information from owner of medical store and store it into the database.

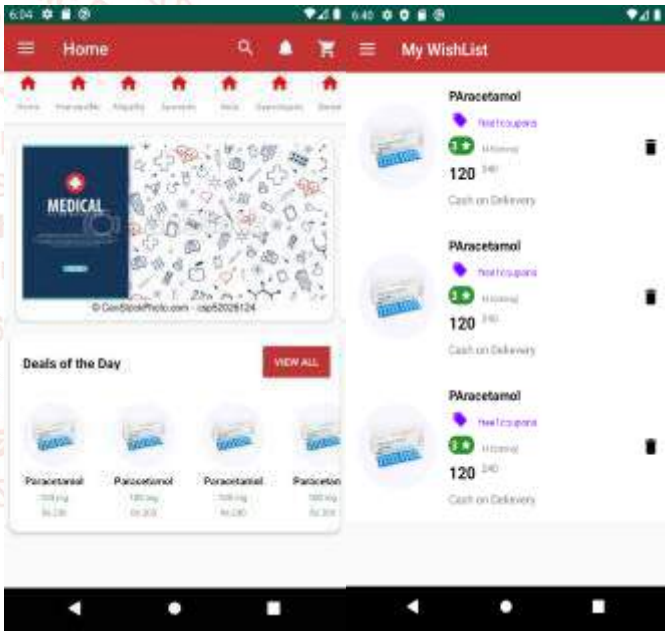

OUTPUT1 **OUTPUT2**

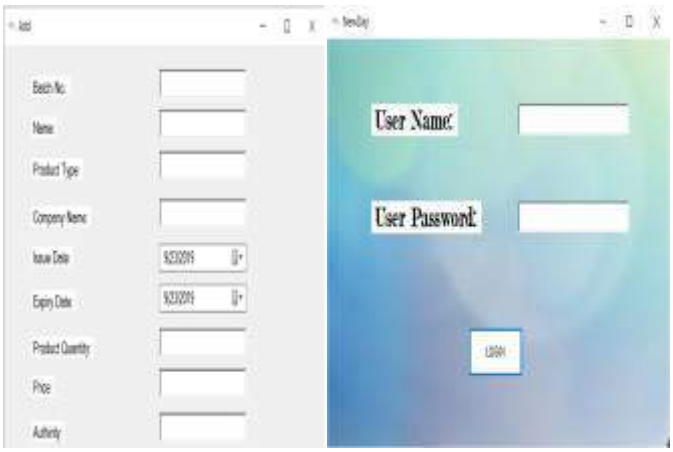

ERP OUTPUT1 **ERP OUTPUT2**

IX. CONCLUSION

The details of the medicine is maintained properly that means inventory check up and E-commerce. Using our application there will be no wastage of the products and medicine. And timely get updates.

X. REFERENCES

[1] Proposing a Distributed Algorithm to Finding Malevolent Entities and Improving Security in E-Commerce Environments Fatemeh Fouladfar Department of Computer, Faculty of Engineering, University of Isfahan, Isfahan, Iran fatemeh

[2] Developing an E-Commerce Website Syed Emdad Ullah, Tania Alauddin and HasanU. Zaman Department of Electrical and Computer Engineering North South University Dhaka, Bangladesh

[3] A Role Oriented Requirements Analysis for ERP Implementation in Medical Service Organizations Hwa Gyoo Park Dept. of U-Healthcare Management, Soonchonyang University.

[4] An Ad Hoc-based ERP for Medical Treatment Provision in Crisis Conditions D. Vassis, B. Zafeiris, C. Skouras Department of Informatics Technological Educational Institute of Athens GR-12210, Athens.